Characterization and application of fusogenic liposomes

Doctoral thesis

Submitted in partial fulfillment of the
requirements for the degree of

Doctor rerum naturalium (Dr. rer. nat.)

to the
Mathematisch-Naturwissenschaftlichen Fakultät der
Rheinischen Friedrich-Wilhelms-Universität Bonn

by

Rejhana Kolašinac

from Novi Pazar, Serbia

Bonn, July 2019

Angefertigt mit Genehmigung der Mathematisch-Naturwissenschaftlichen Fakultät der
Rheinischen Friedrich-Wilhelms-Universität Bonn

1st referee: Prof. Dr. Rudolf Merkel
2nd referee: Prof. Dr. Ulrich Kubitscheck
3rd referee: Prof. Dr. Dirk Menche
4th referee: Priv-Doz. Dr. Gerhild van Echten-Deckert

Date of the oral exam: 22. 01. 2020

Year of the publication: 2020

Acknowledgments

Firstly, I would like to express my sincere gratitude to my Doktorvater, Prof. Rudolf Merkel, for giving me the opportunity to do this work at his institute, as well as for the continuous support, his interest and availability for discussions of results, which have been incredibly helpful and motivating.

Besides my promotor, I would like to thank the other doctoral referees, Prof. Ulrich Kubitscheck, Prof. Dirk Menche, and Priv-Doz. Dr. Gerhild van Echten-Deckert, for accepting to be part of the Ph.D. commission and taking the time to review my work.

My special gratitude goes to my supervisor, Dr. Agnes Csiszar, for providing me with this fascinating and novel project, for guidance and support of my Ph.D. work. Thank you for many discussions, availability and opened door at any time, motivation, critics, advice and of course, sweets. Thank you for the help with paperwork, translations, and finding the apartment when I arrived in Jülich.

Many thanks to our collaboration partners:

- Dr. Sebastian Jaksch and Dr. Marie-Sousai Appavou, for their experimental expertise during SANS measurements and for helping with data evaluation and discussions of the results. Also, I thank Dr. Appavou for the Cryo-TEM experiments and help with analysis of micrographs.
- Dr. Erik Strandberg for the solid-state NMR measurements and discussion of the results.
- Dr. Sabine Dieluweit for freeze-fracture and STEM experiments and for introducing me to the freeze-fracture technique.
- Prof. Bernd Neumaier, Dr. Dirk Bier, Anette Schulze for giving me opportunity to work in their institute, providing ^{131}I and discussion of the results, and help in the laboratory during the experiments, respectively.

I am thankful to all my colleagues at the ICS-7, former and present, for making the working time nicer, for speaking with me in German (sometimes ☺) and for help whenever it was needed.

Big gratitude to our secretary, Claudia Klamandt that made my coming to Germany, first days here, and all the paperwork much easier to handle. Thanks for your patience and willingness to help!

My gratitude goes to Georg Dreissen, and Dr. Ronald Springer for their IT support and their readiness to always help that surely make the life of us students much simpler. Thanks to Georg for writing programs used for analysis in my Ph.D. work and for lessons in Python.

I want to mention the BioSoft fellows and our coordinator, Thorsten Auth, for the stimulating discussions and interesting experiences related to the IHRS graduate school.

I also thank Dr. Bernd Hoffmann for many biological discussions, Dr. Marco Hoffmann and Dr. Tobias Braun for the introduction to the cell culture and help throughout cell experiments at the beginning of my Ph.D. work.

Very special thanks go to Tabea and Jella. For having become my dear friends, for having made me feel at home in a new country and for having taught me German. I thank you for many scientific discussions, revisions of papers and thesis, nice time, many laughs, jokes, coffee breaks, and lunches. Thank you for the nice memories, and I'm looking forward to many more ahead.

Talking about the friends, I want to thank my Algerian (Zeineb) and Palestinian (Ghadeer) friends, for many tasty meals, good time and walks in this beautiful city Jülich. Special gratitude goes to Nour Maraytta, for being such a good friend, many discussion on all the physics I had to deal with, many talks, common meals, and thesis revision!

Finally, I want to thank my family, for love, good thoughts and support, many thanks to my parents, Muharem and Selima, and my siblings, Haris and Selma! Thanks for being there! Hvala vam na svemu! ☺

And, above all, my deepest gratitude goes to my boyfriend, Emin, for biggest support, dedication and encouragement, and patience in the past months. Thank you for your endless love and for being enrichment in my life!

Abstract

Conventional drug delivery strategies use the endocytic pathway to introduce biomolecules like proteins, DNA, or antibiotics into living cells. The main disadvantage of endocytic uptake is the quick intercellular degradation of the cargo. Compared to this, a more promising alternative for efficient molecular delivery is the induction of membrane fusion between liposomes and mammalian cells. Therefore special liposomes with extraordinary high fusion efficiency, so-called fusogenic liposomes (FLs), have been developed for such purposes. Due to complete fusion of the liposomal membrane and the cellular plasma membrane, the cargo molecules can be effectively released into the cell cytoplasm avoiding their degradation. In the last decade, applications relying on FLs became more and more relevant, however, the exact fusion mechanism is still to be elucidated.

Therefore the aims of this work have been to investigate those liposomes and their fusogenicity with living mammalian cells dependent on lipid composition as well as environmental conditions to elucidate the most important factors inducing fusogenic structures within the liposomes.

For structural characterization of the liposomes dynamic light and neutron scattering as well as solid state-NMR, freeze-fracture-STEM, Cryo-TEM, and differential scanning calorimetry were applied. Fusion efficiency was investigated by fluorescence microscopy and flow cytometry using Chinese hamster ovary (CHO) cells as an *in vitro* mammalian cell model.

The first results showed that fusogenic liposomes (FLs) need cationic lipids with inverted conical molecular shapes and aromatic components at a distinct concentration as well as a neutral lipid for the best fusion induction. Neutral lipids with long and unsaturated chains and a small head group (e.g., PEs) do not change the liposomal fusion ability while those with saturated short chains and a big head group (e.g., PCs) do, and in most extreme cases revert the uptake mechanism to endocytosis.

Additionally, a new application of fusogenic liposomes was established. For the first time, cationic liposomes with high fusion ability were successfully used as carrier particles for the delivery of the radionuclide ^{131}I into mammalian breast cancer cells *in vitro*. The FLs reached the cancer cells with high efficiency and delivered their cargo into the cell cytoplasm. The control treatment of human red blood cells did not give positive results on fusion, and in this case, the delivery of the cargo was neglectable. These results considered FLs as an appropriate tool for applications in nuclear medicine.

Further results showed that as the structural reorganization of the liposomal membrane supply the total required driving force to overcome the energy barrier of the different fusion intermediate steps, like in the case of FLs, changes of the fusion conditions such as temperature, osmolality or ionic concentration of the buffer did not influence the fusion success. In the case of the endocytic liposomes (ELs), buffer conditions played a crucial role in successful fusion, however, fusion efficiency remains infinitesimal under physiological conditions.

To elucidate the correlation between efficient membrane fusion and liposomal characteristics, structural investigations of FLs with the best fusion efficiency were also carried out. Here, the simultaneous presence of lipid bilayers and small micelles of around 50 to 100 nm in diameter with high surface curvatures were found. Based on the obtained results, a theoretical mechanism of membrane fusion between FLs and cellular membranes could be proposed. The positively charged lipid is necessary for establishing contact between the two membranes. The micelles are formed by the neutral, phosphoethanolamine, lipids. The lipid bilayer enclosing inverted micelles has a high positive membrane curvature, which is especially favorable for the positively charged lipid molecules. Such curvature stress usually promotes the fusion-stalk formation and subsequent membrane fusion; therefore the proposed fusion mechanism is called a modified stalk mechanism.

Moreover, traces of other three-dimensional (3D) phases with high membrane curvature such us sponge-, inverted hexagonal-, and cubic phases could not be excluded. The present structures are probably metastable precursors, such as a rhombohedral phase, that reduce bilayer stability, which is leading to the pore formation occurring. In comparison to this, ELs formed only lamellar phases shown as non-fusogenic under physiological conditions. These results give rise to the hypothesis that the predominant presence of 3D-like and 3D phases with high membrane curvatures is the most important criterion for efficient membrane fusion induction.

Table of Contents

Chapter 1

1. Introduction

Membrane fusion is an essential process for life. It is simply a merging of two membranes into one, and it can occur between two cells [1], between cell organelles [2-4], or two artificial membranes (lipid vesicles) [5,6], as well as between a cell and an artificial membrane [7-12]. Membrane fusion is significant from numerous points of view, such as trafficking within a cell [4,13-15] and between cells [13], for the mixing of genetic information between organisms [1] and the sculpting of tissues during development [16]. Usually, a fusion between two membranes is induced by some external mediators like proteins, peptides, and viruses, but it can happen without any inducers as it will be discussed later. There are some commonly accepted steps for fusion: membrane aggregation, close apposition of the membranes to fuse, transient destabilization of the bilayers, and mixing of the components to allow two membranes to become one.

Studies on mediated membrane fusion, such as viral fusion, have implicated specific membrane proteins as promoters through bilayer destabilization [17]. The access of viruses, including numerous human pathogens, into the host cell, relies on the fusion between the viral and the host cell membranes [13, 18-21], which may signal the end of the organism's life. However, there are different life processes based on membrane fusion, such as the fusion process mediated by the SNARE proteins [13, 22-25]. Additionally, the benefits of membrane fusion are appreciated to the highly efficient and controlled delivery of important molecules like in controlled protein and nucleic acid delivery.

Based on *in vitro* experiments, a non-mediated fusion between membranes (lipid bilayers) requires energy input, hence even a close and prolonged contact of two membranes may not harvest the fusion under physiological conditions (reviewed in [26]). In theory, any fusion that does not require specialized mediator denote a "spontaneous" fusion [27]. Nevertheless, it has been shown recently that liposomes, such as self-assembled lipid vesicles, can fuse with the cell membrane without any external inducer [9], and because of this special property, they are called fusogenic liposomes.

Liposomes, in general, serve as an adequate model for an examination of the properties and behavior of plasma membrane [28] and investigation of membrane fusion mechanism. In this case, the investigated fusogenic liposomes are able to fuse with the cell membrane easily without proteins, peptides, or viruses present. Therefore, the main goals of the thesis are the systematic investigation of the fusogenic lipid composition, to explore the impact of the conditions that fusion undergoes on the outcome. Additionally, the relation between the lipid phases and possible phase transitions of fusogenic liposomes with their fusogenic ability is crucial for deciphering the fusion mechanism of these liposomes and will be investigated in this thesis.

This chapter aims to introduce the basics of lipids, liposomes, the comparison of the properties of fusogenic liposomes with non-fusogenic ones, their physicochemical properties (lipid phases and phase transition), and known membrane fusion mechanism.

1.1. Liposomes

Liposomes are self-assembling lipid vesicles made of one or several kinds of lipids (Figure 1.1, the chemical structure of 1,2-dipalmitoyl-sn-glycero-phosphatidylcholine (DOPC) lipid is drawn as a representative of phospholipids) with size ranging from nm to μm scale [29-30]. The self-assembly of lipids into liposomes is driven by the hydrophobic effect. The polar head groups of lipids align towards aqueous phases and the apolar chains orient towards each other. A plethora of different amphiphile molecules form membranes (liposomes). When two hydrocarbon chains are esterified to a glycerol backbone, they are called glycerolipids. So-called sphingolipids have the hydrophobic ceramide moiety. The lipid having a phosphate and carbohydrate units in the head group are classified as phospholipids and glycolipids, respectively [31].

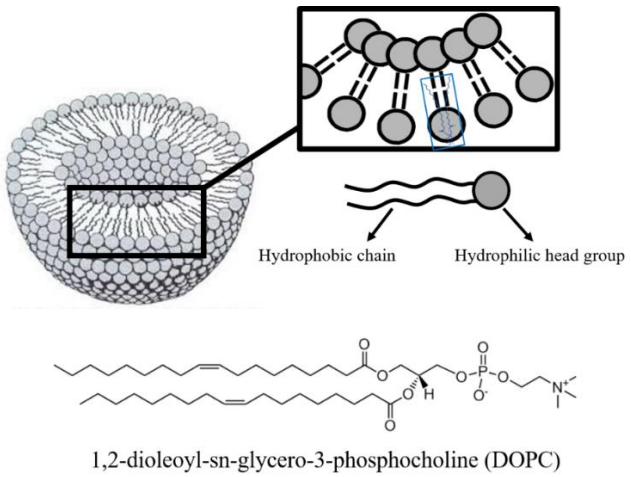

Figure 1.1. Liposome structure (cross-section) and the chemical structure of the phospholipid 1,2-dipalmitoyl-sn-glycero-phosphatidylcholine (DOPC).

The chemical properties of lipid molecules making liposomes determine physical membrane properties such as rigidity, fluidity, as well as the charge of the membrane. Unsaturated phospholipids, in general, make more permeable and less stable bilayers while saturated lipids with long acyl chains form rather rigid, impermeable membrane structures [32,33]. In terms of a number of bilayers, liposomes are classified as unilamellar (one bilayer) or multilamellar (many bilayers). Furthermore, according to their size, they can be small, large, or giant vesicles. Liposomes are often used as either a cell membrane model or a molecular delivery system [34]. The molecular composition of the cell membrane is well

established [35], therefore, many of their biological properties can be deduced in terms of the chemistry and physics of liposomes [36].

Liposomes have been very valuable for test systems for pure science. Many theoretical concepts are developed for understanding the liposomal formation and their behavior [35]. In mathematics, liposomes are applied for research on "topology of 2D surfaces in 3D space governed by bilayer elasticity only", in physics and biophysics for investigation of "aggregation behavior, fractals, soft and high-strength materials, permeability, and phase transitions in 2D", respectively [28]. Liposomes have been used as well in biochemical investigations of conformation and function of membrane proteins, such as ion pumps, purified membrane proteins, or glucose transport proteins reconstructed in their active liposomal form [28, 37]. Liposomes are also very important for applied research. For example, a recent publication that explores the possible *in vivo* delivery of liposome-corona protein [38] (lipid nanoparticle (NP)-corona protein) application in two different liposomal formulations, was published recently. Chatin and coworkers optimized *in vitro* delivery of two functional proteins, the β-galactosidase (β-gal) enzyme and the anti-cytokeratin8 (K8) antibody by liposomal formulations [39].

1.1.1. Comparison of fusogenic and endocytic liposomes

Because of their amphiphilic nature, liposomes can trap hydrophobic molecules in the lipid bilayer as well as hydrophilic molecules in the aqueous lumen [40], and thus they are widely used and applied as delivery systems. In most cases, liposomes are taken up by the cell via endocytosis leading to a low cargo delivery efficiency (Figure 1.2). Thus the commercially available liposomes are here called endocytic liposomes. A liposomal fusion with the cell membrane is a much better way of cargo delivery. It is usually mediated by proteins [41-43] (e.g., SNARE proteins), by membrane connecting tubuli [23], or viral membrane components [44, 45]. The fusion induced by proteins is studied intensely, and there are a lot of details, but these are very complicated mechanisms, and they depend on molecular details. Additionally, having a protein intercalated into the liposomes may trigger an immune response from a cell, and it seems like an expensive approach for clinical application of drug deliveries,. Therefore, having a protein-free membrane fusion is a much better alternative for molecular delivery via liposomes, mentioned here as fusogenic liposomes.

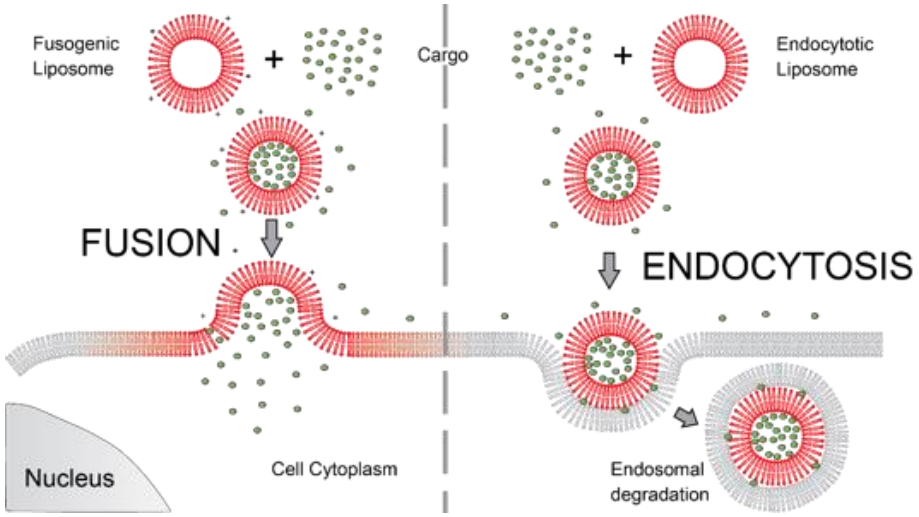

Figure 1.2. Comparison of the cellular uptake of fusogenic (left) and endocytotic liposomes (right). Cargo loaded into fusogenic liposomes is delivered to the cell cytoplasm by membrane fusion directly upon contact. Compared to this, endocytic liposomes (with or without charge) can also be loaded with cargo, but such liposomes are usually taken up via endocytosis, followed by the degradation of most molecules.

Since they were first established and described by Csiszar *et al.* [9], fusogenic liposomes have been of great interest for researchers both as a phenomenon and as a highly efficient delivery tool. In the case of fusogenic liposomes, fusion induction is triggered only by the vesicles made of lipids and aromatic-modified lipids or fluorescent lipid analogs. Precisely, they consist of a positively charged lipid (DOTAP), a neutral phospholipid (DOPE), and an aromatic dye (BODIPY FL-DHPE) at 1/1/0.1 weight ratio [9]. Fusogenic liposomes have a positive surface charge [9] that improves contact with cells, covered by negatively charged glycocalyx [46]. Fusogenic liposomes have been found as nontoxic by Kleusch and colleagues [11]. They have been first used for the delivery of fluorescently labeled lipids [11]. Many fluorescently labeled lipids are used for identification and localization of cellular compartments (e.g., Golgi apparatus or lysosomes) [47,48] or cellular uptake investigation – [49]. Besides the purpose of membrane and cell compartments labeling, fusogenic liposomes can also be used as a delivery system. For example, it can be used for the immune activator lipopolysaccharide [50], nucleic acids (mRNA and siRNA) [51], proteins [12], drugs, and antioxidants (e.g., resveratrol) [8] delivery. They are efficiently used for separation of cell populations based on the specific membrane fusion characteristics [10]. Recently, a novel analytical method for the cellular uptake differentiation (endocytosis or membrane fusion) based on the spectral properties of a single dye, BODIPY FL-DHPE, has been established [7].

1.2. Physico-chemical properties of lipid amphiphiles

1.2.1. Lipid phases

Lipids are natural molecules whose ability to self-assemble in dynamic macrostructures in water has been recognized as thermodynamic phases, depending on the molecular shape of lipids, the solvent content (lyotropic polymorphism), or environmental conditions such as temperature (thermotropic polymorphism) or pressure (barotropic polymorphism) [52-55]. Phases result from the minimization of the free enthalpy (temperature, pressure given) of the full system. The minimization of the free enthalpy results in the assemblies of different geometries.

Lyotropic liquid crystals are phases formed by the addition of solvents. Some examples of lyotropic phase structures are a fluid crystalline phase (L_α), the inverse hexagonal phase (H_{II}), and the inverse bicontinuous cubic phase of crystallographic space group Pn3m (Figure 1.3) [56, 57]. Liquid crystals are self-assembled organized mesophases with properties intermediate between those of crystalline solids and isotropic liquids [57]. In liquid crystals phases, long-range periodicity exists in at least one dimension, while in another dimension there is no periodicity, although the molecules exhibit a dynamical disorder at atomic distances like that in liquids. Accordingly, these materials can also be considered as ordered fluids. Attributable to the short-range disorder, these phases are called liquid crystals [57].

If the lipid molecule forming the bilayer has a cylindrical molecular shape (e.g., phosphocholines), the lamellar phase forms. However, if the lipid has a smaller head group area in comparison to the translational area of the chain region, hexagonal, or cubic phases can be formed (Figure 1.3).

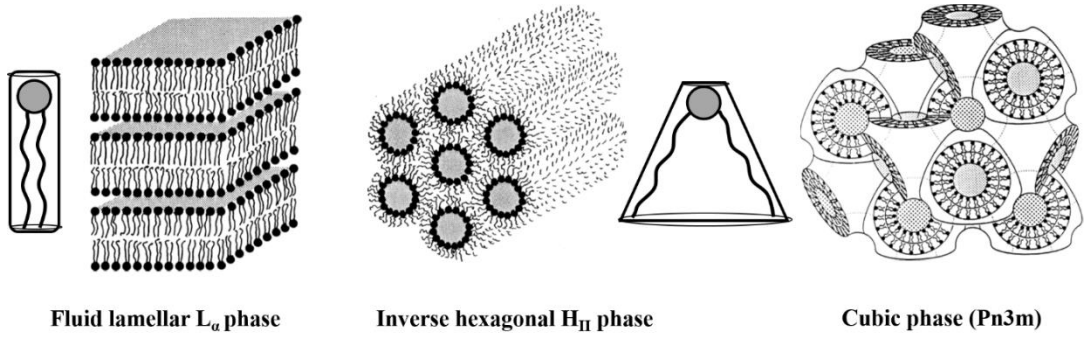

Figure 1.3. Examples of lipid phases. The figure is taken and modified from ref [56].

a) Lamellar phases

Crystalline lamellar (L_C) phases are formed by most of the phospholipids at low temperatures and low hydration levels [55]. These phases characterize high, 3D order, on short and considerable distance, and therefore are real crystals. In the crystalline lamellar phase, the hydrocarbon chains are stiff, fully extended, and regularly aligned on a 2D lattice with almost no lateral diffusion and slow longitudinal rotation [55]. In liquid disordered (L_D) lamellar phase, rapid lateral diffusion occurs, and there is a lower degree of order of the hydrocarbon chains. Over a specific temperature or water content, the hydrocarbon chains convert from the L_C to a fluid phase (L_α, 1D). The lamellar phase consists of about 30 wt% of the solvent and 60 wt% of the lipid. The fluid lamellar phase (L_α) (Figure 1.3) has the smallest surface per polar head compare to other lyotropic structures [58].

b) Hexagonal phases (2D)

The 2D periodicity of highly anisometric molecular aggregates is the feature that characterizes the hexagonal phases [58]. It is highly likely that the most investigated and well-established of them are normal and reverse hexagonal topology phases H_I and $H_{II,}$ respectively (Figure 1.4 [56]) [55]. The relation between surface area per polar head and volumetric occupation of the chain of the lipid is what rules the shape and geometry of supramolecular aggregates in the hexagonal phases [58]. In comparison to the lamellar phases, these have higher relative mobility (fluidity) of lipids forming the hexagonal phase [58]. In the hexagonal phases, the lipids form cylinders with chains inside them (H_I), or chains fill the spaces between the rods and water is inside the cylinders (H_{II}). The H_I usually is not formed by diacyl phospholipids but rather by lysophospholipids, while the H_{II} is extremely common in phospholipids with small and barely hydrated head groups (e.g., phosphoethanolamine) with attractive interactions between polar heads. Although the vast majority of reported hexagonal phases are based on aggregates having a single curved lipid layer (monolayer), a more sophisticated type, complex hexagonal phase, H_C, appears to be based on a hexagonal packing of cylinders formed by curved lipid bilayers [55, 56].

c) Cubic (3D) and rhombohedral phases

There are two types of molecular aggregates in the 3D organization, micelles, and bicontinuous structures (Figure 1.4). So far, there are only six cubic phases identified, two of which are micellar, and all of them are optically isotropic [55, 58].

The rhombohedral (also called rectangular, R) phase exhibits rod-like elements connected three by three in planar 2D hexagonal arrays that are then stacked onto a 3D rhombohedral lattice (Figure 1.4). In the tetragonal phase (square phase, C or K), the structure is formed from rods linked four by four into planar 2D square sheets that are then stacked onto a 3D body-centered tetragonal lattice [55, 58]. Rhombohedral phase, particularly the one of space group R3 discovered by the group of H.W. Huang, is the most suitable phase to learn more about the initial steps of membrane fusion [59]. Depending on the water content this phases can transform back to the lamellar phase (more water) or to the distorted hexagonal phase (dehydrated state) [60, 61].

d) Solution phases (L_1, L_2), and bicontinous sponge phase (L_3)

Micelles are formed either by short-chain phospholipids (typically C6 or C8) or by lysophospholipids in water [53]. They can create different shapes, such as spheres, rods, discs, or inverse micelles, L_2 (Figure 1.4.). These phases are the analogs of liquids: they have local (meso)structure, but the very short-range ordering is insufficient to define a lattice [62]. The aggregates in these mesophases are thus disordered. Nevertheless, they do exhibit many hall-marks of characteristic structures. They are most readily modeled as melts of some of the liquid crystalline mesophases listed above, e.g., sponge phase can be interpreted as a melted cubic phase [58, 62, 63]. Sponge mesophases are characterized by flow birefringence (giving anisotropic optical textures), yet they are isotropic at rest. They are typically viscous, even though to a less extent than bicontinuous cubic mesophases. Their mesostructures are closely related to the bicontinuous cubics. They often form at high (water) dilution, usually in regions of the phase diagram intermediate to lamellar and bicontinuous cubic mesophases. The sponge phase (L_3) is optically isotropic, but it does not display any long-range order. The lipid layer presents local principal curvatures of opposite signs, which characterize a saddle-like topology [55, 58]. There is still a lack of understanding of the differences between the sponge and the cubic phase.

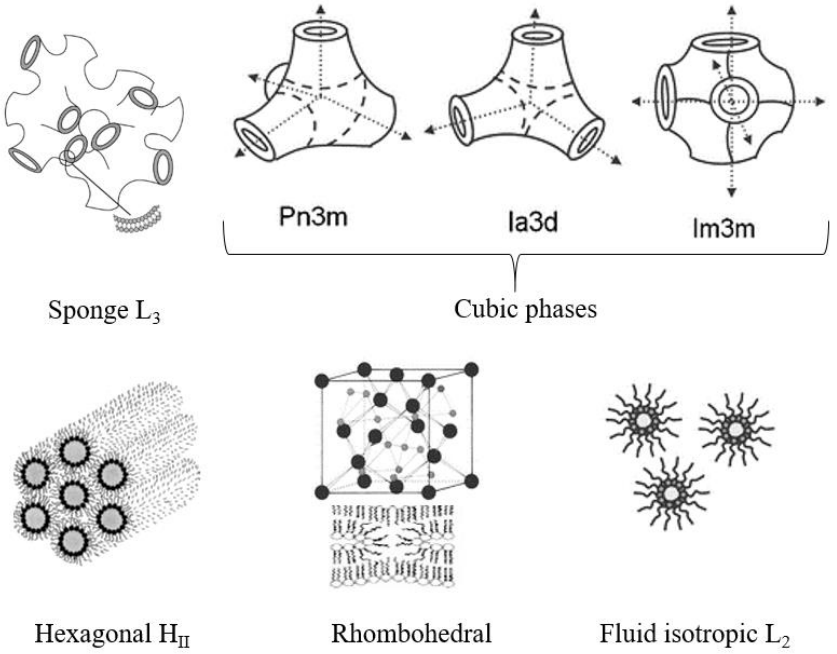

Figure 1.4. Lyotropic lipid phases that can be dispersed into sub-micron size particles. The figure is taken and modified from ref [64] reproduced and modified by permission of The Royal Society of Chemistry.

1.2.2. Phase transitions of lipids

Liposomes can exist in many polymorphic forms (phases), and temperature [65] or water content change-induced [55] interconversions between these forms (phase transitions) readily occur. Identifying number, composition, and structure of contemporary phases are the first steps to understand their phase behavior.

Long-chain phospholipids, depending on their structure, undergo several transitions at precisely defined temperatures. For example, the gel to liquid-crystalline transition (main transition) of 1,2-dipalmitoyl-sn-glycero-phosphocholine (DPPC) happens rather rapidly. Before the main transition, a pretransition can occur (T_p = 5-10 °C below T_m), in which a flat membrane in the gel phase transforms into a periodically undulated bilayer. This transition is called a gel to a 'rippled gel phase' transition and is observed only for sufficiently hydrated lipids such as DPPC in excess water (Figure 1.5 [66]). A prolonged subgel transition between the gel and the crystalline phases is not entirely characterized in structural terms. Each of these transitions has been intensively investigated using different spectroscopic methods or thermal analysis, e.g., differential scanning calorimetry (DSC) [67].

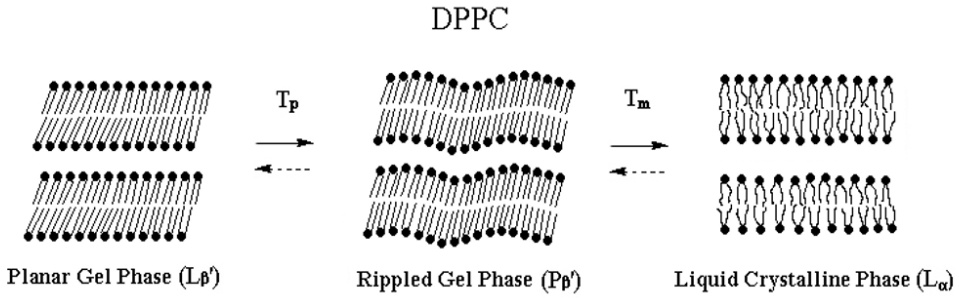

Figure 1.5. Phase transitions of 1,2-dipalmitoyl-sn-glycero-3-phosphocholine (DPPC). Solid arrows – heating transitions. Dotted arrows – cooling transition. © 2013 Smith EA, Dea PK. Published in [66] under CC BY 3.0 license.

In most cases, the information derived from calorimetric measurements is limited to the determination of the phase transition enthalpy (ΔH), entropy (ΔS), and temperature (T_m). In a pure infinitely large system, phase transition should occur at one precisely defined temperature. Real systems, however, show a finite width of the temperature. This can be explained by assuming that only finite size clusters transform cooperatively. If it is assumed that lipids do not melt all spontaneously but rather in clusters of *n* lipids, we have to consider these *n* lipids as the cooperative unit size:

$$\Delta H \rightarrow n\Delta H \tag{1.1}$$

$$\Delta S \rightarrow n\Delta S \tag{1.2}$$

$$K = e^{-\Delta G/RT} \rightarrow K = e^{-n\Delta G/RT} \tag{1.3}$$

$$K = \frac{\text{number of melted lipids}}{\text{number of solid lipids}} \tag{1.4}$$

$$\Delta G = \Delta H - T\Delta S \tag{1.5}$$

where K, as the constant reaction represents a function of temperature and depends on enthalpy (ΔH), ΔS is entropy change, ΔG is standard Gibbs free energy change (equation 1.5), R is a gas constant, and T is the absolute temperature. The coupling between the bilayers as well as within bilayers both sharpen the phase transition. In general, the larger the cooperative unit size, the narrower the transition peak. If the cooperative unit size approaches an infinite number of molecules, the transition half-width also becomes infinitely small.

Furthermore, the thermodynamic and kinetic properties of lipid phase transitions vary considerably [65], and the transition may not always occur under equilibrium conditions [65]. The temperatures (T_m, T_p, T_s), the enthalpy change of the phase transitions (ΔH_m, ΔH_p, ΔH_s), as well as the width and shape of the transition curves determined by calorimetry, are all related to the purity of the system and the nature of the transition [68]. One of the main determinants of phospholipid phase behavior is the lipid chains. For instance, the longer the chain length, the higher the phase transition temperatures. The effects of chain unsaturation are reasonably complex. The complexity comes from the degree of unsaturation, the geometry of the double bonds, and their location along the hydrocarbon chains. Typically, *trans* double bonds have a negligible effect on the lipid packing within the bilayers, and thus on T_m. On the contrary, the presence of a single *cis* double bond may result in a significant decrease of T_m, which can be assigned to modification of the lipid packing within the bilayer.

The packing of lipid molecules within the membrane gives it the specific degree of order, and change of the packing and higher mobility of the lipids (e.g., during phase transition) usually leads to membranes disorder. For instance, when the L_α phase undergoes a phase transition to the inverse cubic phase (Q_{II}), double layers change their prime organization notably. Tanford [69] and Israelachvili [70, 71] first proposed two different concepts of packing of molecules in the liposomes. Tanford suggested the concept of opposing forces to express the standard free energy change on aggregation quantitatively. Israelachvili and colleagues proposed the concept of molecular packing parameters and demonstrated how the size and the shape of the aggregate at equilibrium can be predicted from a combination of molecular packing considerations and general thermodynamic principles [70]. The critical packing parameter (CPP) can be calculated via the formula given in figure 1.6A [70]. It is a dimensionless number. Once the optimal surface area a_0, hydrocarbon chain volume v, and critical length l_c are specified for a given molecule, one may ascertain which structures the molecules can pack into within these geometric constraints [70]. Figure 1.6A illustrates how the different interactions occurring at the headgroup and chain regions determine v/a_0l_c and, in turn, the critical or limiting packing shapes that the molecules can adopt in the structures they assemble into. Figure 1.6B shows the gradation in preferred structures with increasing v/a_0l_c from spherical micelles ($v/a_0l_c \leq 1/3$) to nonspherical (ellipsoidal) micelles ($1/3 < v/a_0l_c < 1/2$) to cylindrical or rod-like micelles ($v/a_0l_c \approx 1/2$) to various interconnected structures ($1/2 < v/a_0l_c < 1$) to vesicles and extended bilayers ($v/a_0l_c \approx 1$) and finally to a family of "inverted" structures ($v/a_0l_c > 1$). Each of these structures corresponds to the minimum sized aggregate in which all the amphiphiles have minimum free

energy [70]. In concentrated systems, the preferred structures are also determined by the interactions between the aggregates, "mesophase" structures.

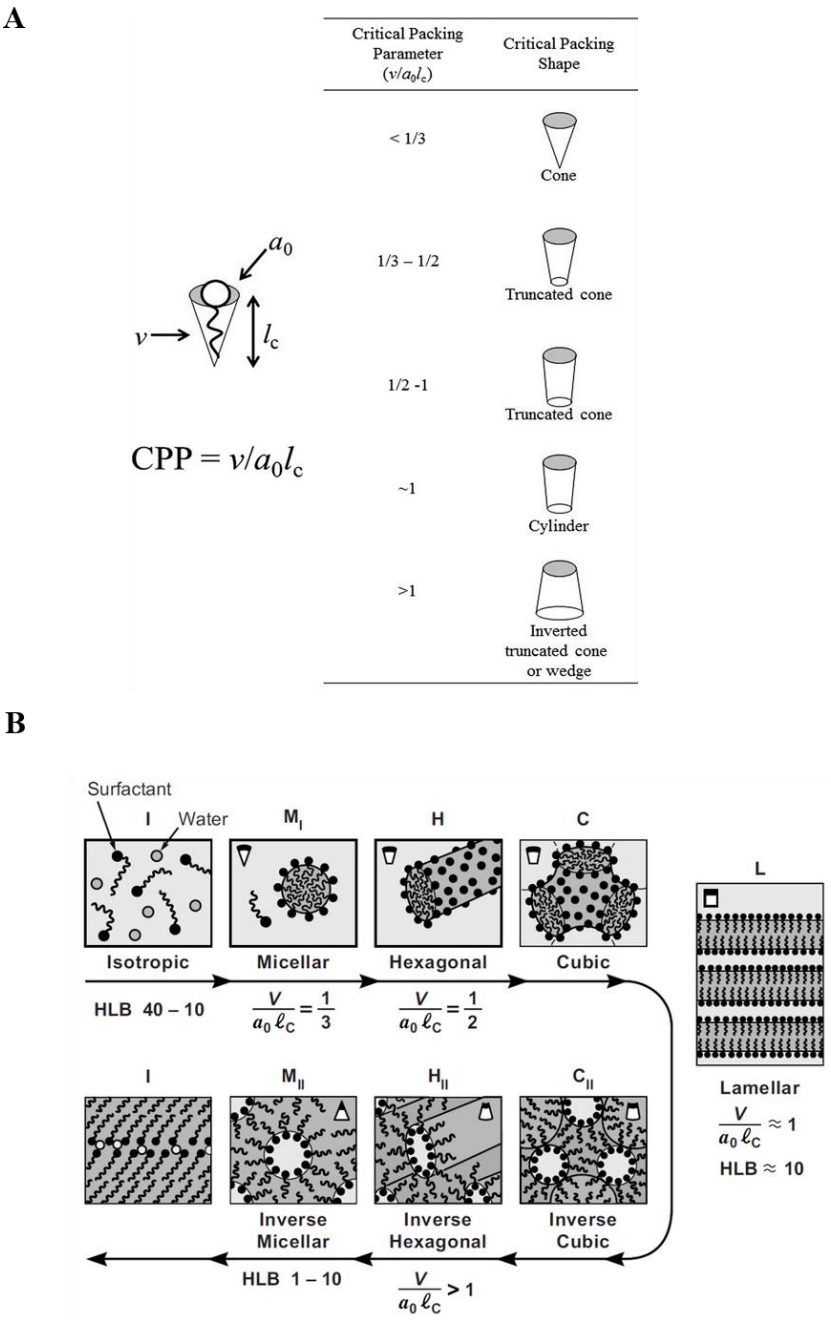

Figure 1.6. Molecular shapes and critical packing parameters of surfactants and lipids and the structures formed (A). The dimensionless CPP is linearly proportional to the hydrophile-lipophile balance or HLB number [72], which is traditionally used to designate amphiphiles that form oil-in-water micelles or inverted water-in-oil micelles in surfactant-water-oil mixtures (B). The figure is adopted and redrawn from reference [70].

1.3. Protein-free membrane fusion

Intermediates in the lamellar nonlamellar phase transitions of membrane systems containing phosphatidylethanolamine (e.g., 1,2-dioleoyl-sn-glycero-3-phosphoethanolamine (DOPE)), or other lipids with similar properties, have been implicated in facilitating membrane fusion. Siegel [73], together with Epand [74], worked on the phase behavior of DOPE and analyzed the conditions when the fusion of two membranes occurs via the so-called stalk-mechanism, the merging of the lipid monolayers (Figure 1.7B (2) [73]). Experiments done with DOPE liposomes revealed the intervesicular mixing of lipids when transitions from lamellar to inverse phases were observed [75, 76]. Therefore, the hypothesis that the formed structures (like small lipid particles) during this event are essential for membrane fusion has been established (Figure 1.7A [77]) [74]. Accordingly, fusion passages are primarily formed when two membranes merge. They connect the proximal monolayers of the membrane, which curves within the passage, that is energetically highly disadvantageous. It leads to an expansion of the fusion passage and formation of a hemifusion (trans-monolayer-contact, TMC, Figure 1.7B (3) [77]) where the lumen of two liposomes is separated only by one bilayer of lipids. Its breakage leads to the creation of the fusion pore (Figure 1.7B (4) [77]).

The observations of such phase transformations are obtained from DOPE`s phase behavior [74]. Even though they are probable, its states are not detectable. It was postulated, however, that lipids with negative spontaneous curvature, such as PE lipids, have little effect on the free energy of the stalk barrier [25]. In contrast, the same group claimed the lipid shape plays a crucial role in overcoming the hydration repulsion between two membranes, and that this lowers the total work required to form a stalk [25].

The proposed fusion mechanism is very well studied from a theoretical and experimental point of view [22, 25, 45, 73, 74, 78-87]. The stalk appears as a (meta)stable intermediate structure. In consequence, there are at least two free energy barriers to overcome during the process of membrane fusion: the free energy barrier associated with the stalk formation, and the free energy barrier associated with the opening of the fusion pore. The prediction of the energy barrier was calculated by different groups [25, 87-90], having results compatible with each other with activation energy ~ 30 k_BT [87] (Figure 1.8. [87]). François-Martin and co-workers postulated that if a fusion barrier of high energy (Figure 1.8B) can be split into several barriers that of low energy (Figure 1.8A), the fusion is facilitated [87].

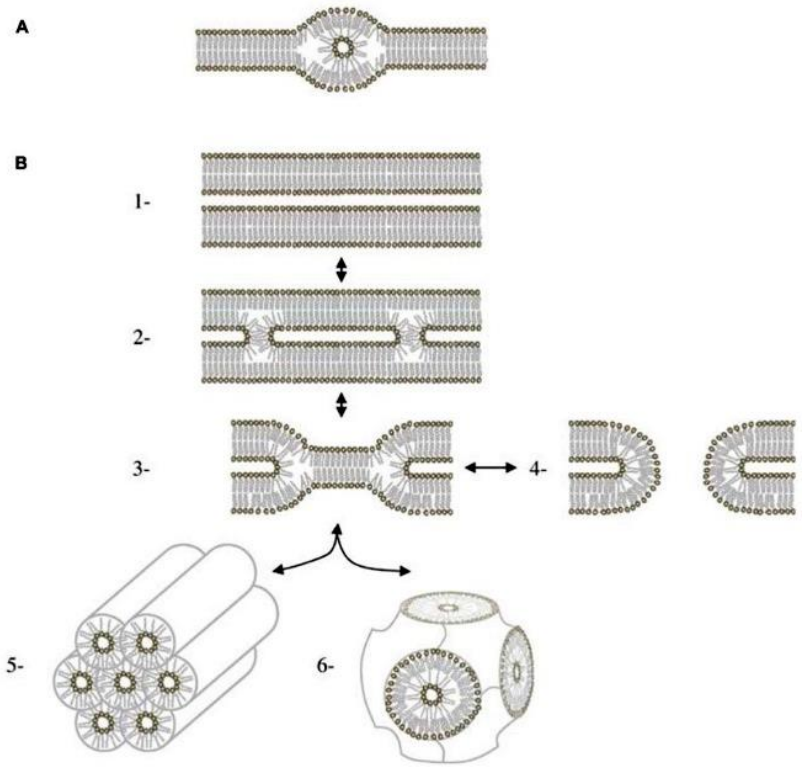

Figure 1.7. H_{II} phase in bilayers. (A) The lipidic particle, as described by Siegel [91] **(B)** Mechanisms of membrane fusion involving H_{II} via the stalk intermediate. (1) The adjunct of two bilayers. (2) Formation of cylindrically symmetrical stalks. (3) Two different types of structures can be formed at the hemifusion intermediate. When the bilayer in the central of the hemifusion intermediate breaks, then it forms a fusion pore (4). The systems that are near the lamellar/H_{II} phase frontier, hemifusion intermediates can also aggregate to form H_{II} phase (5) Accumulation of fusion pores in sufficient numbers leads to the formation of a cubic phase (6). Figure adapted from Jouhet (Siegel) [73, 77].

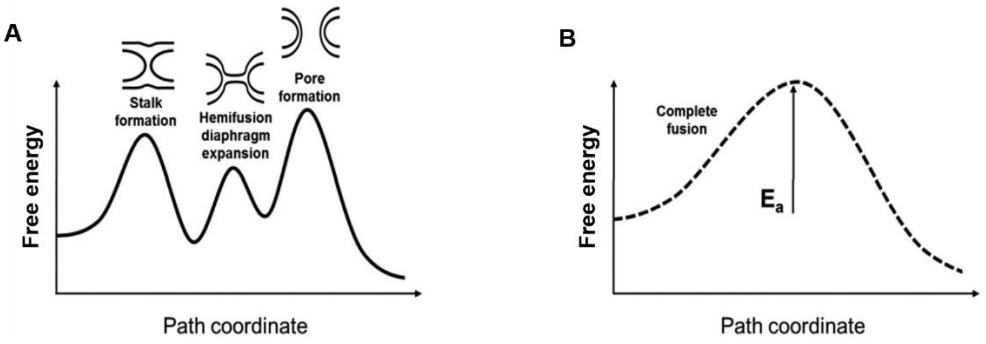

Figure 1.8. The energy of membrane fusion. (Left) The energy diagram of the membrane fusion steps. (Right) The energy diagram of the complete fusion pathway [87]. The overall probability of transition to the fused state as a pathway with a single activation barrier has to be larger than any of the individual energy barriers that separate successive transient intermediate states in a reaction process. The figure is adopted from [87].

Chapter 2

2. Materials and methods

This chapter provides information about the chemicals, materials, biomaterials, and methods for the preparation of samples, obtaining data via various techniques and analysis of the results.

2.1. Materials

2.1.1 Lipids

The lipids used for this work (presented in figures 2.1.-2.3), in powder form or dissolved in chloroform, were purchased from Avanti Polar Lipids (Alabaster, AL, USA) and used without further purification. The exceptions are fluorescently labeled lipids: *N*-(4,4-difluoro-5,7-dimethyl-4-bora-3a,4a-diaza-*s*-indacene-3-propionyl)-1,2-dihexadecanoyl-*sn*-glycero-3-phosphoethanolamine, triethylammonium salt (BODIPY FL DHPE, Figure 2.3), 2-(4,4-difluoro-5,7-dimethyl-4-bora-3a,4a-diaza-*s*-indacene-3-dodecanoyl)-1-hexadecanoyl-*sn*-glycero-3-phosphocholine (β-BODIPY FL C_{12}-HPC, Figure 2.3) and 1,1'-dioctadecyl-3,3,3',3'-tetramethylindotricarbocyanine iodide ($DiIC_{18}$ (7), DiR, Figure 2.3) that were purchased from Invitrogen (Eugene, OR, USA) as lyophilized powders or dissolved in chloroform (Merck, KGaA). The fluorescently labeled Bodipy derivatives from Avanti are similar by a structure to the Bodipy lipids available from Invitrogen (Figure 2.3). One difference is in the coupling of Bodipy to the head or chain region of the lipids. Another functional difference is that Bodipy lipids from Avanti do not form dimers and therefore do not have dimer signal detected via fluorescence spectroscopy, probably because of the symmetrical coupling to the lipid that is absent in the case of the lipids from Invitrogen. Lipids stock solutions were stored in glass vials at -20 °C not longer than six months. Fluorescently labeled lipids stock solutions were stored in dark glass vials at -20 °C maximum three months.

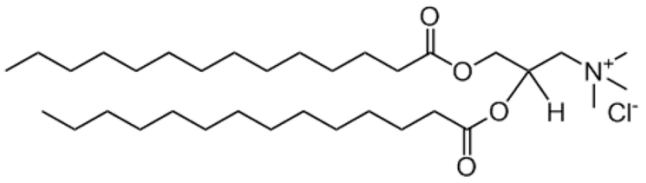

1,2-dimyristoyl-3-trimethylammonium-propane (chloride salt)
(DMTAP)
Mw = 590 g/mol

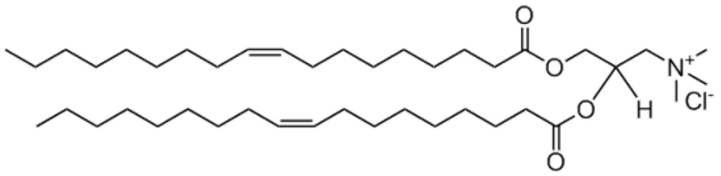

1,2-dioleoyl-3-trimethylammonium-propane (chloride salt)
(DOTAP)
Mw = 698 g/mol

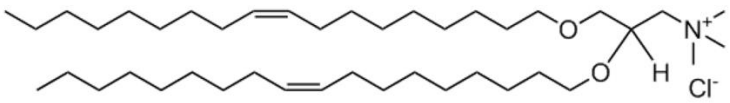

1,2-di-O-octadecenyl-3-trimethylammonium propane (chloride salt)
(DOTMA)
Mw = 671 g/mol

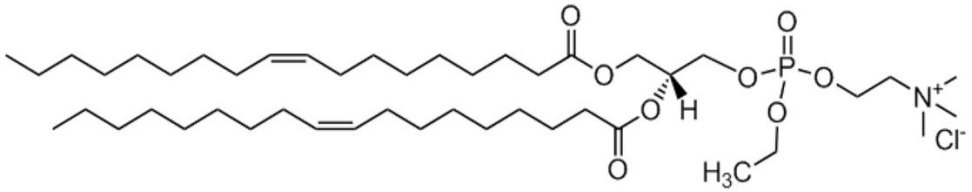

1,2-dioleoyl-sn-glycero-3-ethylphosphocholine (chloride salt)
(DOEPC)
Mw = 850 g/mol

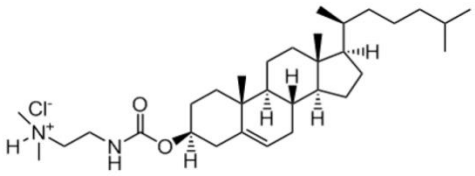

3ß-[N-(N',N'-dimethylaminoethane)-carbamoyl]cholesterol hydrochloride
(DC Choesterol)
Mw = 537 g/mol

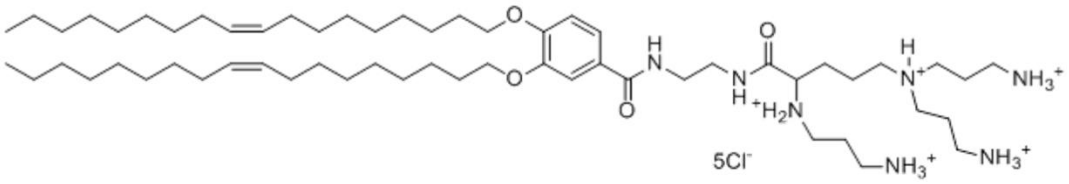

N1-[2-((1S)-1-[(3-aminopropyl)amino]-4-[di(3-amino-propyl)amino] butylcarboxamido)ethyl]-3,4-di[oleyloxy]-benzamide
(MVL5)
Mw = 1165 g/mol

Figure 2.1. Overview of positively charged lipids: their IUPAC names, corresponding abbreviations, structural formulas, and molecular weights (Mw).

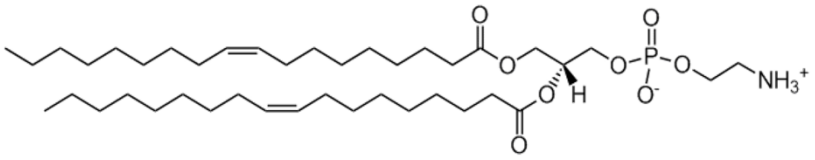

1,2-dioleoyl-sn-glycero-3-phosphoethanolamine
(DOPE)
Mw = 744 g/mol

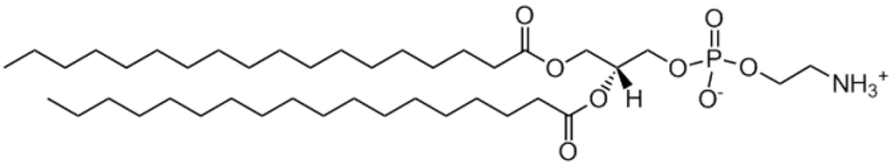

1,2-distearoyl-sn-glycero-3-phosphoethanolamine
(DSPE)
Mw = 748 g/mol

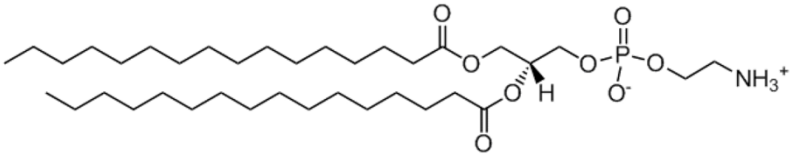

1,2-dipalmitoyl-sn-glycero-3-phosphoethanolamine
(DPPE)
Mw = 692 g/mol

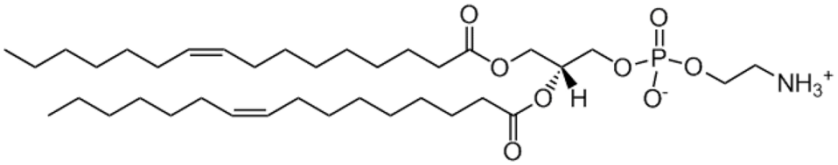

1,2-dipalmitoleoyl-sn-glycero-3-phosphoethanolamine
(DPaPE)
Mw = 688 g/mol

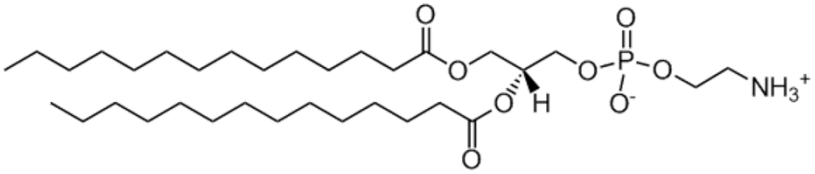

1,2-dimyristoyl-sn-glycero-3-phosphoethanolamine
(DMPE)
Mw = 636 g/mol

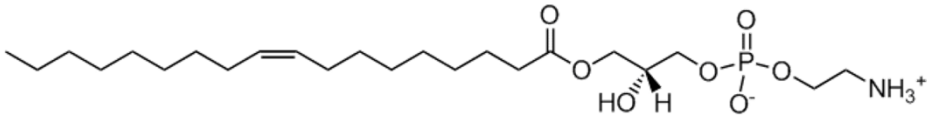

1-oleoyl-2-hydroxy-sn-glycero-3-phosphoethanolamine
(Lyso PE)
Mw = 480 g/mol

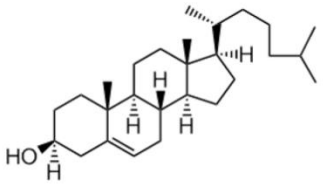

Cholesterol
(Cholesterol)
Mw = 387 g/mol

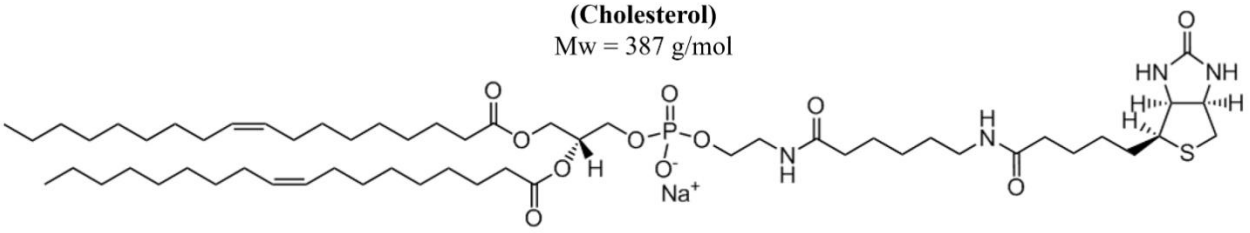

1,2-dioleoyl-sn-glycero-3-phosphoethanolamine-N-(cap biotinyl) (sodium salt)
(Biotinylcap-DOPE)
Mw = 1105 g/mol

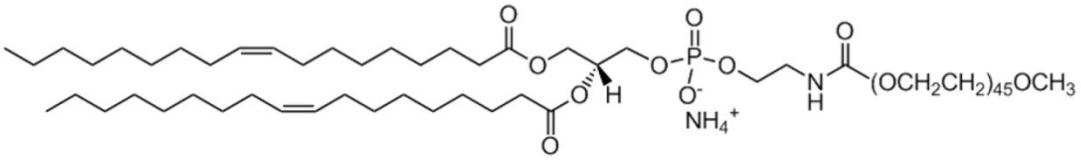

1,2-dioleoyl-sn-glycero-3-phosphoethanolamine-N-[methoxy(polyethylene glycol)-2000]
(ammonium salt) **(PEG2000-DOPE)**
Mw = 2801 g/mol

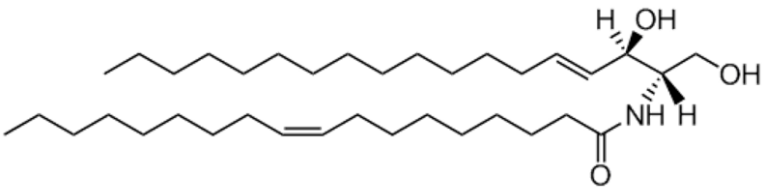

N-oleoyl-D-erythro-sphingosine
(CER)
Mw = 564 g/mol

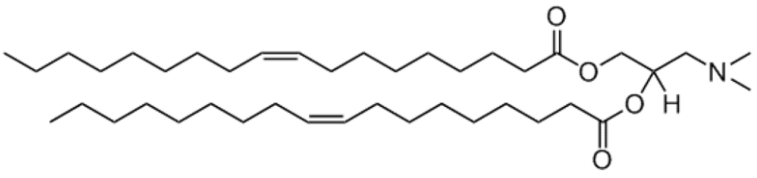

1,2-dioleoyl-3-dimethylammonium-propane
(DODAP)
Mw = 648 g/mol

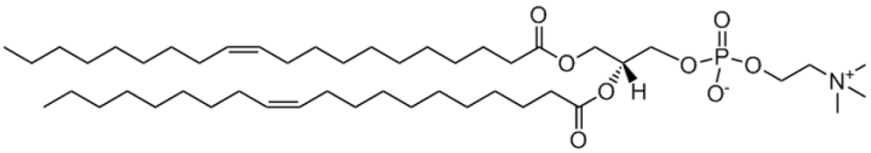

1,2-dioleoyl-sn-glycero-3-phosphocholine
(DOPC)
Mw = 786 g/mol

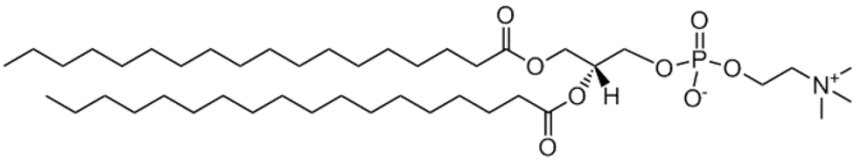

1,2-distearoyl-sn-glycero-3-phosphocholine
(DSPC)
Mw = 790 g/mol

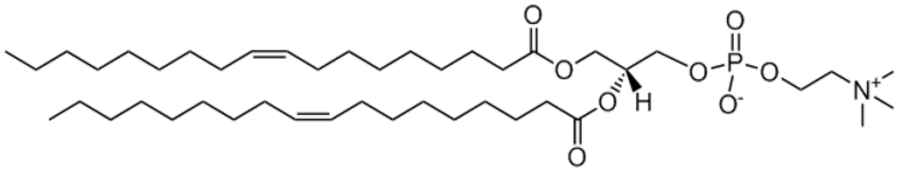

1,2-dieicosenoyl-sn-glycero-3-phosphocholine
(DEPC)
Mw = 842 g/mol

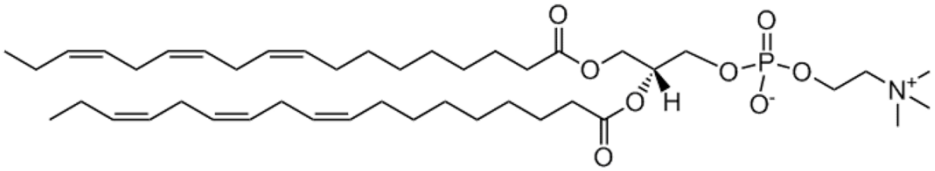

1,2-dilinolenoyl-sn-glycero-3-phosphocholine
(DLiPC)
Mw = 778 g/mol

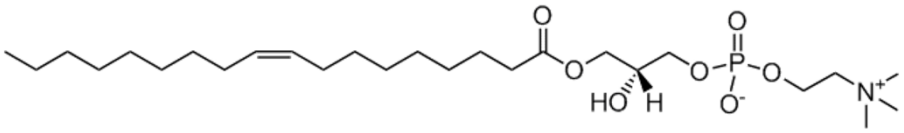

1-oleoyl-2-hydroxy-sn-glycero-3-phosphocholine
(Lyso PC)
Mw = 522 g/mol

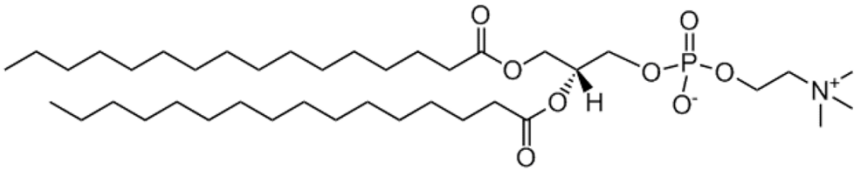

1,2-dipalmitoyl-sn-glycero-3-phosphocholine
(DPPC)
Mw = 734 g/mol

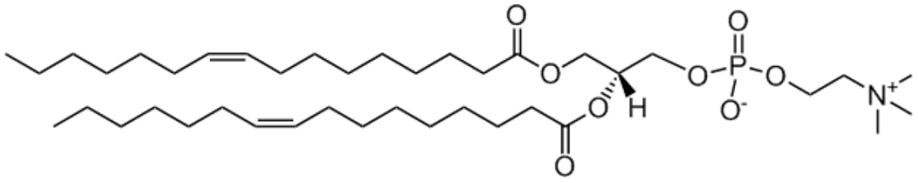

1,2-dipalmitoleoyl-sn-glycero-3-phosphocholine
(DPaPC)
Mw = 730 g/mol

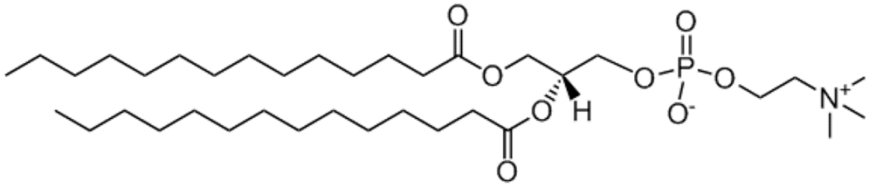

1,2-dimyristoyl-sn-glycero-3-phosphocholine
(DMPC)
Mw = 678 g/mol

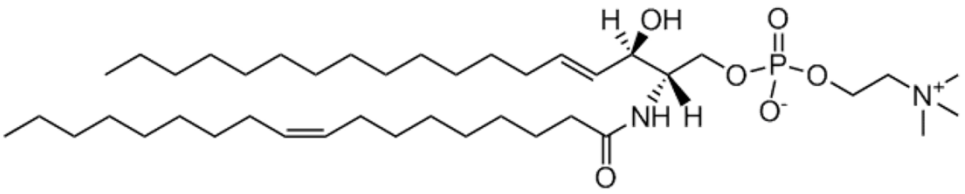

N-oleoyl-D-erythro-sphingosylphosphorylcholine
(SM)
Mw = 729 g/mol

Figure 2.2. Overview of neutral lipids: their IUPAC names, corresponding abbreviations, structural formulas, and molecular weights (Mw).

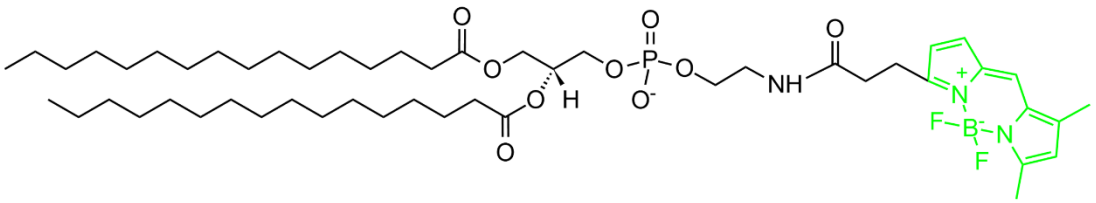

(*N*-(4,4-Difluoro-5,7-Dimethyl-4-Bora-3a,4a-Diaza-*s*-Indacene-3-Propionyl)-1,2-Dihexadecanoyl-*sn*-Glycero-3-Phosphoethanolamine, Triethylammonium Salt)
(BODIPY FL-DHPE)
Mw = 1067 g/mol

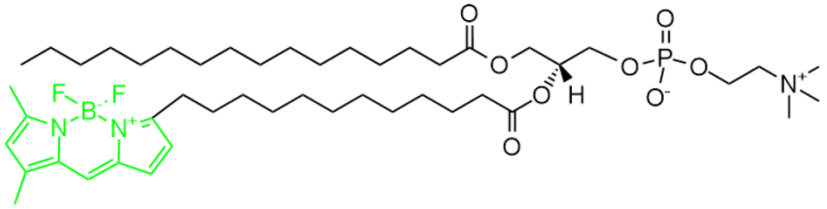

(2-(4,4-Difluoro-5,7-Dimethyl-4-Bora-3a,4a-Diaza-*s*-Indacene-3-Dodecanoyl)-1-Hexadecanoyl-*sn*-Glycero-3-Phosphocholine)
(βBodipy-C12HPC)
Mw = 896 g/mol

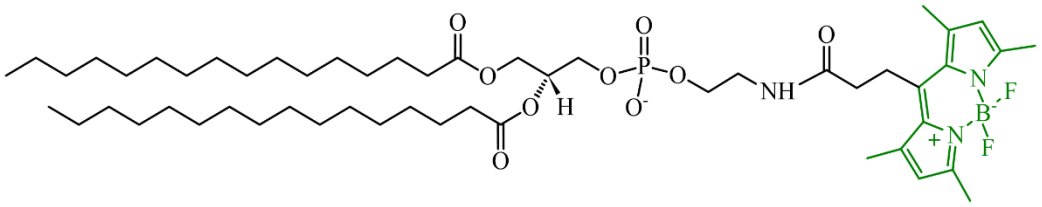

1,2-dioleoyl-sn-glycero-3-phosphoethanolamine-N
[(dipyrrometheneboron difluoride) butanoyl]
(TFPE-head)
Mw = 1077 g/mol

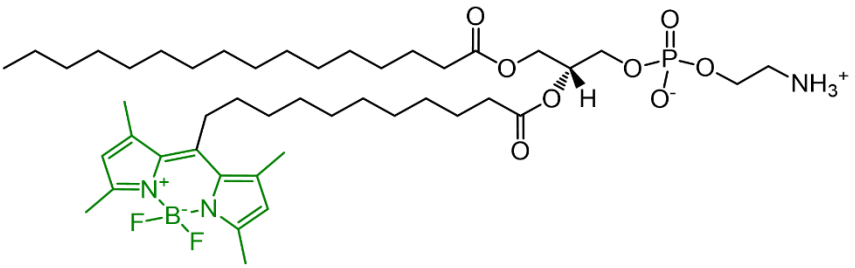

1-palmitoyl-2-(dipyrrometheneboron difluoride)undecanoyl-sn-glycero-3-phosphoethanolamine
(TFPE-chain)
Mw = 868 g/mol

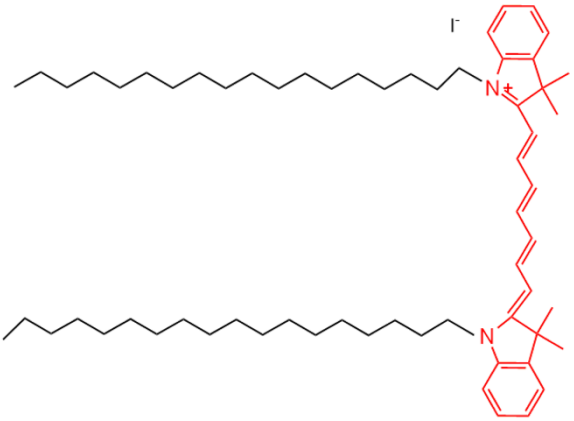

1,1'-Dioctadecyl-3,3,3',3'-
Tetramethylindotricarbocyanine Iodide,
DiIC$_{18}$ (7), DiR
Mw = 1013 g/mol

Figure 2.3. Overview of fluorescently labeled lipids: their IUPAC names, corresponding abbreviations, structural formulas, and molecular weights (Mw).

2.1.2. Buffers

Phosphate buffered saline (PBS) was prepared from 137 mM NaCl; 2,7 mM KCl; 1,47 mM KH_2PO_4; 8,1 mM Na_2HPO_4 (all from Sigma-Aldrich, Taufkirchen, Germany) in ultrapure water, provided by a water purification system (Millipore, San Francisco, CA, USA). Phosphate buffer (PB) was made by the same recipe as PBS without NaCl (2,7 mM KCl; 1,47 mM KH_2PO_4; 8,1 mM Na_2HPO_4, Sigma-Aldrich, Taufkirchen, Germany). Glucose solutions were done by dissolving glucose (Sigma-Aldrich, Taufkirchen, Germany) in ultrapure water to make 30 mM or 290 mM solution. For the experiments with the radionuclide ^{131}I and ^{127}I, 160 mM sucrose (Sigma-Aldrich, Taufkirchen, Germany) solution was made by the same procedure as glucose solutions. As standard liposomal buffer, 20 mM N-2-hydroxyethylpiperazine-N-2 ethane sulfonic acid (HEPES, VWR, Darmstadt, Germany) was used. HEPES and PBS in D_2O were prepared according to the protocol described above (Sigma-Aldrich, Taufkirchen, Germany).

The pH of all buffers was adjusted to 7.4. Buffer osmolalities were determined using a freezing point osmometer (Osmomat 030, Gonotec GmbH, Berlin, Germany) prior to each experiment and set to desired osmolality (HEPES-30mOsm/kg, PBS-290 mOsm/kg, PB-30 mOsm/kg, Glucose 290 mOsm/kg or 30 mOsm/kg and sucrose 160 mOsm/kg). Buffers were

either aliquoted in small amounts and kept at -20 °C (HEPES, sucrose) or kept at 4 °C and renewed every month.

2.1.3. Iodine isotopes

The radionuclide, ^{131}I, 5 mCi, 0.1M NaOH (pH 12-14) was purchased from PerkinElmer (Hamburg, Germany). Sodium iodide, NaI, (ACS reagent, ≥ 99.5%, ^{127}I) was purchased from Sigma Aldrich (Taufkirchen, Germany).

2.1.4. Glass substrates

For treatment with the various liposome formulations, cells were plated in handcrafted glass-bottom dishes one day before the experiments. Thin-corrected high-precision round cover glasses (80 µm ± 20 µm, d = 25 mm, VWR, Darmstadt, Germany) were glued to the underside of pre-drilled (∅: 18 mm) plastic culture dishes (∅: 3 cm, Greiner Bio-One). As adhesive, cross-linked polydimethylsiloxane (PDMS) prepared from a vinyl-terminated PDMS polymer blend and a methylhydrosiloxane-dimethylsiloxane copolymer with a catalyst at a mixing ratio of 10:1 w/w (Sylgard 184, Dow Corning Co., MI) was used. For complete cross-linking, the freshly glued glass-bottom dishes were stored at 60 °C for at least two hours. Before use, the glass bottom dishes were sterilized with UV light.

2.1.5. Additional material used for the work

a) The material used for the preparation of liposomes

2-(4-(2-Hydroxyethyl)- 1-Piperazinyl) Ethansulfonsäure (HEPES)	Sigma-Aldrich, Taufkirchen, Germany
Balls stainless steel unhardened 1.000 mm N0 - Material 1.4301 - Quality G100	Kugel-Winnie, Bamberg, Germany
Chloroform	Merck Millipore, Darmstadt, Germany
Deuterium oxide, D_2O	Sigma-Aldrich, Taufkirchen, Germany
Ethanol, p.a.	Merck, Darmstadt, Germany
Glass micropipettes, disposable, different sizes	Merck, Darmstadt, Germany
Glass vials (different sizes)	VWR, Darmstadt, Germany
Parafilm	Pechiney Plastic Packaging, Chicago, IL, USA
Pasteur pipettes	VWR, Darmstadt, Germany
Pipette tips (different sizes)	Starlab, Hamburg, Germany
Radionuclide ^{131}I (in 0.1 M NaOH)	PerkinElmer, Hamburg, Germany
Reaction tubes (1.5 ml and 2 ml)	Eppendorf, Wesseling-Berzdorf, Germany
Reaction tubes (15 ml and 50 ml)	Greiner Bio-one, Frickenhausen, Germany
Sodium iodide, NaI (^{127}I)	Sigma-Aldrich, Taufkirchen, Germany

b) The material used for cell culture and treatment of cells

24-well plate	Greiner Bio-one, Frickenhausen, Germany
96-well plate	Greiner Bio-one, Frickenhausen, Germany
Cell culture dishes, 3 cm, 18 mm opening	Greiner Bio-one, Frickenhausen, Germany
Cell culture flasks (25 cm^2, 75cm^2)	BD Bioscience, Fernwald, Germany
Cover glass 170±5 µm	Marienfeld, Lauda-Koenigshofen, Germany
DMEM/F12	Thermo Fisher Scientific, Darmstadt, Germany
DMEM/F12 Glutamax	Thermo Fisher Scientific, Darmstadt, Germany
DRAQ5 Fluorescent Probe Solution	Thermo Fisher Scientific, Darmstadt, Germany
Fetal Bovine Serum, FBS	Sigma-Aldrich, Taufkirchen, Germany
Fibronectin from human Placenta	BD Bioscience, Fernwald, Germany
FIX&PERM Solution A	Thermo Fisher Scientific, Darmstadt, Germany
Hoechst 33342 Fluorescent Probe Solution	Thermo Fisher Scientific, Darmstadt, Germany
NucBlue Fluorescent Probe Solution	Thermo Fisher Scientific, Darmstadt, Germany
Penicillin/Streptomycin (10.000 U/ml)	Sigma-Aldrich, Taufkirchen, Germany
Pipette tips (different sizes)	Starlab, Hamburg, Germany
Reaction tubes (1.5 ml and 2 ml)	Eppendorf, Wesseling-Berzdorf, Germany
Reaction tubes (15 ml and 50 ml)	Greiner Bio-one, Frickenhausen, Germany
Sylgard-184 Silicone Elastomer Kit	Dow Corning, Wiesbaden, Germany
Trypsin/EDTA 0,05%	Thermo Fisher Scientific, Darmstadt, Germany

2.2. Preparation of liposomes

In all cases of liposomes preparation, the following steps were kept constant. First, lipids were mixed in chloroform (Merck Millipore, Darmstadt, Germany) at the desired ratio. Second, the chloroform was evaporated under vacuum for at least 30 min and a maximum of 24 h. Third, dry lipid film was hydrated by desired buffer or ultrapure water at different total lipid concentrations, vortexed (when multilamellar liposomes were used) and most of the time sonicated in an ultrasonic bath (Sonocool, Bandelin electronic GmbH, Berlin, Germany) for 20 min at 5 °C, to form unilamellar vesicles. Prepared liposomes were not kept longer than two days at 4 °C, or longer than a month at -20 °C.

2.2.1. Liposomes used in Dechipering the Functional Composition of Fusogenic Liposomes [92]

Liposomes were prepared as described above. As a buffer, 20 mM HEPES was used.

a) Variation of DOTAP concentration in liposomes

To prove the importance of the cationic lipid in fusogenic liposomes, they were prepared by varying the DOTAP concentration, as the most commonly used positively charged lipid, and keeping the concentrations of neutral lipid, DOPE, and BODIPY FL-DHPE constant (for IUPAC names, structures and molecular weight see chapters 2.1.2.-2.1.4). The desired molecular ratios of lipids in the liposomes used in chapter 3 are shown in table 2.1.

a) Variation of cationic lipid in liposomes

Cationic lipids of different molecular shapes were used for the preparation of fusogenic liposomes to test the influence of molecular shape on fusion efficiency. Here, the neutral lipid (DOPE) and the dye (BODIPY-head) were kept constant. The compositions of these liposomes used in chapter 3 and the corresponding ratios are given in table 2.1.

b) Variation of dye and its concentration in liposomes

The second component of fusogenic liposomes, according to Csiszar et al.[9] is an aromatic component (fluorescent dye). In chapter 3, the systematic study of the importance of this component has been done by varying the dye and its concentration. Three types of dyes were chosen: BODIPY FL-DHPE, βBodipy-C12HPC, and DiR (IUPAC names, structures, and

molecular weights are shown in chapters 2.1.2.-2.1.4). The concentration of positively charged lipid and neutral lipid was kept constant while the concentration of the dye was varied (1/1/0.01-0.1 mol/mol). Two kinds of liposomes were prepared: liposomes containing DOPE/DOTAP/dye (in chapter 3 called fusogenic liposomes-FLs) and liposomes consisting of DOPC/DOTAP/dye (in chapter 3 called endocytic liposomes-ELs).

Additionally, non-aromatic components were tested in order to prove the importance of the presence of a π electron system in the composition of liposomes. Here the liposomes were prepared with a non-fusogenic concentration of DiR and with a presumed concentration of non-aromatic components for fusion induction. Liposomal compositions are given in table 2.1.

c) Variation of neutral lipid

To explore the influence of the neutral lipid on the liposomal fusion efficiency, a systematic analysis was carried out varying the neutral lipid components regarding its head group, chain length, and chain saturation. Hence, DOTAP and BODIPY FL-DHPE were kept at constant concentrations. Liposomal compositions are given in table 2.1.

2.2.2. Composition of liposomes used in Influence of Environmental Conditions on the Fusion of Cationic Liposomes with Living Mammalian Cells [93]

In the experiments where the fusion conditions were tested, several neutral lipids with different head groups, chain lengths, and saturation were applied. As cationic lipid, only DOTAP has been used. As an aromatic compound, either TFPE-head, TFPE-chain, or DiR (for IUPAC names, structures, and molecular weight see chapters 2.1.2.-2.1.4) were systematically applied. Lipids were mixed in chloroform at proven molar ratio (1/1/0.1 mol/mol) for fusion induction according to previous studies [9] at 2 mg/ml total lipid concentration. After evaporation of the solvent under vacuum for 30 min, liposomes were hydrated in ultrapure water to avoid the presence of ions and sonicated for 20 min to achieve the unilamellar formation of liposomes. Membrane fusion with CHO cells was analyzed in four different buffers: PBS, PB, Glucose 30 mOsm/kg, and Glucose 290 mOsm/kg (for a detailed description of buffers see section 2.1.5 and for the treatment of the cells see section 2.3.2). For pH dependency test, the pH of PBS was adjusted by adding 1M HCl or 1M NaOH. Liposomal compositions are given in table 2.2.

2.2.3. Preparation of liposomes used in Understanding of Phase Behavior of Fusogenic Liposomes and its Correlation with the Fusion Ability

In brief, lipids were mixed in chloroform at a distinct molar ratio. Then chloroform was evaporated under vacuum for 30 min, and dry lipid film was hydrated in 20 mM HEPES buffer in D_2O or ultrapure water. Afterward, liposomes were vortexed vigorously for 15 min until the lipid film was hydrated, and multilamellar vesicles were formed.

a) **Liposomes used for DSC:** DOPE/DOTAP/TFPE-head (FLs) and DOPC/DOTAP/TFPE-head (ELs) were mixed at a molar ratio of 1/1/0.1 at 20 mg/ml total lipid concentration in 20 mM HEPES buffer dissolved in D_2O. As a control sample, DPPC or DMPC liposomes were used at the same concentration and in the same buffer. Samples were stored at -20 °C not longer than one week and rethawed and vortexed again before the measurement.

b) **Freeze-fracture/STEM experiments:** Liposomes consisting of either DOPE/DOTAP/DiR (FLs) or DOPC/DOTAP/DiR (ELs) were prepared at a molar ratio of 1/1/0.1 at 10 mg/ml total lipid concentration in 20 mM HEPES buffer. They were stored at -20 °C not longer than a month. Liposomes were vortexed and incubated at the desired temperature before the experiments.

c) **Liposomes for Cryo-TEM imaging:** Liposomes consisting of either DOPE/DOTAP/TFPE-head (FLs) and DOPC/DOTAP/TFPE-head (ELs) were mixed at a molar ratio of 1/1/0.1 at a total lipid concentration of 5 mg/ml in 20 mM HEPES buffer. Before the experiments, liposomes were vigorously vortexed.

d) **Liposomes utilized for SANS experiments**: Fusogenic, as well as endocytic liposomes with different compositions, were prepared to analyze the liposomal thermotropic behavior. The liposomal compositions are summarized in table 2.3. The total lipid concentration was set to 20 mg/ml. After evaporation of chloroform, the lipid film was resuspended in 20 mM HEPES buffer dissolved in D_2O (99 atom % D, Sigma-Aldrich, Taufkirchen, Germany) and vortexed vigorously without additional sonification. Samples were stored at -20°C until usage. One hour before measurements, samples were thawed and vortexed vigorously before transferred into quartz cuvettes (110-QS, quartz glass, Suprasil, 1 mm path length, Hellma, Müllheim, Germany) for SANS measurements.

e) Falling sphere viscosimetry experiments: The same liposomal compositions used for SANS measurements (molar ratios and concentrations), were used for the falling ball viscosimetry experiments in order to find out the rheological behavior of those liposomal mixtures.

f) Liposomes prepared for solid-state ^{31}P NMR: Liposomes for solid-state NMR were prepared using typically 10 mg of other lipids and 0.5 mg of the fluorescent lipid. Fluorescent lipids were purchased as chloroform solutions, and the concentration was tested before use. Other lipids were purchased as a powder, weighed, and dissolved in chloroform. Lipid solutions in chloroform were mixed in a glass vial and dried under vacuum at least 3 h. 150 µl of 10 mM HEPES buffer was added, and the vial was vortexed vigorously, but not sonicated. Samples were placed at -20°C in a freezer and taken out after at least 1 h, thawed and vortexed vigorously again. Samples were not heated above room temperature. This freeze-thaw-vortex cycle was repeated five times. Finally, samples were stored at -20°C. Shortly before NMR measurements, the samples were taken out of the freezer and vortexed for the final time. Afterward, the samples were transferred to a plastic container and placed in the NMR sample holder. Liposomal compositions used for solid-state NMR experiments are shown in table 2.4.

2.2.4. Preparation of liposomes used in Delivery of the Radionuclide ^{131}I to Cancer Cells using Fusogenic Liposomes as Nanocarriers

a) Preparation of liposomes with radionuclide ^{131}I

The experiments with radionuclide ^{131}I have been performed in the controlled area of the Institue of Neuroscience and Medicine-5: Nuclear Chemistry (INM5, Research Center Juelich, Germany). All the necessary measures and security measurements were taken before and after the performance of the experiments.

Liposomes were prepared by mixing DOPE, DOTAP, and DiR in chloroform (EMSURE grade, VWR, Darmstadt, Germany) at the molar ratio of 1/1.2/0.3 mol/mol and by mixing DOPC and DiR at the molar ratio 2/0.005 mol/mol. The total lipid concentration in both mixtures was 4 mg/ml. Chloroform was evaporated under vacuum for 30 min. The dry lipid film was hydrated in 20 µl of ^{131}I solution diluted in a sugar solution (160 mOsm, 0.1µCi/µl, 940 pM/µl) and incubated for 20 min with constant vortexing until all the lipid film was

hydrated. Then, 250 µl of sugar solution (160 mOsm) was added, and the liposomes with intercalated ^{131}I were vortexed for an additional 10 min. The liposomal suspensions with intercalated ^{131}I , into two Eppendorf tubes (Sigma Aldrich, Taufkirchen, Germany) and 1 ml of cold PBS (Thermo Fisher Scientific, Waltham, USA) was added. The prepared solutions were centrifuged at 0 °C for 30 min in an Eppendorf Centrifuge 5417R (Eppendorf, Wesseling-Berzdorf, Germany) at 25.000 × g (Figure 2.4). As control samples, the ^{131}I solution and one-quarter of the ^{131}I solution in 1 ml of sugar/PBS buffer (1/4 ratio) were prepared. After separation, sample activities were determined using a γ-counter (Turku, Finland) for 30 seconds.

b) Preparation of liposomes with ^{127}I

The preparation of ^{127}I isotope containing liposomes was comparable to that described above with small modification; the dry lipid film was hydrated in a ^{127}I solution diluted in a sugar solution (160 mOsm) to a final concentration of 940 pM/µl.

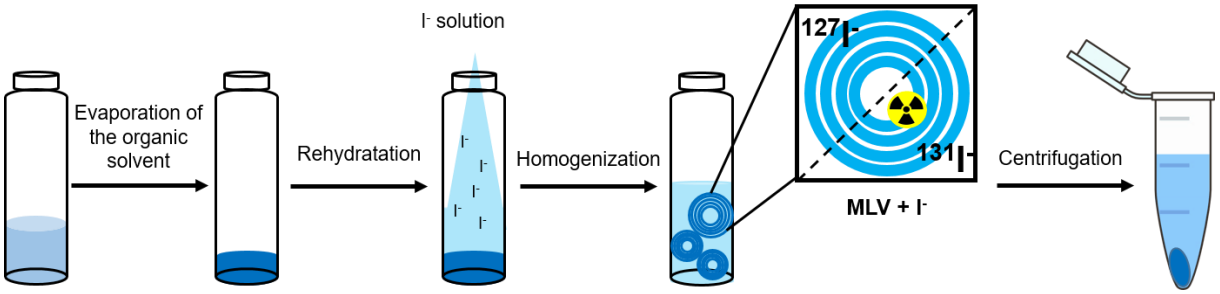

Figure 2.4. Preparation of iodine loaded liposomes. After evaporation of the organic solvent, the dry lipid mixture was rehydrated in iodine-containing buffer whereby multilamellar liposomes formed spontaneously containing iodine isotopes between the lamellas. Iodine loading efficiency was determined on liposomes separated from the free solution by centrifugation.

Table 2.1. Liposomal compositions used in Chapter 3.

Liposomal components	**Molar ratios**
DOPE/DOTAP/BODIPY FL-DHPE	1/0-1/0.1
DOTAP/ BODIPY FL-DHPE	2/0.1
DOPE/DOTAP/ BODIPY FL-DHPE	1/1/0.1
DOPE/DOTMA/ BODIPY FL-DHPE	1/1/0.1
DOPE/DMTAP/ BODIPY FL-DHPE	1/1/0.1
DOPE/DOEPC/ BODIPY FL-DHPE	1/1/0.1
DOPE/DC-Cholesterol/ BODIPY FL-DHPE	1/1/0.1
DOPE/MVL5/ BODIPY FL-DHPE	1/1/0.01-0.1
DOPE/DOTAP/ BODIPY FL-DHPE	1/1/0.01-0.1
DOPC/DOTAP/ BODIPY FL-DHPE	1/1/0.01-0.1
DOPE/DOTAP/ βBodipy-C12HPC	1/1/0.01-0.1
DOPC/DOTAP/ βBodipy-C12HPC	1/1/0.01-0.1
DOPE/DOTAP/DiR	1/1/0.01-0.1
DOPC/DOTAP/DiR	1/1/0.01-0.1
DOPE/DOTAP/ BODIPY FL-DHPE	1/1/0.1
DMPE/DOTAP/ BODIPY FL-DHPE	1/1/0.1
DPPE/DOTAP/ BODIPY FL-DHPE	1/1/0.1
DPaPE/DOTAP/ BODIPY FL-DHPE	1/1/0.1
DSPE/DOTAP/ BODIPY FL-DHPE	1/1/0.1
LysoPE/DOTAP/ BODIPY FL-DHPE	1/1/0.1
DOPC/DOTAP/ BODIPY FL-DHPE	1/1/0.1
DSPC/DOTAP/ BODIPY FL-DHPE	1/1/0.1
DPPC/DOTAP/ BODIPY FL-DHPE	1/1/0.1
DPaPC/DOTAP/ BODIPY FL-DHPE	1/1/0.1
DMPC/DOTAP/ BODIPY FL-DHPE	1/1/0.1
DEPC/DOTAP/ BODIPY FL-DHPE	1/1/0.1
DLiPC/DOTAP/ BODIPY FL-DHPE	1/1/0.1

Table 2.2. Liposomal compositions used in Chapter 4.

Liposomal components	**Molar ratios**
DPPE/DOTAP/ TFPE-head	1/1/0.1
DPPC/DOTAP/ TFPE-head	1/1/0.1
DPaPE/DOTAP/ TFPE-head	1/1/0.1
DPaPc/DOTAP/ TFPE-head	1/1/0.1
DSPE/DOTAP/ TFPE-head	1/1/0.1
DSPC/DOTAP/ TFPE-head	1/1/0.1
DOPE/DOTAP/ TFPE-head	1/1/0.1
DOPC/DOTAP/ TFPE-head	1/1/0.1
DPPE/DOTAP/ TFPE-chain	1/1/0.1
DPPC/DOTAP/ TFPE-chain	1/1/0.1
DPaPE/DOTAP/ TFPE-chain	1/1/0.1
DPaPc/DOTAP/ TFPE-chain	1/1/0.1
DSPE/DOTAP/ TFPE-chain	1/1/0.1
DSPC/DOTAP/ TFPE-chain	1/1/0.1
DOPE/DOTAP/ TFPE-chain	1/1/0.1
DOPC/DOTAP/ TFPE-chain	1/1/0.1
DPPE/DOTAP/ DiR	1/1/0.1
DPPC/DOTAP/ DiR	1/1/0.1
DPaPE/DOTAP/ DiR	1/1/0.1
DPaPc/DOTAP/ DiR	1/1/0.1
DSPE/DOTAP/ DiR	1/1/0.1
DSPC/DOTAP/ DiR	1/1/0.1
DOPE/DOTAP/ DiR	1/1/0.1
DOPC/DOTAP/ DiR	1/1/0.1

Table 2.3. Liposomal compositions used for SANS experiments.

Liposomal components	**Molar ratios**
DOPE/DOTAP/ BODIPY FL DHPE	1/1/0.1
DOPC/DOTAP/ BODIPY FL DHPE	1/1/0.1
DOPE/DOTAP/ TFPE-head	1/1/0.1
DOPC/DOTAP/ TFPE-head	1/1/0.1
DOPE/DOTAP/ TFPE-chain	1/1/0.1
DOPC/DOTAP/ TFPE-chain	1/1/0.1
DOPE/DOTAP/ DiR	1/1/0.1
DOPC/DOTAP/ DiR	1/1/0.1

Table 2.4. Liposomal compositions used for ^{31}P NMR experiments.

Liposomal components	**Molar ratios**
DOPC	
DOPE	
DOPC/DOTAP	1/1
DOPE/DOTAP	1/1
DOPE/ Biotinylcap-DOPE	2/0.1
DOPC/DOTAP/ Biotinylcap-DOPE	1/1/0.1
DOPE/DOTAP/ Biotinylcap-DOPE	1/1/0.1
DOPE/DiR	2/0.1
DOPC/DOTAP/DiR	1/1/0.1
DOPC/DOTAP/DiR	1/1/1
DOPE/DOTAP/DiR	1/1/0.1
DOPE/TFPE-head	2/0.1
DOPC/TFPE-head	2/0.1
DOPE/TFPE-chain	2/0.1
DOPC/TFPE-chain	2/0.1
DOPE/DOTAP/TFPE-head	1/1/0.1
DOPC/DOTAP/TFPE-head	1/1/0.1
DOPE/DOTAP/TFPE-chain	1/1/0.1
DOPC/DOTAP/TFPE-chain	1/1/0.1
DOPE/DOPC	3/1

2.3. Cell culture

Chinese hamster ovary cells, Subtype K1 (CHOs), were ordered from American Type Culture Collection (ATCC, Manassas, VA, USA) and used as a standard for experiments with mammalian cells. Additionally, an epithelial human breast cancer cell line, MDA-MB-231, purchased from Sigma-Aldrich (Taufkirchen, Germany) was used for the experiments in Delivery of the radionuclide ^{131}I to cancer cells using fusogenic liposomes as nanocarriers. Both cell lines were maintained in DMEM-F12 (Sigma-Aldrich, Taufkirchen, Germany) supplemented with 10% fetal bovine serum (FBS) (Thermo Fisher Scientific, Waltham, MA), 10.000 units penicillin and 10 mg/mL streptomycin (both Sigma-Aldrich) in 25 cm^2 or 75 cm^2 cell culture flasks. During culture, cells were kept at 37°C and 5% CO_2 in a saturated humid atmosphere. Cell density never exceeded 80% confluence. Prior to the experiments, cells were seeded on glass substrates and cultivated 24h at 37°C and 5% CO_2 in a saturated humid atmosphere. Approximately 50.000 cells per dish were seeded and let to divide to 100 000 for the experiment. Blood cells were treated in pureblood obtained from the healthy volunteer. For each liposomal sample, around 20 µl of full blood was supplied.

2.3.1. Cell culture and liposomal treatment performed in Deciphering the Functional Composition of Fusogenic Liposomes [92] (Chapter 3)

For the experiments performed in chapter 3, Chinese Hamster Ovary K1 (CHOs) cells were used. Before the treatment, cells were cultivated as described above. For microscopy and flow cytometry analyses, 30.000 cells were seeded on fibronectin (BD Biosciences, San Jose, CA, USA) coated (10 µg/mL, 30 min) glass surfaces one day before the treatment.

Prior to experiments, 10 µL of the liposome stock solutions (described in chapter 2.2.1. and summarized in Table 2.1) were diluted 1/50 with phosphate-buffered saline (PBS) (Sigma-Aldrich). Cells cultivated on a Petri dish (Ø = 3.5 cm) were incubated in liposome solution (pH 7.4) for 5 min at 37 °C. Subsequently, liposome solutions were replaced by fresh medium, and the internalized cellular fluorescence was analyzed by confocal fluorescence microscopy. Afterward, cells were trypsinized, collected, and analyzed by flow cytometry [92].

2.3.2. Cell culture and liposomal treatment performed in Influence of Environmental Conditions on the Fusion of Cationic Liposomes with Living Mammalian Cells [93] (Chapter 4) and Understanding the Phase Behaviour of Fusogenic Liposomes and its Correlation with the Fusion Ability (Chapter 5)

Experiments were performed on Chinese Hamster Ovary K1 cells (CHOs). Before microscopy, glass surfaces (∅ = 3.5 cm Petri dish) were coated with human fibronectin (10 µg/mL, BD Biosciences, San Jose, CA, USA) for 30 min at 37 °C and 50.000 cells were seeded on them and cultivated for 24 h.

Cell nuclei were stained for 15 min at 37 °C with DRAQ5 (red fluorescence, Thermo Fischer Scientific) or Hoechst 33342 (blue fluorescence, Thermo Fischer Scientific) according to the manufacturer's protocols. Furthermore, 10 µL of the liposome stock solutions (described in chapter 2.2.2. and summarized in Table 2.2) were diluted 1/50 with PBS, PB, or glucose solution of defined osmolality (30 mOsm/kg and 290 mOsm/kg, the recipes of buffers are described in chapter 2.1.5) and cells on glass substrates (~ 100 000 of cells) were incubated in these solutions for 5 minutes in the incubator (37 °C and 5% CO_2, saturated humid atmosphere). After the treatment, the dilution of liposomes was exchanged with fresh, pre-warmed cell culture medium.

For temperature-dependent experiments, 10 µL of the liposomal stock solutions (see chapter 2.2.2. and Table 2.2), stored at 4 °C no longer than 24 h, were diluted 1/50 with phosphate buffer saline (PBS, 290 mOsm/kg) at room temperature. First, liposomes and cells were left for 5 min at room temperature. Immediately afterward cells were incubated with liposomal solutions at 4 °C, 20 °C, 30 °C or 37 °C for 5 minutes, whereafter it was exchanged by fresh, pre-warmed cell culture medium and samples were analyzed by laser scanning microscopy [93].

2.3.3. Cell culture and liposomal treatment performed in Delivery of the Radionuclide ^{131}I to Cancer Cells using Fusogenic Liposomes as Nanocarriers (Chapter 6)

Experiments were implemented on an epithelial human breast cancer cell line, MDA-MB-231, purchased from Sigma-Aldrich (Taufkirchen, Germany). Before the treatment, glass surfaces (∅ = 3.5 cm Petri dish) were coated with fibronectin (c = 10 µg/mL) (BD Biosciences, San Jose, CA, USA) for 30 min at 37 °C and 50,000 cells were seeded on them and cultivated for 24 h before the experiments.

For blood cells treatment, 60 µl of fresh blood was collected from a healthy volunteer and diluted by adding 60 µl of PBS. The sample was divided into six Eppendorf tubes and immediately treated for 5 min at 37 °C with pellet and supernatant of centrifuged liposomal solution (see chapter 2.2.4 for preparation of liposomes and the following description of treatment). After treatment, cells were centrifuged at 1.500 rcf, at room temperature, for 5 min.

a) Treatment of cells with radionuclide ^{131}I/liposomes

After separation of liposomes (compositions are described in chapter 2.2.4.) into pellet and supernatant by centrifugation, cells were treated with it for 5 minutes at 37 °C on a warming plate (Bel-Art™ SP Scienceware™ CultureTemp 37°C) under non-sterile conditions. For measurements of ^{131}I activity, MDA-MB-231 cells were trypsinized with a trypsin–EDTA solution (Sigma-Aldrich) for 5 min, and subsequently collected in fresh media into suitable plastic sample holders for activity analysis. Simultaneously, blood cells were centrifuged, and the cell pellets were collected into the sample holders for activity analysis. Samples activities were determined using a Hidex Automatic γ-counter (Turku, Finland) for 5 min.

b) Treatment of cells with a ^{127}I/liposomes and free liposomes

For microscopy imaging of MDA-MB-231 cell, nuclei were stained for 15 min with DAPI (blue fluorescence, Eugene, OR, USA) according to the manufacturers' protocols. The DAPI solution was replaced by fresh media, and cells were relaxing for 15 min at 37 °C before the treatment with the liposomes (see chapter 2.2.4). Both MDA-MB-231 cells and blood were treated with free liposomes and with ^{127}I intercalated into liposomes for 5 min at 37 °C in an incubator with 5% CO_2 and a saturated humid atmosphere. After cellular treatment, liposome solutions were replaced by fresh cell culture medium, and the internalized cellular fluorescence was analyzed by laser scanning microscopy. Subsequently, cells were trypsinized with a trypsin–EDTA solution (Sigma-Aldrich) for 5 min and collected with fresh media into a 96 well plate (Sigma-Aldrich) for flow cytometry analyses. Blood cells were centrifuged, and cell pellets were diluted into 300 µl of PBS, of which 100 µl was dropped on a glass substrate for microscopy imaging, and 200 µl was used for flow cytometry experiment.

2.4. Scattering techniques

The organization of molecules within colloidal systems is of significant importance when the relationships between molecular structure and physical properties are studied. The scattering techniques are based on interactions of incident radiations, for example, light or neutrons and particles. Therefore, the quantitative information on size, shape, and structure of colloidal particles can be obtained using the scattering techniques. Since scattering is a broad field, and many parts of it are out of the scope of this thesis, for more about its fundamentals, please refer to [94-105]. This chapter focuses only on three special techniques, small-angle neutron scattering (SANS), dynamic light scattering (DLS), and electrophoretic light scattering (ELS), used in this thesis.

2.4.1. Small-angle neutron scattering (SANS) – Theory

In this work, SANS was applied for the identification of the liposomal phases and the internal liposomal structures, as this technique is particularly suitable for the investigation of structures within sizes ranging from 0.5 nm to several hundreds of nanometers [95, 97]. To reach this goal, SANS instruments use a typical wavelength of neutrons between 0.5 and 20 Å, and the deflection of collimated radiation (scattering angle) is between 0.1-10° (small-angle scattering) [99]. Depending on the wavelength of the incoming radiation, small-angle scattering corresponds to the magnitude of a scattering wave vector $\vec{Q}$ in the range of 10^{-3} to 0.6 $Å^{-1}$. The scattering vector and the basic principle of scattering [97, 99, 103, 104] are shown in Figure 2.5. The figure shows a scattering process in which radiation is deflected by an object from straight propagation where the incident and scattered waves are plane waves of particular wavelengths λ and λ' (strictly monochromatic) and propagation directions $\vec{k_i}/k_i$ and $\vec{k_s}/k_s$.

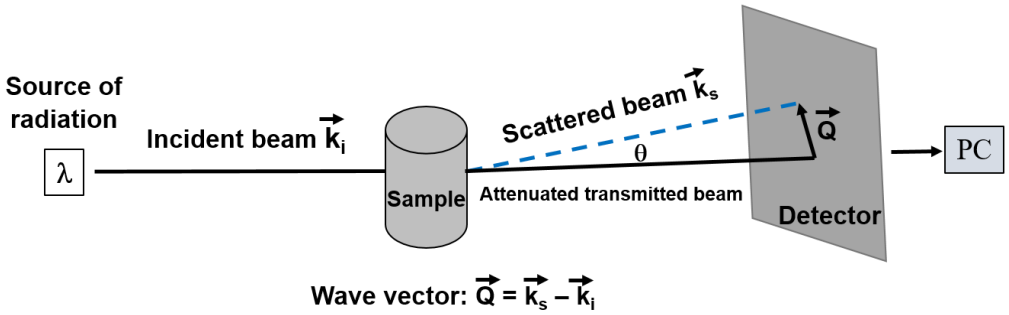

Figure 2.5. The schematic representation of scattering geometry.

The scattering vector $\vec{Q}$ is defined by the relation in equation 2.1 and describes the momentum transfer during the scattering process [95, 97, 104]:

$$|\vec{Q}| = |\vec{k}_s - \vec{k}_i| = Q = \frac{4\pi}{\lambda} \sin\frac{\theta}{2} \tag{2.1}$$

here, $\vec{k}$ ($\vec{k_i} = 2\pi\lambda^{-1}$) is the modulus of the incident wave vector with the wavelength λ and $\vec{k_s}$ is one of the scattered waves. The confined angle is called the scattering angle θ. Equation 1 holds only for static scattering where $\vec{k_i} = \vec{k_s}$. In an elastic small-angle scattering experiment, only the magnitude of the scattering vector is considered, which is related to a length in the reciprocal space. In the following discussion, it will be assigned the unit nm^{-1}. For the summation of the individual scattered waves, the phase shift, δ, between the incident and scattered waves has to be taken into account and is provided by equation 2.2 [95, 97, 104]:

$$\delta \equiv \vec{k}_i \cdot \vec{r}_{ij} - \vec{k}_s \cdot \vec{r}_{ij} = \vec{Q} \cdot \vec{r}_{ij} \tag{2.2}$$

where $\vec{r}_{ij}$ is the vector between the two propagation centers (*i*, *j*), which produces the phase difference. Basically, the $\vec{r}_{ij}$ is the distance between the nucleus *i* and *j*. The total amplitude of the three-dimensional Fourier transform of $\rho(\vec{r})$ of the scattering ensemble is provided by equation 2.3 [95, 97, 104]:

$$A(Q) = \sum_i b_i e^{-i\vec{Q}\vec{r}} = \iiint_V \rho(\vec{r}) e^{-i\vec{Q}\vec{r}} d^3\vec{r} = \int_V \rho(\vec{r}) e^{-i\vec{Q}\vec{r}} d^3 r \tag{2.3}$$

Here, the vector $\vec{r}_{ij}$ results from $\vec{r} = \vec{r}_{ij} = \vec{r}_i - \vec{r}_j$. This relation takes into account that the integration is done over the total scattering volume V. The detector signal correlates with the absolute squared amplitude of the scattered wave.

The scattering of the incident wave takes place at individual scattering centers. The relative position of the individual scatterers is provided by a radial distribution function. The scattering length density (SLD) distribution $\rho(r)$ is the direct link to the structure of the probed sample [95, 97, 104].

$$\rho(r) = \sum_i \rho_i(r) b_i \tag{2.4}$$

where b_i is the scattering length of the different species embodied in the sample and their density distribution ρ_i (r) concerning the number of individual scatterers per volume unit. The

interaction between radiation and matter is quantified by scattering length, and it is characteristic of the different scattering specimens and the radiation [95, 97, 104].

The differential scattering cross-section is an adequate quantitative expression for the ratio between an incident and scattered radiation (equation 2.3). For small-angle scattering by monodisperse particle dispersions, it can be written as [102, 107]:

$$\frac{d\sigma(Q)}{d\Omega} = n\Delta\rho^2 P(Q)S(Q) \tag{2.5}$$

where n is the number density of particles Δρ represents the scattering contrast between the particles and the solvent, P(Q), and S(Q) are the particle form factor and the structure factor, respectively. The particle form factor is defined by the morphology of the individual particles (equation 2.6) and satisfies the condition of $P(0) = V$ with V being the particle volume. The structure factor provides evidence of the interaction between the particles, *c*, (equation 2.7), and the resulting interference of scattering from different particles, *n*, (equation 2.7). The scattering intensity can be described as a product of form and structure factor (equation 2.8).

$$P(Q) = \int \rho_j(r) e^{iQr} dV \tag{2.6}$$

$$S(Q) = \frac{1}{1 - nc(Q)} \tag{2.7}$$

$$I(Q) = P(Q) \cdot S(Q) \tag{2.8}$$

The contribution of the structure factor is most conspicuous at low Q-values. At large Q, only the inner structure of the particle is visible, but not its arrangement in space [99].

2.4.2. Small-angle neutron scattering (SANS) - Measurements

SANS experiments were carried out at the small-angle scattering set-up KWS-2, operated by JCNS at Forschungsneutronenquelle Heinz Maier-Leibnitz (MLZ), FRM II (Münich, Germany) [107]. The help for the performed experiments was kindly provided by **Dr. Sebastian Jaksch** and **Dr. Marie-Sousai Appavou**, instrument scientists at KWS-2 at Forschungsneutronenquelle Heinz Maier-Leibnitz (MLZ), FRM II (Münich, Germany). A source wavelength of 7 Å ($\Delta\lambda/\lambda$ = 10%) and a detector system based on an array of ^{3}He tubes with a resolution of 8 mm were used for data collection. Sample-detector distances (SDD) of

1.58, 7.58, and 19.48 m were set to cover a Q-range of 0.002-0.221 $Å^{-1}$. The exposure time was adjusted to 5 min, 10 min, and 20 min for 1.58, 7.58, and 19.48 m SDDs, respectively.

The liposomal compositions and preparation used for the SANS measurements are given in chapter 2.2.3 (d). Samples were filled in quartz glass cuvettes with a 1 mm thickness (Hellma Optic GmbH, Jena, Germany) and placed in an aluminum holder with plastic cover. The measurement temperature of 37 °C was controlled by a Peltier element combined with a water bath and controlled by a water thermostat. The scattering intensity of the empty cuvette and the solvent D_2O were subtracted from the sample scattering. The resulting intensities were azimuthally averaged. All data corrections were performed with the software QtiKWS (JCNS, Jülich, Germany), while for data analysis the software SasView version 4.2.0 (sasview.org) was used.

2.4.3. Model functions used for the SANS data fitting

The help for data fitting was kindly provided by **Dr. Sebastian Jaksch** (JCNS). All fit functions contained a scale factor I_0 and background I_b, i.e., they were of the form:

$$I(Q) = I_0 \cdot f(Q) + I_b \tag{2.9}$$

where **Q** denotes the scattering vector. The scale factor contains the scattering volume and the scattering length density difference between solvent and structure.

The lamellar model, equation 2.8, provides the scattering intensity, *I (Q)*, for a lyotropic lamellar phase. A uniform scattering length density and random distribution in solution are assumed which results in

$$f(Q) \propto \frac{1 - \cos(Q\sigma)}{\sigma Q^4} \tag{2.10}$$

where σ denotes bilayer thickness [108].

The ellipsoid model, equation 2.9, is calculated from the form factor for randomly oriented ellipsoids of revolution with uniform scattering length density. It is given by:

$$f(Q) = \frac{[\sin(Qr) - \cos(Qr]^2}{9(Qr)^6} \text{ with } r = \sqrt{R_b^2 \sin^2\alpha + R_a^2 \cos^2\alpha} \tag{2.11}$$

where α denotes the angle between the rotational axis of the ellipsoid and the *Q*-vector, R_a is its radius along this axis and R_b the radius perpendicular to it. The orientation of the ellipsoid is numerically averaged over a sphere to give the final fit model [104].

As the final model, a general power law was used:

$$f(Q) = \|Q\|^{-m} \tag{2.12}$$

2.4.4. Dynamic Light Scattering (DLS) – Theory

Colloidal particles in a solvent are in constant movement due to their thermal energy [110]. The speed of this so-called Brownian motion can be determined from the fluctuation of the scattering light pattern produced by the moving particles, a technique called dynamic light scattering (DLS) [101, 109, 110]. The speed of the particles is more precisely described by the translational diffusion coefficient D. The relationship between the speed of Brownian motion of a particle and its size is defined in the Stokes-Einstein equation [109]:

$$d_H = \frac{kT}{3\pi\eta D} \tag{2.13}$$

where: d_H is the hydrodynamic diameter, k is the Boltzmann's constant, T is the absolute temperature, η represents the viscosity of the solvent, and D is the diffusion coefficient of the particle. The hydrodynamic diameter (d_H), also called the Stokes-Einstein diameter or Stokes diameter is the diameter of a hard-sphere that diffuses at the same speed as the particle or molecule being measured. The hydrodynamic diameter (d_H) depends, besides the size of the particle core, on surface structures as well as the ionic composition of the medium.

Because diffusing particles are moving with random velocities in random directions, the intensity of the scattered light *I*(t), is a fluctuation function. For fast diffusing particles, *I*(t) is fluctuating fast and for slow particles more sluggishly. The "speed of fluctuations" can be mathematically defined by the correlation function g_2 (t) [94, 109, 111] defined as:

$$g_2(t) = \frac{\langle I(t'-t)\cdot I(t')\rangle - \langle I^2(t')\rangle}{\langle I^2(t')\rangle} \tag{2.14}$$

where the angular brackets < > denote averaging over t'. Here g_2 (t) represents the "memory" of a fluctuating signal, metaphorically speaking. A lengthy calculation shows that the correlation function of light scattered by a set of different scatters is given by [94, 111]:

$$g_1(Q,t) = \sum_{i=1}^{n} G_i(\Gamma_i)e^{(-\Gamma_i t)} \tag{2.15}$$

with $\Gamma_i = Q^2 D_i$, scattering wave vector $Q = 4\pi n / \lambda \sin(\theta/2)$ and G_i as the total scattering strength of the particles of sort *i*. The index of refraction of solvent is n, λ represent the wavelength of the light and θ the angle of observation with respect to the incoming light.
The measured intensity correlation function g_2 is simply the square amplitude of g_1 [94, 111]:

$$g_2(Q,t) = |g_1(q,t)|^2 \tag{2.16}$$

2.4.5. Dynamic Light Scattering (DLS) – Measurements

Liposomal size distribution was determined using the instrument Zetasizer Nano ZS (Malvern Instruments (Malvern, UK) in back-scattering mode with a non-invasive backscatter optics (NIBS) at 173° angle [94]. The instrument was equipped with a Helium-Neon laser (633 nm). The laser power was automatically set using the appropriate attenuator. The measurement temperature of 20 °C was set by a Peltier element.

Prior to measurements, 20 µl of liposome stock solutions were diluted with 180 µl of ultrapure and filtrated water (Milli-Q Gradient A10, Merck Millipore, Darmstadt, Germany) and filled in a quartz micro-cuvette (Hellma Optics, Jena, Germany). All measurements were performed at 20 °C and repeated three times at 1 min intervals. Data were collected from three independently prepared samples and analyzed using the instrument software (DTS from Malvern Instruments). Reported data are mean peak position and its standard deviation (mean (s.d.)).

2.4.6. Electrophoretic light scattering (ELS) - Theory

Zeta potential (ζ), also known as electrokinetic potential, is a physical property exhibited by any particle in suspension. It is the potential at the slipping/shear plane of a colloid particle moving in an electric field (Figure 2.6). In other words, the zeta potential represents the potential difference between the electric double layer of electrophoretically mobile particles and the layer of dispersant around them [94, 110, 112].

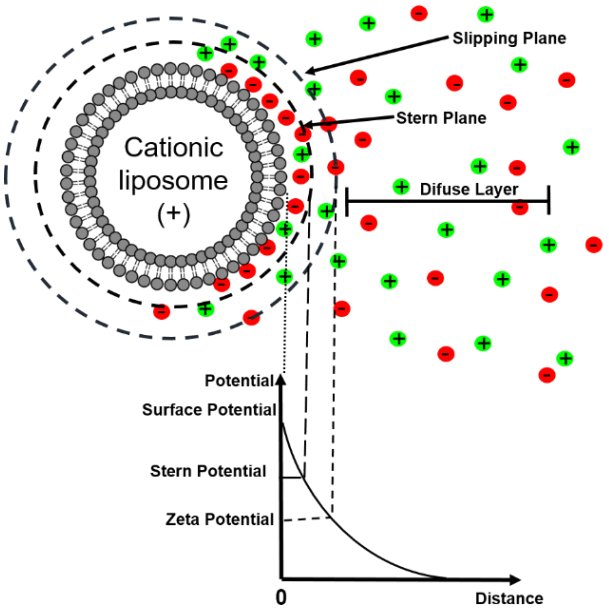

Figure 2.6. Schematic representation of zeta potential

It is the electrophoretic mobility measured directly with the conversion to zeta potential being inferred from theoretical considerations. The essence of the traditional microelectrophoresis system is a cell with electrodes at either end, between which a potential is applied. Particles move towards the electrode of opposite charge; their velocity is measured and expressed in unit field strength as their mobility [94, 110, 112]. The velocity of a particle in an electric field is commonly referred to as its electrophoretic mobility (U_E). Zeta potential is related to the electrophoretic mobility (U_E) by the Henry equation :

$$U_E = \frac{2\varepsilon\zeta f(\kappa a)}{3\eta} \qquad (2.17)$$

where ζ is zeta potential, ε represents dielectric constant, η is viscosity. The units of κ, termed the Debye length, are the reciprocal length and κ^{-1} is a measure of the "thickness" of the electrical double layer. The parameter a refers to the radius of the particle and, therefore κa measures the ratio of the particle radius to electrical double layer thickness. Electrophoretic determinations of zeta potential are most commonly made in aqueous media and moderate electrolyte concentration. F(κa) in this case is 1.5, and this is referred to as the Smoluchowski approximation [94, 112].

Therefore calculation of zeta potential from the mobility is straightforward for systems that fit the Smoluchowski model, i.e., particles larger than about 0.2 μm dispersed in electrolytes containing more than 10^{-3} M salt.

2.4.7. Electrophoretic light scattering (ELS) - Measurements

In this work, the zeta potential of the liposomes was characterized by Nano ZS (Malvern Instruments Inc, Malvern, UK). Before measurements, liposomes were diluted 1:50 in ultrapure and filtrated water (Milli-Q Gradient A10, Merck Millipore, Darmstadt, Germany). All measurements were performed at 20 °C and repeated three times at 1 min intervals, with a minimum of 10 runs per sample. Data were collected from three independently prepared samples and analyzed using the instrument software (DTS from Malvern Instruments). Reported data are mean peak position and its standard deviation (mean (s.d.)).

2.5. Flow cytometry

2.5.1. Flow cytometry – Theory

Flow cytometry is a well-established technique in cell biology to determine various physical and chemical properties of cell populations based on light scattering and fluorescence detection. For more about the flow cytometry, please refer to the literature [113, 114]. In brief, a flow cytometer consists of four basic components: fluidic system, laser(s), optics, and electronics/external computer system. Cells are usually suspended in a fluid and inserted into the flow cytometer where they become separated by aspiration into a capillary. The detection of the signals, forward (at 10° to the laser beam) and side scattered light (90° to the laser beam), allows conclusions about the cellular size and surface properties. Furthermore, the fluorescent intensities of distinct cell-specific staining can also be detected.

2.5.2. Flow cytometry – Measurements

Cellular fluorescence intensities were analyzed using a flow cytometer (Guava easyCyte 8HT, Merck Millipore, Billerica, MA, USA) equipped with a guava Flowcell II (Merck Millipore) and a 75 mW argon-ion laser to excite the BODIPY fluorophores at 488 nm. The emitted monomer signal was measured using a 525/30-nm band-pass optical filter (green channel) while the dimer signal of this dye was collected using a 690/50-nm band-pass optical filter (red channel) [7]. For each sample, a minimum of 10,000 cells was collected. Data were analyzed using the InCyte Software for Guava easyCyte HT Systems (Merck Millipore).

Prior to analysis, cells were trypsinized with trypsin–EDTA solution (Sigma-Aldrich) for 5 min, subsequently washed with phosphate-buffered saline (PBS) (pH 7.4) and centrifuged for 5 min at 200× g. Analyses were carried out either on living cells in PBS or on fixed cells. Cell fixation was carried out using a cell fixation reagent (Solution A from Fix&Perm cell permeabilization kit from Life Technologies, Carlsbad, CA, USA). All measurements were performed at least three independent experiments in duplicates. The analysis was performed as described by Braun and co-workers [7]. Briefly, cells were selected and quantified using a two-dimensional dot plot of the forward scatter signal (FSC) vs. side scatter signal (SSC) (both logarithmic plots). Photomultiplier sensitivities of the green (monomer) and red (dimer) channels were adjusted to the detected signal intensities of untreated CHOs below ten counts. During analysis, no compensation was required. “Endocytosis” and “Fusion” gates were determined based on the two-dimensional dot plot of green vs. red channels (both log plots) using endocytic and fusogenic liposomes, respectively (Figure 3.2).

2.6. Differential Scanning Calorimetry (DSC)

Thermotropic phase transitions of lipid suspensions were analyzed by differential scanning calorimetry (DSC). The DSC is a fundamental thermodynamic measurement essential for the understanding of molecular interactions and the design of thermal processes. DSC measures excess heat capacity (C_p) of a sample (at constant pressure), or more precisely, the difference in C_p between sample and reference. It is then straightforward to calculate the excess heat capacity of the system as it undergoes the thermotropic transition [68, 115]. For more details please refer to [66, 68, 115-119].

2.6.1. DSC – theory

A system under constant pressure and temperature conditions, where virtually all phase transitions occur, is best described by the Gibbs free energy. The standard Gibbs free energy change for a chemical reaction is given by:

$$\Delta G = \Delta H - T\Delta S = -RTInK \tag{2.18}$$

where ΔH and ΔS are the standard enthalpy and entropy of the reaction, respectively. The temperature where the transition from one state (state A) of the system to another (state B) happens (e.g., for lipids from gel to liquid crystalline phase) is the melting temperature T_m. Here, the Gibbs energy change is zero, and transition (melting) temperature is the ratio of enthalpy and entropy changes:

$$T_m = \Delta H/\Delta S \tag{2.19}$$

The enthalpy versus temperature function for the system is shown in Figure 2.7. The heat capacity is defined as the differential of heat with respect to the temperature. The excess heat capacity function [68, 115] C_p, given by

$$c_p = \left(\frac{d\Delta H}{dT}\right)_P = \frac{K(T)}{(1+K(T))^2} \cdot \frac{\Delta H^2}{RT^2} \tag{2.20}$$

The heat capacity function is instantly obtained by DSC. The integral under the C_p curve represents the enthalpy change for the transition from state A to state B (ΔH). The phase transition temperature can be determined from the maximum of the C_p curve (Figure 2.7). From the T_m = $\Delta H/\Delta S$ ratio, the entropy or enthalpy change of the transition can be calculated [68, 115].

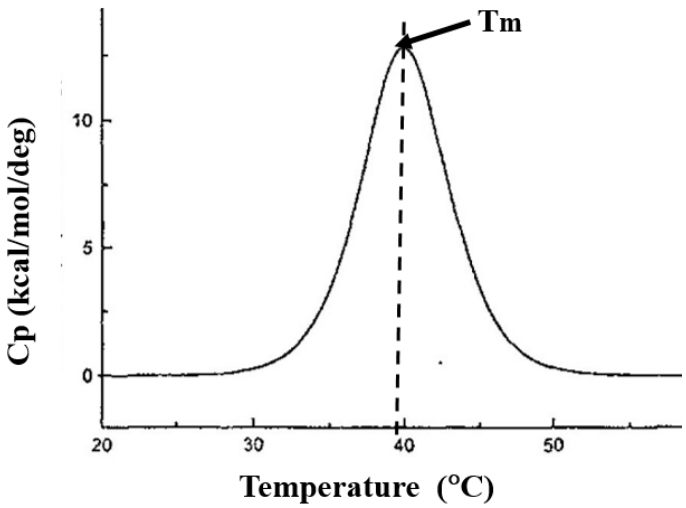

Figure 2.7. Schematic representation of the DSC thermogram of melting at ~ 40°C. The temperature dependence of the enthalpy difference. The figure is taken and modified from ref [68].

2.6.2. DSC - Measurements

To determine the liposomal thermal properties, a multi-cell DSC (MC DSC) (TA Instruments, New Castle, DE USA) was used. The instrument was designed to run one reference and three samples simultaneously in removable Hastelloy ampoules sealed with O-rings to prevent loss of volatiles.

Liposomes were prepared, as described in chapter 2.2.3.a. Samples were first incubated for 48 h at 4 °C so that equilibrium within the sample has been achieved. An empty sample holder was used as a reference. The measurements were performed in the temperature range from 5 °C to 65 °C with 1 °C/min heating/cooling rate. Heating and cooling scans were recorded one after another four times in total.

2.7. Microscopy techniques

Cells, untreated and treated with liposomes and liposomes themselves, were also analyzed by microscopy. Cells were analyzed by widefocal and confocal laser scanning microscope (cLSM), light microscopy, while liposomes were imaged by (scanning) transmission electron microscope ((S)TEM) combined with specific sample preparation techniques, i.e., Cryo-TEM and freeze-fracture/STEM. Since microscopy is a broad field, and some parts of it are out of the scope of this thesis, for more about its fundamentals please refer to [120-137].

2.7.1. Microscopy techniques applied for live cell experiments

The viability and density of cells during culture were observed using a light microscope Axiovert 40 CFL (Carl Zeiss MicroImaging GmbH, Jena) equipped with 20x/0.25 Ph1 air objective (Carl Zeiss). Further microscopic analyses were carried out with an inverse confocal microscope (LSM 710 from Carl Zeiss MicroImaging GmbH, Jena) equipped with a 25 mW argon ion laser (458/488/514 nm), two (1.2 mW and 5 mW) helium-neon lasers (543/633 nm) and a near UV laser (405 nm). The BODIPY FL, as well as both TFPE dyes, were excited at a wavelength of 488 nm, and their fluorescence emissions were detected using a band pass filter BP 495–550 nm (green channel). Hoechst 33342 was excited by the 405 nm laser line, and its emission was detected using a BP 505/90. The lipid analog DiR and DRAQ5 were excited using the 633 nm laser line, and the emitted signal was collected through the long pass filter LP 650 nm. For imaging, a Plan-Apochromat 40×/1.40 Ph3 (Carl Zeiss) objective was used. To maintain appropriate culture conditions, the microscope was equipped with an incubator (Incubator XL 2, Carl Zeiss). Temperature and CO_2 were kept constant at 37 °C and 5%, respectively. The images were analyzed using ZEN software (Carl Zeiss). The sample preparation prior to imaging has been described in chapter 2.3.

2.7.2. Analysis of images

The algorithm for quantification of the fusion efficiency based on the fluorescence micrographs was developed by Georg Dreissen (Forschungszentrum Jülich GmbH, ICS-7: Biomechanics). The code was implemented in Matlab (R2017, Mathworks, Natick, MA).

Briefly, in the first step, individual cells were segmented using the nuclei channel. This image was first smoothed (Gaussian filter, standard deviation 3 pixels, pixel size 173 nm throughout), and morphological opening (disk-shaped structuring element of radius 9 pixels)

was performed. The bright nuclei were segmented using the mean grey value of the image as an intensity threshold. Subsequently, morphological opening and closing (both with a disk of radius 5 pixels) were performed on the mask. Next, the watershed transformation was used to separate overlapping nuclei and to segment cells. Therefore, the distance transform of the negative mask was calculated and multiplied by -1. Then local minima (depth less than 2) were eliminated from this resulting image, and finally, the watershed transform was applied. Next, the dividing lines between the "watershed" areas of neighboring nuclei, computed by the watershed transform, were used as the shape of the corresponding cell.

In the second step, the fluorescent lipid signal incorporated into living cells was analyzed. Since the many small, bright spots in the images indicated lumps, endocytic, or not fused liposomes, they had to be removed. Therefore, the image was first smoothed (Gaussian filter, standard deviation of 3 pixels), then local bright spots were detected using the algorithm described in the work of Hersch at al. [138]. In brief, the local z-score of the image was calculated within a 91x91 pixel environment and segmented using a threshold of 2 for the z-score. Only regions with area below 100,000 pixels were accepted. Each region was then enlarged by morphological dilation disk of radius 3 pixels. On the smoothed image, all spots identified by the z-score segmentation were replaced by pixel values calculated by inward interpolation from the greyscale values at the rim of the spot. Spot detection and interpolation of grey values were performed twice.

Using the processed intensity image from the second part of the program and the cell label image from the first part, the average grey value intensity for each cell was calculated individually. By using the same manually chosen threshold for all images, all cells were separated into fused (all cells with an average grey value above the threshold) and non-fused (all cells below the threshold) cells.

2.7.3. Microscopy techniques applied for the liposomal experiments

a) Cryo-TEM

The preparation of liposomes is described in chapter 2.2.3. The sample preparation, as well as Cryo-TEM experiments, were carried out by **Dr. Marie-Sousai Appavou** (MLZ, Münich, Germany). Prior to experiments, samples were preincubated at 20 °C or at 37 °C for 10 min. Subsequently, 5 µl of FLs or ELs (described in chapter 2.2.3) were dropped on a

patterned S7/2 carbon-coated copper grid. After a few seconds, excess solution was removed by blotting with filter paper. The samples were cryo-fixed by rapid immersing into liquid ethane at -180 °C in a cryo-plunge (EMGP Leica GmbH) where the temperature was set to 20 °C and the relative humidity at 80% prior to vitrification. The specimen was placed into a cryo-transfer holder (HTTC 910, Gatan, Munich, Germany) and transferred to a JEM 2200 FS EFTEM instrument (JEOL, Tokyo, Japan). Experiments were carried out at temperatures around -180 °C. The transmission electron microscope functioned at an acceleration voltage of 200 kV. Zero-loss filtered images were taken under reduced dose conditions (<10 000 e^-/nm^2). All images were recorded digitally by a bottom-mounted 16 bit CMOS camera system (TemCam-F216, TVIPS, Munich, Germany). To avoid any saturation of the gray values, proportional to a certain number of electrons per pixel, all the measurements were taken with intensity below 15, 000 gray value.

b) Freeze-fracture/Scanning Transmission Electron Microscopy (FF/STEM)

The freeze-fracture technique has been established and used for investigating biological structures such as cells, membranes, or the distribution of proteins within membranes, and it has been usually combined with electron microscopy. More about freeze-fracture can be found in the literature [63, 136, 139, 140].

FF/STEM experiments were carried out by **Dr. Sabine Dieluweit** (Forschungszentrum Jülich GmbH, ICS-7: Biomechanics, Jülich, Germany). The preparation of liposomes is described in chapter 2.2.3. Prior to measurements, a small drop (1-2µl) of the ELs and FLs sample equilibrated at room temperature for 30 min, was frozen in liquid ethane (cooled down by liquid N_2). Afterward, frozen samples were inserted into a freeze-fracture etching machine BAF 400T (Balzers, Lichtenstein), and the system was set up on vacuum and equilibrated for 30 min. Cutting and etching were performed in the temperature range of -114 °C to -117 °C and a pressure range of 6 mbar to 10 mbar. Evaporation of platinum/carbon at 45° following evaporation of carbon at 90° with a rotating sample resulted in a replica. The replicas (Pt/C layer thickness of around 2 nm and C layer thickness in the range between 20-30 nm) were separated from the sample drop by floating on a detergent (TritonX100 (1%), Sigma-Aldrich, Taufkirchen, Germany) solution and water followed by transfer on an EM copper grid (Athene old, Plano, Wetzlar, Germany) which were analyzed in STEM (STEM II, Magellan 400, FEI company, Hillsboro, OR, USA, HNF) with an acceleration voltage of 25 kV, and 0.1 nA, current in a bright field mode.

2.8. Falling ball viscometry

2.8.1. Falling ball viscometry - Theory

Formally, viscosity (η) is the ratio of the shear stress (*F*/*A*) to the velocity gradient ($\Delta v_x/\Delta z$ or dv_x/dz) in a fluid [141].

$$\eta = \frac{\frac{F}{A}}{\frac{\Delta v_x}{\Delta z}} \tag{2.21}$$

A Newtonian fluid is one in which the viscosity is just a constant number. A non-Newtonian fluid is one in which the viscosity is a function of some variable like shear stress or time. The conventional expression for determining viscosity η from the velocity of a falling sphere is Stokes' law [141]:

$$\eta = \frac{(\gamma_s - \gamma_f)d^2 g}{18v} \tag{2.22}$$

in which d is the sphere diameter, γ and γ_f are the densities of a sphere and fluid, respectively, g the local acceleration of gravity, and ν the sphere fall velocity. Stokes' law applies for slow, steady fall of a sphere through an infinite Newtonian medium [141]. In the usual experimental apparatus, the sphere falls along the axis of a cylindrical tube, hence a wall correction must be applied to Stokes' law if the falling sphere and the cylindrical tube having diameters on the same order of magnitude. Moreover, the fall may not be slow. Therefore an inertial correction may also be required [141].

2.8.1. Falling ball viscometry - Measurements

The falling ball viscometer described for this work was developed from a glass capillary of 100 µl volume and ~ 1 mm inner diameter, positioned perpendicular to the working surface and refilled by the liposomal solution of 10 mg/ml concentration (see chapter 2.2.3 and figure 2.8). The falling sphere was a ball of stainless steel (section 2.1.9) with a diameter of less than 1 mm and a weight of ca. 0.0042 g. Sketching paper placed behind the capillary served to calibrate distances. The movement of the sphere was recorded via a digital camera (Canon, EOS 600D EF-S 18-55 III kit). The effect of the wall correction [142] of the capillary was not taken into consideration because at the dimensions used here; the correction factor depends very

strongly on the ratio of sphere and capillary diameter. Therefore, only relative values were determined. Comparability was ensured by using the same type of capillary and the same type of sphere.

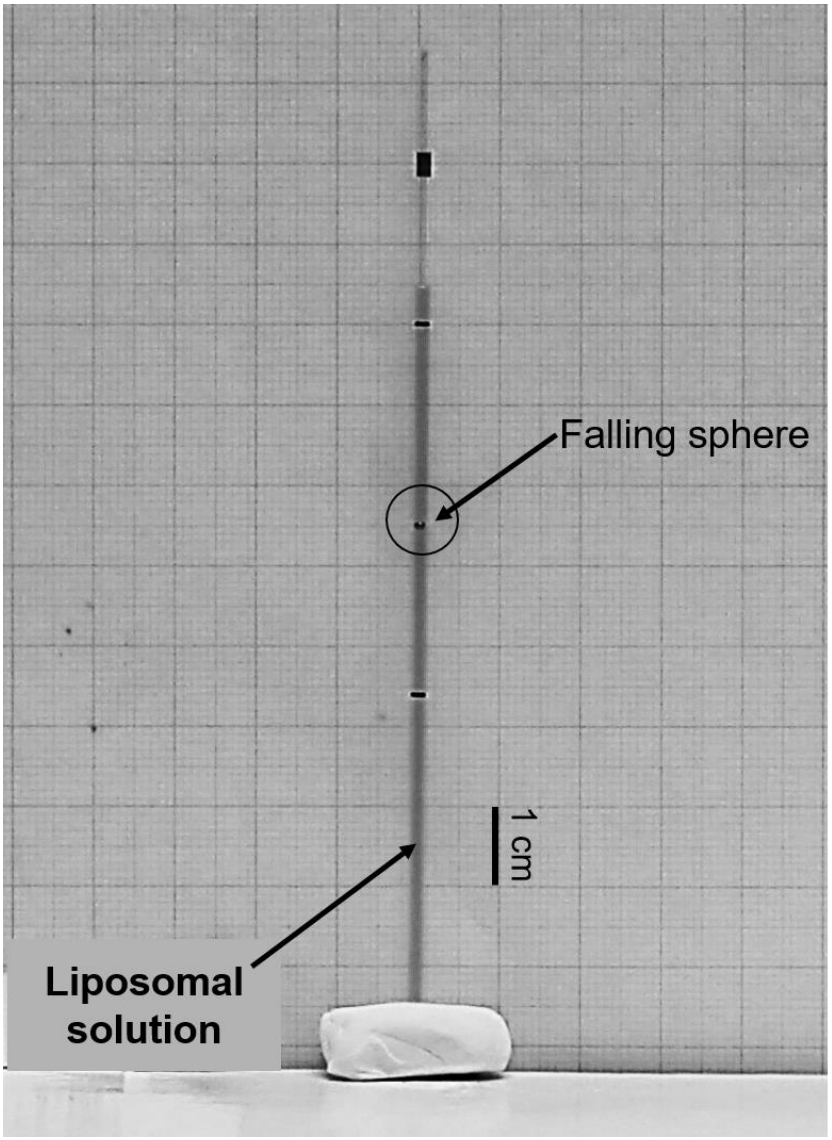

Figure 2.8. Falling sphere viscosity experiments set up.

2.9. Solid-state NMR

2.9.1. Solid-state NMR - General

NMR is mostly applied to determine the structure of organic molecules in solution. In liquid samples, rapid isotropic molecular motion causes the averaging of various orientation-dependent interactions, called anisotropic interaction, and results in well-resolved spectra with narrow peaks. In crystals, large membrane vesicles, or powders, there is no motion-induced averaging because molecules are mostly held rather rigidly, and anisotropic interactions persist. Therefore, broad and complicated spectra are obtained. The technique for the study of solid or quasi-solid samples is called solid-state NMR (SSNMR). For the basics of NMR with a particular focus on solid-state NMR, please refer to the literature [143-152].

A special SSNMR technique, phosphorus NMR (^{31}P NMR), is frequently used to study liquid crystals containing phosphorus atoms such as phospholipid membranes [149]. Here, the line-shape is a sensitive measure of liposomal phases and their structural changes. If lipids are in the form of dry powder, it becomes possible to observe all the principal axis contributions in the spectrum. When the membrane is in a liquid state, fast axial motions cause an averaging in the principal axis. Depending on the temperature, some phospholipids, such as phosphatidylethanolamines, can form inverted hexagonal phases where lipid molecules form cylindrical structures. Therefore, rotation around the cylinder axis causes a further averaging out of anisotropy. If the axial motion is fast enough, it is also possible to average out all the anisotropic motion and observe only the isotropic chemical shift (Figure 2.9.).

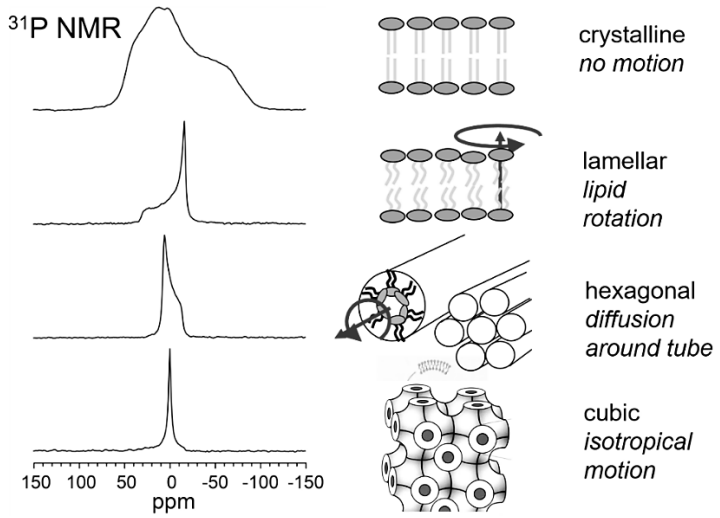

Figure 2.9. Lipid phases and the corresponding ^{31}P NMR spectra. The figure is taken and modified from the lecture of **Dr. Erik Strandberg** (KIT, Karlsruhe, Germany).

2.9.2. Solid-state NMR - Measurements

NMR experiments and corresponding figures were provided by **Dr. Erik Strandberg** (KIT, Karlsruhe, Germany). A detailed description of the preparation of the liposomes used for SSNMR experiments for this work is given in chapter 2.2.3 (f). All NMR experiments were carried out on a Bruker Avance 500 MHz spectrometer (Bruker Biospin, Karlsruhe, Germany). ^{31}P-NMR measurements were performed on a flat-coil ^{31P}/^{1}H probe head built in-house using a Hahn echo sequence [151] with a 90° pulse of 3.5 µs, a 30 µs echo time and 13 kHz ^{1}H SPINAL-64 decoupling [152] during acquisition. The acquisition time was 10 ms, and the recycle time was 1 s. Typically, 3,000-10,000 scans were collected. For temperature series, a waiting time of 1 h was used between measurements for temperature equilibration. The temperature in the sample inside the probe was calibrated using a methanol sample . Measurements were carried out at 4, 20, 30, 37, 50, and 60 °C.

^{19}F-NMR experiments were performed on a flat-coil ^{19}F/^{1}H goniometer probe head built in-house by using an "anti-ringing" sequence (to reduce background signals from the probe) , a 3.9 µs 90° pulse, a 1 s relaxation delay time, 500 kHz spectral width, 4096 data points and 24 kHz proton decoupling with a SPINAL-64 sequence. Between 1,000 and 5,000 scans were collected depending on signal strength. Spectra were referenced from a ^{1}H-NMR spectrum at 30 °C, in which the water signal was set to 4.7 ppm, and the corresponding ^{19}F or ^{31}P reference frequency was calculated from the gyromagnetic ratios of ^{1}H and ^{19}F or ^{31}P .

Chapter 3

3. Deciphering the Functional Composition of Fusogenic Liposomes

The most common uptake mechanism of mammalian cells is endocytosis. However, it has several drawbacks, such as time-consuming, low efficiency of delivery, or cargo degradation. As introduced in the first chapter, the novel cationic liposomes are able to fuse with the cellular plasma membrane with extraordinary high efficiency and without external inducers like fusion proteins or peptide, within a few minutes. Although those liposomes are well established in many fields of life sciences in the meantime, a systematic investigation of their composition and its influence on the fusion ability was missing. This chapter presents a study where each of the three essential components of fusogenic liposomes was steadily varied in order to determine its impact on fusion induction and efficiency.

The major part of this chapter is published in Kolasinac et al., *Deciphering the Functional Composition of Fusogenic Liposomes,* International Journal of Molecular Sciences, 2018, ***19***, 346 [92].

3.1. Introduction [92]

Positively charged liposomes have been well known in cell biology, and biotechnology since the first cationic lipid N-[1-(2,3-dioleoyloxy)propyl]-N,N,N-trimethylammonium chloride (DOTMA) was synthesized by Felgner and co-workers and successfully used to introduce plasmid DNA to kidney cells [153]. This lipid-based transfection, also called lipofection, uses the attractive electrostatic interaction between the negatively charged nucleic acids and the positively charged liposomes to build liposome/DNA complexes [153, 154]. Neutrally or negatively charged liposomes used before were not able to attach to nucleic acids and transfer them through cellular membranes into the nuclei of mammalian cells where the genetic information can be readout. Therefore, cationic liposomes became increasingly popular in biotechnology. Several research groups focused on the improvement of transfection efficiency by changing the liposomal composition, while others elucidated the lipid/DNA complex, called lipoplex, structures [154-156], and their cellular uptakes [80, 157-160].

In the last decades, novel cationic lipid analogs have been synthesized to minimize toxicity. At present, 1,2-dioleoyl-3-trimethylammonium-propane (DOTAP) is one of the most favored and characterized cationic lipids [161]. In most cases, cationic lipids are used in combination with different neutral lipids or helper lipids, e.g., phosphoethanolamines, phosphocholines, or cholesterol. Such co-lipids, at the same time, decrease lipoplex toxicity and simultaneously increase transfection efficiency. It was observed by several research groups that the addition of a neutral lipid with a small head group and long, unsaturated fatty acid chains, e.g., 1,2-dioleoyl-3-glycero-phosphatidylethanolamine (DOPE), to the cationic lipids resulted in liposomes, that partially formed the inverted hexagonal (H_{II}) phase in combination with the lamellar phases (L) [162]. In lipoplexes composed of the same lipid mixture and additional plasmid DNA, H_{II} structures have been found even more. The inverted hexagonal lipid phase, together with other 3D phases, like hexagonal or cubic phases, may serve as intermediate structures for membrane fusion [45, 74]. Therefore membrane fusion has been postulated as the main uptake route of such lipoplexes. However, investigations of the last decades clearly show that endocytosis plays a crucial role in the cellular uptake of cationic liposomes while the contribution of membrane fusion is negligible [159, 163]. Considering the slow dynamics of endocytosis and the fact that this process delivers the molecules of interest to the lysosomes where most of them are degraded, the low efficiency of lipofection can be explained.

Csiszar et al. showed that the addition of an aromatic molecule as a third component to the usual cationic and neutral lipid mixture (DOPE/DOTAP) dramatically improves the membrane fusion efficiency of liposomes with the plasma membrane of mammalian cells [9]. Due to their extraordinarily high fusion efficiency, such liposomes have been called fusogenic liposomes (FLs). They have been successfully used for the delivery of different kinds of molecules, e.g., nucleic acids [164], purified proteins [12], polyphenols [8], anti-cancer therapeutics [165], fluorescent lipids [11], or nanoparticles [166]. The authors analyzed liposomes containing DOPE as neutral lipid, DOTAP as cationic lipid component at an equimolar ratio, and also fluorescently labeled lipids at ca. 5 mol %. Such molecules are fluorescent, and because of that property, their cellular uptake was monitored by fluorescence microscopy [92].

Unfortunately, until now, no systematic analysis has been carried out on the relative importance of the different components for fusion induction. This work aims at filling this gap. Therefore, the systematic variation of the liposomal composition and the concentration of each component, the cationic lipid, the neutral helper lipid, and the aromatic compound has been done. Liposomal characteristics like hydrodynamic diameter and zeta potential distributions were determined by dynamic and electrophoretic light scattering, respectively. Liposomal uptake by Chinese hamster ovary cells (CHOs) was visualized by fluorescence microscopy, while the fusion efficiency of liposomes, with the same cells, was quantified by flow cytometry. The main goal of this study was to elucidate the interplay of liposomal composition, physicochemical characteristics, and fusion capacity [92].

3.2. Results [92]

3.2.1. Changing the lipid composition of FLs: The importance of Cationic Lipids

Two kinds of liposomes were prepared to investigate the role of positively charged lipids in liposomes. One type of liposomes contained 1,2-dioleoyl-3-trimethylammonium-propane (DOTAP), a quaternary amine with +1 net charge in the head group range, and the others carried 1,2- dioleoyl-3-dimethylammonium-propane (DODAP), a ternary amine without charge at pH 7.4 but with the same hydrophobic moiety (Figure 3.1A) [92]. These two lipids have comparable structures but different charges. They were entrenched into liposomes together with DOPE as neutral component and BODIPY FL DHPE as an aromatic component. The molar ratio of lipids making liposomes was 1/1/0.1 mol/mol (DOPE/(DOTAP or DODAP)/BODIPY FL DHPE). Hydrodynamic size and zeta potential distributions of liposomes were measured using dynamic and electrophoretic light scattering (DLS), respectively. Figure 3.1B shows that both kinds of liposomes had similar monomodal size distributions with maxima around 200 nm. However, their zeta potentials differed sharply. DOTAP containing liposomes had a zeta potential of + 41 mV (s.d. 10 mV, n=3) whereas liposomes enclosing DODAP had a negative zeta potential of – 30 mV (s.d. 10 mV, n=3) at physiological pH as shown in Figure 3.1C.

Chinese hamster ovary (CHO) cells, as a typical mammalian cell line, were treated by the above-described liposomes to test their fusogenicity. Cellular uptake of liposomes was visualized by fluorescence microscopy, while phase contrast micrographs generated information about cell numbers and morphology (Figure 3.1D). When CHO cells were treated with liposomes containing DOTAP, a homogenous membrane staining was detected. This indicated the complete mixing of liposomal and cellular membranes. In contrast to this, no liposomal uptake of CHOs was detected upon incubation with liposomes containing the neutral lipid DODAP. In both cases, cell morphologies remained unchanged and healthy.

To examine the role of the positive charge of FLs in more detail, liposomes containing DOTAP as a charged component, DOPE as helper lipid, and BODIPY FL-DHPE as aromatic component were prepared with varying DOTAP content between 0% and 95%. Zeta potentials were determined as previously described. Liposomes without DOTAP had a negative potential around −20 mV, at physiological pH, while increasing DOTAP concentration resulted in more and more positive values (Figure 3.2A). Similar zeta potentials were found at 50 mol % and 95 mol % of DOTAP content. This indicated saturation at about +40 mV.

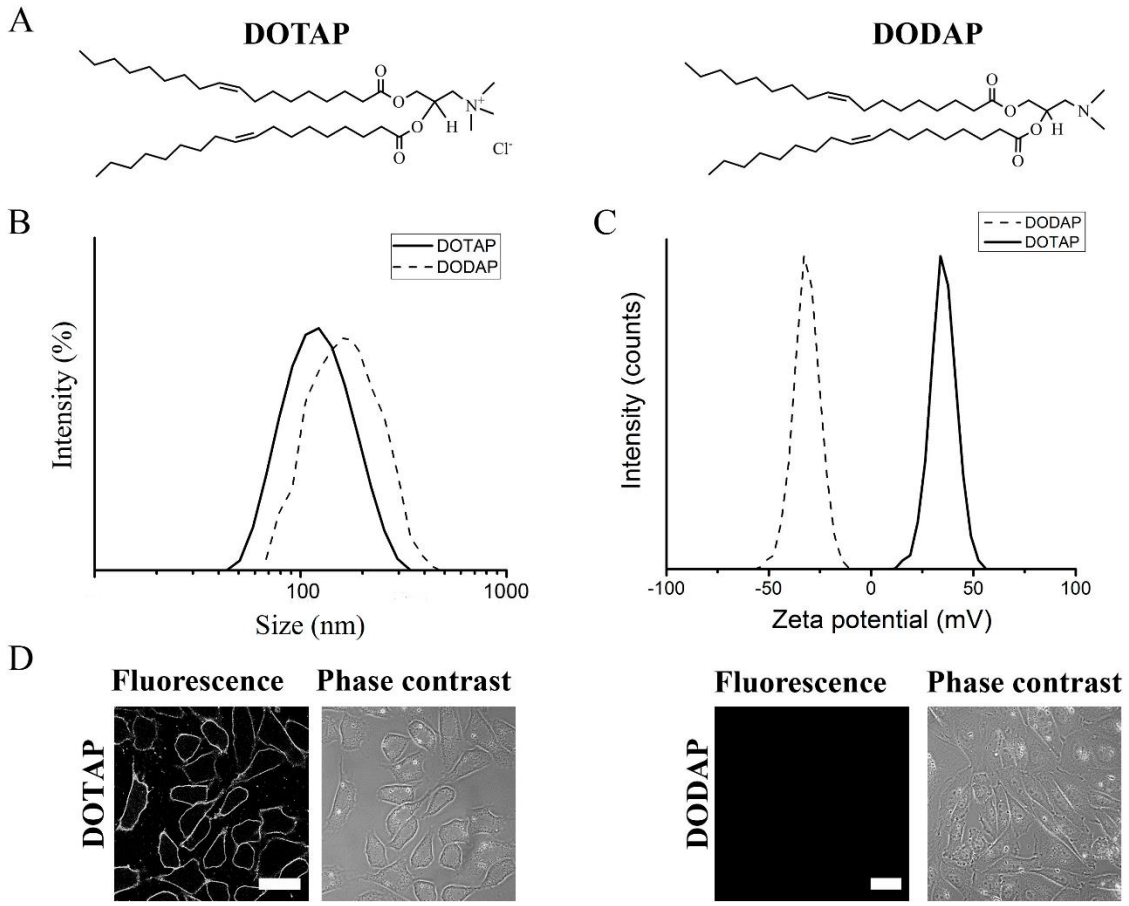

Figure 3.1. (**A**) Chemical structures of the positively charged lipid 1,2-dioleoyl-3 trimethylammonium-propane (DOTAP) and the neutral lipid 1,2-dioleoyl-3-dimethylammonium-propane (DODAP). (**B**) Hydrodynamic size and (**C**) zeta potential distributions of liposomes containing DOPE/DOTAP/BODIPY FL-DHPE and DOPE/DODAP/BODIPY FL-DHPE (1/1/0.1 mol/mol). (**D**) Fluorescence and phase contrast micrographs of CHO cells after treatment with liposomes containing DOTAP or DODAP. Scale bars, 20 μm [92].

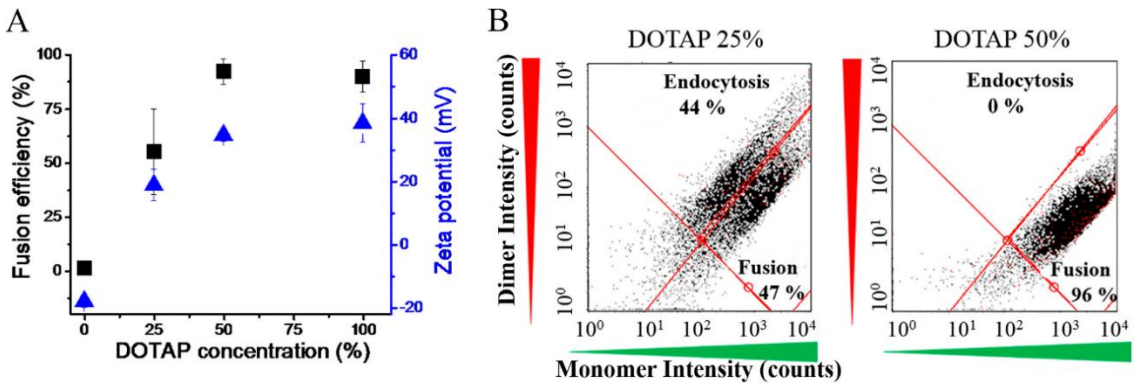

Figure 3.2. (**A**) Liposomal zeta potential (blue triangles) and fusion efficiency (black squares) at varying cationic lipid concentration. Bars indicate standard deviations (n=3). (**B**) Flow cytometry dot plots to determine the cellular uptake pathway and its efficiency. Liposomes always contained the aromatic tracer BODIPY FL-DHPE. Its monomer signal was detected in the green, its dimer signal in the red channels after incubation with Chinese hamster ovary cells (CHO). Endocytic liposomal uptake resulted in a nearly equal dimer and monomer signals of the tracer, while a high monomer and a low dimer signal were detected in the case of membrane fusion [92].

The fusion efficiency increased with an increasing zeta potential of liposomes. However, saturation occurred at a DOTAP concentration of about 50 mol %. Fusion efficiencies reached approximately 90%.

The same liposomes were applied on CHO cells, and membrane fusion efficiency was analyzed by flow cytometry using the concentration-dependent spectral changes of BODIPY FL. This technique allowed the statistical analysis of multiparametric data with high reliability. It also accompanied the qualitative analysis of the cellular uptake of liposomes attained by fluorescence microscopy. The specific concentration-dependent spectral changes of BODIPY FL were used for this technique instead of a FRET pair. The sharp emission peak appeared in the green spectral range (monomer signal) when the labeled liposomes were internalized by membrane fusion because of the dilution of the dye within the cellular plasma membrane. When the cellular uptake is endocytosis, the BODIPY FL tracers remain at high local concentrations within the endosomes and therefore can interact among themselves building dimer pairs. Their interaction influenced the spectral properties resulting in a red-shifted emission peak (dimer signal) that was absent at low concentrations (Figure 3.2B).

To explore the role of the positively charged component, six cationic lipids with different molecular shapes were embedded into FLs containing DOPE and BODIPY FL DHPE constant. The molar ratio of the components was 1/1/0.1 mol/mol (DOPE/cationic lipid/BODIPY FL DHPE). The following cationic lipids were used: DMTAP, DOTAP, DOTMA, DOEPC, MVL5, and DC-cholesterol (IUPAC names of lipids are listed in Chapters 2.1.1.-2.1.4.). Hydrodynamic diameters, zeta potentials, and fusion efficiencies of liposomes with CHO cells were determined as described above. The results are summarized in Table 3.1. While all liposomes had more or less the same sizes between 140 nm and 215 nm and zeta potentials between +30 mV and +40 mV, fusion efficiencies differed strongly. Liposomes containing the cationic lipids DOTAP or DOTMA were able to fuse with CHOs with efficiencies above 90%. On the contrary, liposomes with DMTAP or DOEPC showed efficiencies of only ca. 30%. This value was even further reduced to 20% or even 0% in the case of liposomes with MVL5 and DC-cholesterol, respectively [92].

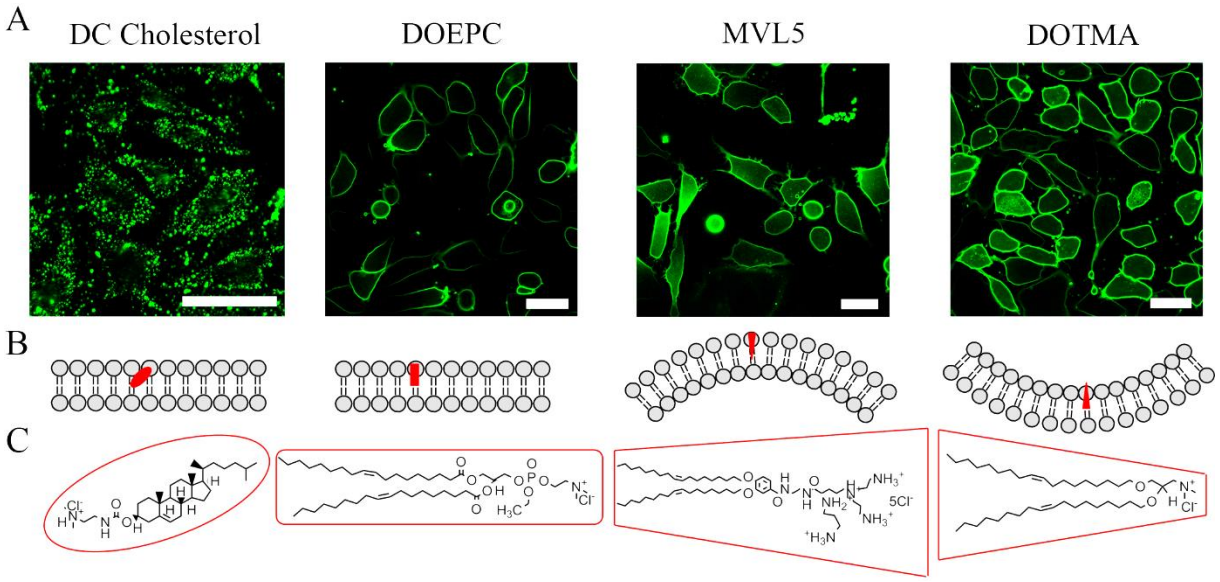

Figure 3.3. (**A**) Fluorescence micrographs of CHO cells after treatment with liposomes containing DC Cholesterol, DOEPC, MVL5, or DOTMA as cationic lipid, DOPE as neutral component and BODIPY FL-DHPE as fluorescent component (1/1/0.1 mol/mol). Scale bars, 20 µm.[92] (**B**) Favored membrane curvature of the reported cationic lipids. (**C**) Chemical structures of DC Cholesterol, DOEPC, MVL5, and DOTMA, used as cationic lipids in FLs. Putative molecular shapes are indicated by red lines [92].

Table 3.1. Characteristics of FLs containing different cationic lipids: the molecular shape of lipids, fusion efficiency of liposomes with CHO cells, zeta potentials (ς) and hydrodynamic sizes (d) of liposomes containing the respective cationic lipid, DOPE as helper lipid and BODIPY FL-DHPE as a fluorescent molecule (1/1/0.1 mol/mol). Efficiencies of endocytosis and fusion give together 100%. Average values of at least three independent measurements and their standard deviations are given [92].

Cationic Lipids	Molecular Shape	Fusion eff. (s.d.) (%)	ζ (s.d.) (mV)	d (s.d.) (nm)
DOTAP	conical	92 (6)	41 (10)	214 (45)
DOTMA	conical	95 (4)	42 (12)	126 (36)
DMTAP	cylindrical	35 (7)	31 (6)	149 (39)
DOEPC	cylindrical	33 (6)	41 (19)	164 (8)
DC-Cholesterol	cylindrical	1 (1)	42 (1)	136 (1)
MVL5	inv. conical	20 (2)	26 (8)	152 (7)

3.2.2. Changing the lipid composition of FLs: Importance of the aromatic component

To test the role of the aromatic component, liposomes were prepared containing DOTAP as a cationic lipid, DOPE as a helper lipid (1/1 mol/mol), and BODIPY FL DHPE, βBODIPY-C_{12}HPC or DiR as an aromatic component with varying amounts of the aromatic molecules. Total lipid ratios were set between 1/1/0.01 and 1/1/0.1 mol/mol. CHO cells were treated with these liposomes, and the fluorescence signals of dyes were observed by fluorescence microscopy. Depending on fluorophore concentration, two different characteristic staining patterns occurred (Figure 3.4A, and Figure 3.5A). A green speckled signal on the cell surfaces was recorded in the low BODIPY-FL-DHPE concentration range (0.01 mol/mol $\leq n_{Bodipy\ FL\text{-}DHPE}/n_{DOTAP} \leq$ 0.05 mol/mol) (Figure 3.4A: left image). This pattern is typical for endocytic uptake [7]. With increasing BODIPY FL-DHPE concentration, furthermore cell shapes became visible due to homogenously stained plasma membranes upon membrane fusion, and above a distinct dye concentration ($n_{Bodipy\ FL\text{-}DHPE}/n_{DOTAP} \geq$ 0.05 mol/mol) all CHO cells showed completely stained plasma membranes (Figures 3.4A-3.6A: top right images). This signal was characteristic of highly efficient membrane fusion between liposomal and cellular membranes [7]. Based on the fluorescence signal of the BODIPY FL dye coupled to the DHPE lipid, the quantification of the internalized liposomal signal was carried out by flow cytometry. In the whole dye concentration range, the signal intensity increased linearly with increasing BODIPY FL-DHPE concentration (slope 0.87 counts/dye ratio). Similar behavior was detected when BODIPY FL-DHPE was replaced by a chain labeled lipid-like βBODIPY-C_{12}HPC or by carbocyanine fluorescent dye DiR (Figures 3.4-3.6) [92].

Liposomes with different compositions were also analyzed in the same way. Here, DOPE was replaced by DOPC, and the concentration of the aromatic component was varied in the same range as described above. In the whole dye concentration range from 0.01 to 0.1 mol/mol, such liposomes resulted in the same speckled fluorescence pattern upon incubation with CHO cells (Figures 3.4A). Flow cytometry analysis revealed increasing signal intensity incorporated by cells with increasing dye concentration. The absolute intensity values obtained by DOPC containing liposomes were comparable with those containing DOPE in the low dye concentration range (0.01 mol/mol $\leq n_{\text{Bodipy FL-DHPE}}/n_{\text{DOTAP}} \leq$ 0.05 mol/mol), while they were significantly lower at higher dye concentrations ($n_{\text{Bodipy FL-DHPE}}/n_{\text{DOTAP}} \geq$ 0.05 mol/mol) (slope 0.1 counts/dye ratio). The same trend was observed when BODIPY FL-DHPE was replaced by βBODIPY-C_{12}HPC or by the carbocyanine fluorescent dye DiR (Figures 3.4A-3.6A) [92].

To validate the importance of the aromatic component, it was replaced by the non-aromatic molecules cholesterol, biotin, and PEG2000 coupled to DOPE (Biotinylcap-DOPE and PEG2000-DOPE, respectively). For visualization BODIPY FL-DHPE was incorporated into the liposomes at a non-fusogenic concentration. Liposomes were composed as follows: DOPE/DOTAP/non-aromatic molecule/BODIPY FL-DOPE 1/1/0.1/0.02 mol/mol. In a control sample, DiR was used at its fusogenic concentration to release fusion, and the fluorescence emission of BODIPY FL-DOPE was recorded in the green channel, as shown in Figure 3.7. This pattern revealed a homogenously distributed green fluorescence in the plasma membrane of CHO cells, identified as a membrane fusion pattern (control sample). In all other cases, green, speckled signals typical for endocytic processes were detected (Figure 3.7.). Liposomal size and zeta potentials, however, were similar to those of fusogenic liposomes (Table 3.2). Nevertheless, these liposomes were not able to fuse with CHO cells [92].

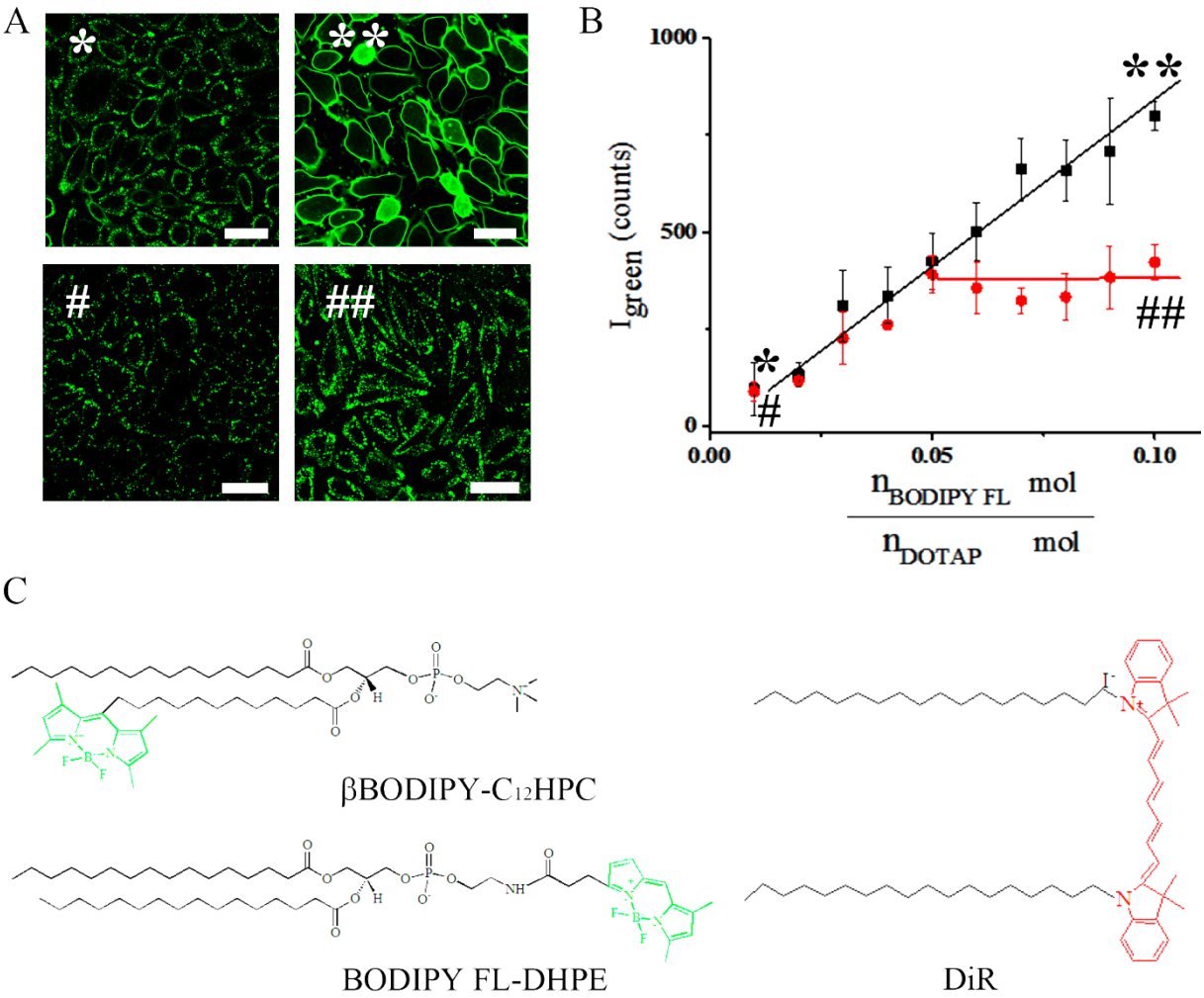

Figure 3.4. Importance of the aromatic component. (**A**) Fluorescence micrographs of CHO cells treated with liposomes containing BODIPY FL-DHPE as an aromatic component in fusogenic liposomes (FL) at 0.01 (*) and 0.1 (**) mol/mol concentration as well as in endocytotic liposomes (EL) at the same concentrations (# and ##). Scale bars, 20 µm. (**B**) The intensity of the green signal indicating fusion efficiency dependence on dye concentration in FLs (black) and ELs (red) determined by flow cytometry. The signal intensity median of the whole cell population was plotted vs. BODIPY FL-DHPE molar ratio to the cationic DOTAP amount in the liposomes ($n_{Bodipy\ FL\text{-}DHPE}/n_{DOTAP}$ mol/mol). Measurement points with standard deviations are shown as squares (FL) and circles (EL), respectively. Lines represent linear fits. (**C**) Molecular structures of the chain labeled lipid βBODIPY-C12HPC, the head labeled lipid BODIPY FL-DPHE, and the lipophilic membrane dye DiR incorporated in FLs as fluorescent components. The aromatic molecular parts are colored green and red, representing their spectral emissions [92].

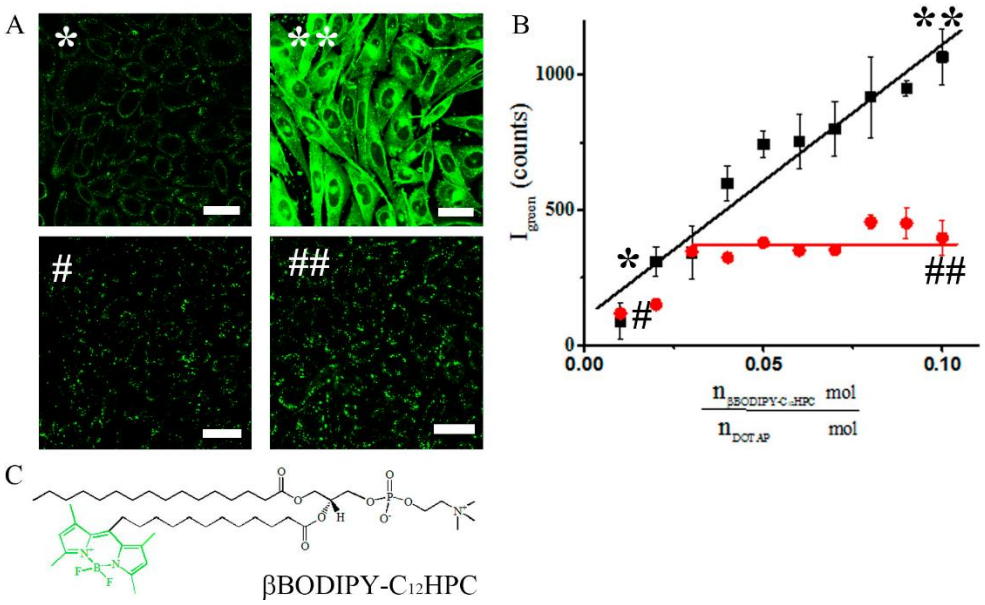

Figure 3.5. Importance of the aromatic component. (**A**) Fluorescence micrographs of CHO cells treated with liposomes containing βBodipy-C_{12}HPC as an aromatic component in FLs at 0.01 (*) and 0.1 (**) mol/mol concentration as well as in ELs at the same concentrations (# and ##). Scale bars, 20 µm. (**B**) The intensity of the green signal indicating fusion efficiency on dye concentration in FLs (black squares) and ELs (red circles). Measurement points with standard deviations are shown. Lines represent linear fits [92].

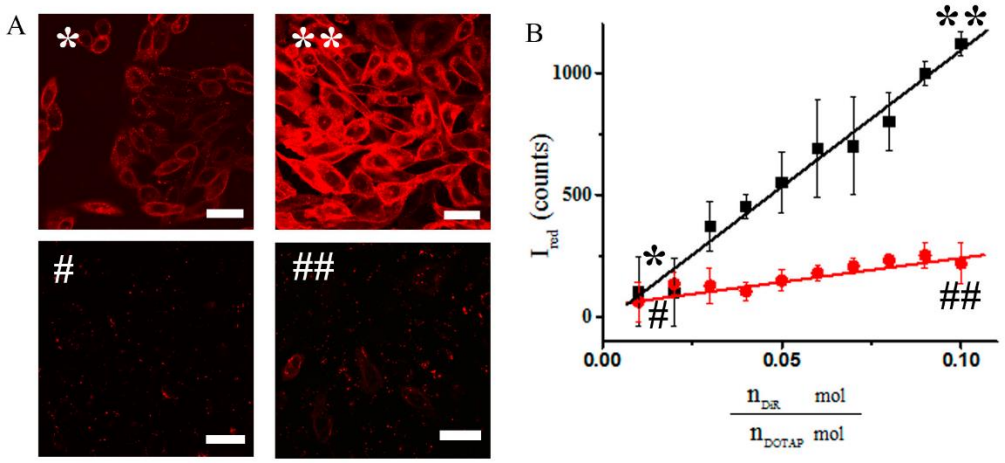

Figure 3.6. Importance of the aromatic component. (**A**) Fluorescence micrographs of CHO cells treated with liposomes containing DiR as an aromatic component in FLs at 0.01 (*) and 0.1 (**) mol/mol concentration as well as in ELs at the same concentrations (# and ##). Scale bars, 20 µm. (**B**) The intensity of the green signal indicating fusion efficiency on dye concentration in FLs (black squares) and ELs (red circles). Measurement points with standard deviations are shown. Lines represent linear fits [92].

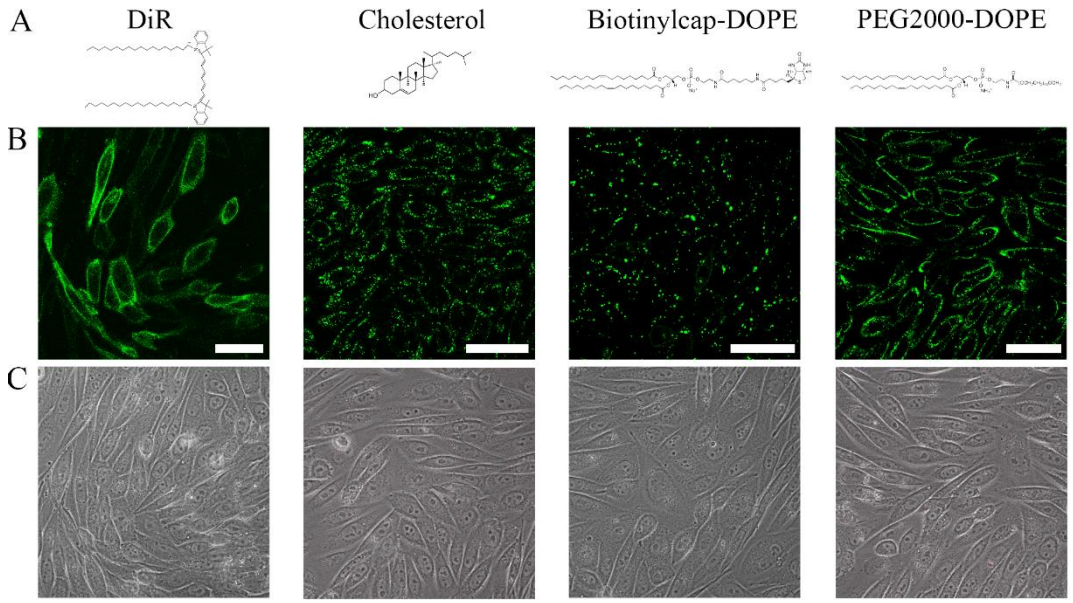

Figure 3.7. (**A**) Chemical structures of the aromatic DiR used as control, and the non-aromatic cholesterol, 1,2-dioleoyl-sn-glycero-3-phosphoethanolamine-*N*-(cap-biotinyl) (Biotinylcap-DOPE), and 1,2-dioleoyl-sn-glycero-3-phosphoethanolamine-*N*-[methoxy(polyethyleneglycol)-2000] (PEG2000- DOPE). (**B**) Fluorescence and (**C**) phase contrast images of CHO cells treated with liposomes containing non-aromatic instead of aromatic component, DOTAP as cationic lipid, DOPE as neutral lipid, and BODIPY FL-DHPE as a fluorescent tracer (0.1/1/1/0.02 mol/mol). In all cases, the green fluorescence of BODIPY FL-DHPE is seen as it was used at a non-fusogenic concentration. Scale bars, 50 μm [92].

Table 3.2. Characteristics of liposomes containing non-aromatic molecules as third components and DOPE/DOTAP/BODIPY FL-DHPE (0.1/1/1/0.02 mol/mol). The aromatic BODIPY FL-DHPE was used below its critical fusogenic concentration. Fusion efficiency of liposomes with CHO cells, as well as liposomal zeta potential (ζ)and hydrodynamic size (d) are listed. Average values of at least three independent measurements and their standard deviations are given [92].

Cationic Lipids	**Fusion eff. (s.d.) (%)**	**ξ (s.d.) (mV)**	**d (s.d.) (nm)**
Biotinylcap-DOPE	0 (0)	59 (7)	116 (29)
PEG2000-DOPE	8 (2)	64 (5)	165 (31)
Cholesterol	0 (0)	65 (4)	124 (19)
DiR	90 (7)	64 (3)	165 (2)

3.2.3. Changing the lipid composition of FLs: Importance of the neutral lipids

As shown above (Figure 3.2A), positively charged liposomes containing only a cationic lipid and an aromatic molecule, here a fluorescent dye, were able to fuse with the plasma membrane of mammalian cells. The additional helper lipid was not mandatory. However, neutral lipids can stabilize the formed liposomes and reduce cell toxicity. Therefore, the influence of neutral lipids on cellular uptake pathway and fusion efficiency was studied here. For this purpose, neutral lipids with different head groups, phosphocholine (PC), phosphoethanolamine (PE), and ceramide, with varying chain lengths from C14 to C22, as well as with saturated or unsaturated acyl chains were applied (see Table 3.3.). Liposome composition was neutral lipid/DOTAP/BODIPY FL-DHPE 1/1/0.1 mol/mol. Liposomal size and zeta potential distributions were determined as described above. Liposomes were incubated with CHO cells, as described in chapter 2.3.1. and their cellular uptake and fusion efficiency were monitored by fluorescence microscopy and flow cytometry. All results are presented in Table 3.3 [92].

3.2.3.1. Effect of the head group

All investigated liposomes containing lipids with a phosphoethanolamine (PE) or phosphocholine (PC) as a head group were analyzed by DLS, and any significant differences neither in size nor in zeta potential were found between PE and PC containing liposomes. Subsequently, the liposomal uptake mechanism and fusion efficiency were analyzed. The chemical structure of DOPC as an example for PCs and DOPE for PEs are shown in Figure 3.8A. Liposomes containing these lipids were incubated with CHO cells, and liposomal uptakes were visualized by microscopy. As shown in Figure 3.8B, in the case of DOPC, a speckle signal of the fluorescent BODIPY FL-DHPE was detected. This indicated endocytic cellular uptake [92].

In contrast, a homogenous green fluorescent signal was observed in the plasma membrane of CHO cells when liposomes contained DOPE as neutral lipid. This fluorescent pattern proved membrane fusion between liposomes and cell membranes. Additional flow cytometry analyses revealed much higher fusion efficiency in the case of liposomes containing DOPE (87%, s.d. 8%, n=3) compared to those with DOPC (7%, s.d. 3%). Similar trends were

noticed for all PCs and PEs tested (Table 3.3 and Figure 3.9) as well as for sphingolipids with small (ceramide) and large (sphingomyelin) head groups (Figure 3.10.) [92].

Table 3.3. Characteristics of liposomes containing different neutral lipids, DOTAP as cationic component, and BODIPY FL-DHPE as fluorescent component (1/1/0.1 mol/mol): head group, chain length, number of double bonds, and molecular shape of the neutral lipid component, fusion efficiency of liposomes with CHO cells, as well as liposomal zeta potential (ς), and hydrodynamic size (d). Efficiencies of endocytosis and fusion give together 100%. Average values of at least three independent measurements and their standard deviations are given [92].

Lipid	Head group	Chain lenght	Double bonds	Molecular shape	Fusion eff. (s.d.) (%)	ς (s.d.) (mV)	d (s.d) (nm)
DMPE	PE	14	0	conical	54 (15)	62 (4)	242 (14)
DPPE	PE	16	0	conical	69 (5)	60 (5)	140 (20)
DPaPE	PE	16	1	conical	93 (5)	69 (2)	109 (24)
DSPE	PE	18	0	conical	79 (9)	67 (8)	170 (14)
DOPE	PE	18	1	conical	87 (8)	68 (1)	124 (31)
LysoPE	PE	18	1	inv.conical	4 (2)	65 (3)	99 (4)
DMPC	PC	14	0	cylindrical	1 (1)	55 (12)	141 (64)
DPPC	PC	16	0	cylindrical	1 (0)	57 (5)	140 (55)
DPaPC	PC	16	1	cylindrical	2 (1)	65 (8)	205 (60)
DSPC	PC	18	0	cylindrical	48 (11)	50 (4)	141 (4)
DOPC	PC	18	1	cylindrical	7 (3)	58 (9)	176 (96)
DLiPC	PC	18	3	cylindrical	56 (17)	55 (3)	121 (15)
DEPC	PC	20	1	cylindrical	15 (3)	56 (7)	183 (103)
LysoPC	PC	18	1	inv.conical	3 (1)	45 (1)	131 (46)
SM	PC	18	1	cylindrical	3 (1)	58 (4)	120 (25)
CER	OH	18	1	conical	88 (9)	56 (9)	154 (10)

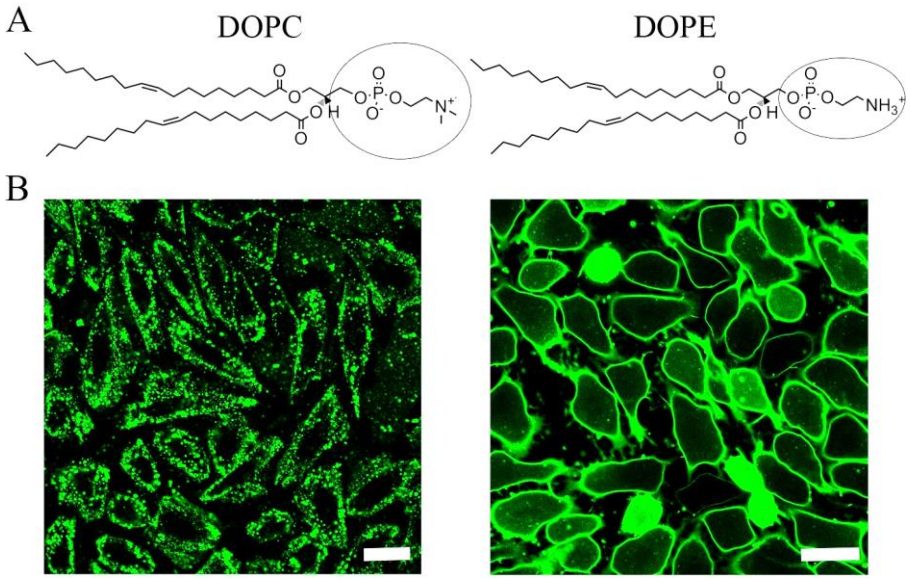

Figure 3.8. (**A**) Chemical structures of the neutral lipids 1,2-dioleoyl-*sn*-glycero-3-phosphocholine (DOPC) and 1,2-dioleoyl-*sn*-glycero-3-phosphoethanolamine (DOPE). (**B**) Fluorescence micrographs of CHO cells treated with liposomes containing DOPC (**left**) or DOPE (**right**) as neutral lipid, DOTAP as cationic lipid, and BODIPY FL-DHPE as fluorescent component (1/1/0.1 mol/mol). Scale bars, 20 μm [92].

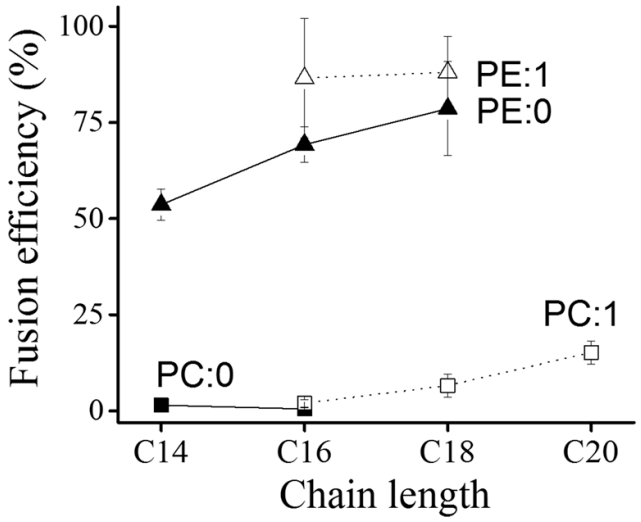

Figure 3.9. Liposomal fusion efficiency vs. neutral lipid component. Fusion efficiency of liposomes containing a neutral lipid component with different chain lengths and chain saturations as well as DOTAP and BODIPY FL-DHPE (1/1/0.1 mol/mol) was determined on CHO cells by flow cytometry. Symbols: saturated chains—filled symbols, unsaturated chains—open symbols, PCs—squares, PEs—triangles [92].

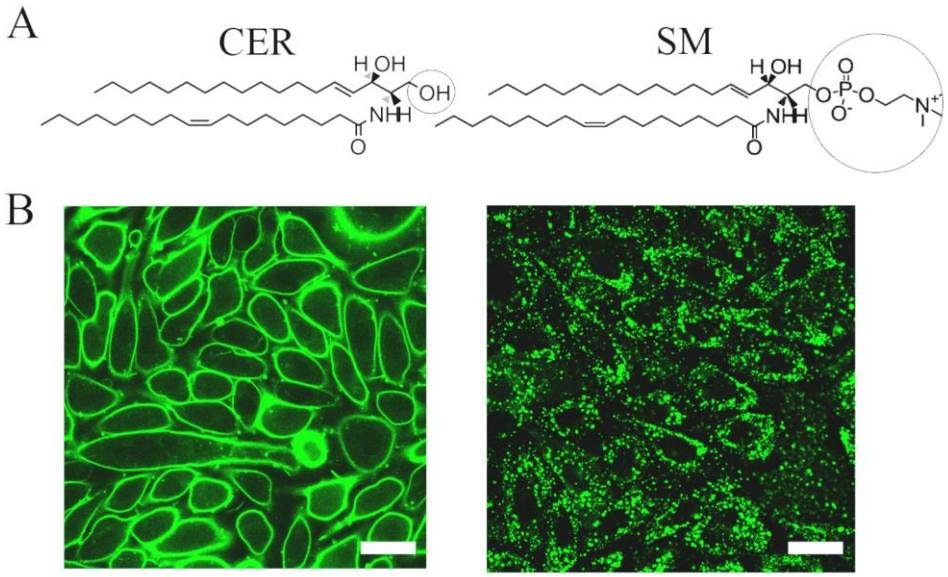

Figure 3.10. (**A**) Chemical structures of the neutral lipids N-oleoyl-D-erythro-sphingosine ceramide (CER) and N-oleoyl-D-erythro-sphingosylphosphorylcholine (SM). (**B**) Fluorescence micrographs of CHO cells treated with liposomes containing CER or SM as neutral lipid, DOTAP as cationic lipid, and BODIPY FL-DHPE as fluorescent component (1/1/0.1 mol/mol). Scale bars, 20 μm [92].

3.2.3.2. Effect of the chain length and saturation

The influence of acyl chain length and saturation of the neutral lipid were also investigated. Neutral lipids with 14, 16, 18, and 20 carbon atoms (C14–C20), with or without one double bound in the acyl chains were used, and the formed liposomes were characterized. Neither liposomal sizes nor zeta potentials varied systematically with chain length or saturation (Table 3.3). Additional flow cytometry analyses revealed that fusion efficiency increased with increasing acyl chain length. Moreover, chain unsaturation also increased the fusion ability of liposomes, especially in the case of neutral lipids with PE head groups (Figure 3.9) [92].

3.3. Discussion [92]

Cationic liposomes, in general, are known as carrier particles for DNA plasmids and are frequently used for transfection. The most popular formulation has been the equimolar mixture of the cationic lipid DOTAP and the neutral phospholipid DOPE. Its uptake pathway has been described as mostly endocytosis [163, 167]. Lipid molecules with an aromatic group added at around 5 mol % concentration to DOPE/DOTAP liposomes converted the endocytic uptake of liposomes to membrane fusion [9]. In recent years, many applications of such liposomes have been established. In this endeavor, it was noted that slightly varying liposomal compositions were needed to deliver different biological macromolecules to living cells [8, 10-12, 50, 165]. However, a systematic study about the influence of liposomal composition on membrane fusion efficiency has still been missing. Therefore, we set out to systematically explore the role of the different molecules constituting of FLs. To do so, all three components, the cationic lipid, the neutral helper lipid, and the chromophore, as well as their amount in the liposomes, were systematically varied, and the liposomes and their fusion ability were characterized [92].

3.3.1. Importance of the cationic lipid component

Cationic lipids, overall, are not considered as natural lipids. They have been synthesized for the particular application of transfection [153, 168-170]. Some of them are listed in Table 3.1. Based on their attractive electrostatic interactions with negatively charged nucleic acids (DNA, mRNA, siRNA, etc.), they can complex such molecules. The most prominent cationic lipid 1,2-dioleoyl-trimethylammonium-propane (DOTAP) has been analyzed here in combination with the neutral lipid DOPE and the fluorescently labeled BODIPY FL-DHPE with a varying concentration between 0 and 95 mol %. DOPE liposomes, in general, are classified as fusogenic due to the conical effective molecular shape of DOPE. Although Siegel and co-workers showed intermediate fusion states by electron microscopy [74], the fusogenicity of DOPE alone seems to be insufficient for fusion with complex biomembranes. With increasing cationic lipid concentrations, membrane fusogenicity increased (Figure 3.2.). Notably, a correlation between liposomal fusion ability and positive zeta potential, as is characteristic of the liposomal surface charge has been found [92].

To find out the role of the cationic lipids in membrane fusion in more detail, different cationic lipids were analyzed in the presence of a dye but without a neutral phospholipid like DOPE. We found marked differences in the fusion efficiencies of the respective liposomes,

although they all had similar zeta potentials (Table 3.1.). These results can be understood from the molecular shapes of the cationic lipids. According to Kumar, membrane lipids can be classified into three general shape categories: inverted conical, cylindrical, and conical [171]. The shape of a membrane lipid depends on the relative sizes of its polar head group and its apolar tails [52, 172]. If the head group and tails have similar cross-sectional areas, the molecule has a cylindrical shape. Lipids with a small head group and long unsaturated chains mostly have inverted conical shapes, while those chains occupy less area than their head groups when they are of conical shape. We realized that the cationic lipids DOTAP or DOTMA with conical molecular shape were able to fuse with the cellular plasma membrane with efficiencies above 90%, while lipids with more cylindrical shapes like DMTAP or DOEPC fused with an efficiency of only ca. 30% with the cell membrane. This value was reduced even further to 20% if the cationic lipid had a rather inverted conical shape like MVL5 [92].

As shown in Figure 3.3. and described by Chernomordik and Kozlov [45, 80, 81], the tendency of lipids to form curved layers correlates with their effective molecular shapes. Molecules with an effective conical shape tend to form monolayers with negative curvature, which is a necessary prerequisite for the formation of the fusion intermediate state [92].

3.3.2. Importance of the neutral lipid component

Most liposomal formulations used for gene delivery contain a neutral or helper lipid component besides the cationic lipids [173-175]. Figure 3.2A implies that the incidence of a neutral (or zwitterionic) lipid is not obligatory for membrane fusion events. On the other hand, it can profoundly influence the liposomal uptake, as reported by Braun *et al*. [7]. They have replaced DOPE by DMPC and detected endocytosis events instead of membrane fusion. This effect leads to the systematic investigation of the influence of the neutral lipid by changing lipid head group and acyl chains. Phosphocholine (PC), phosphoethanolamine (PE), and ceramide (CER) were tested. We observed increasing fusion abilities with decreasing head group size (Figures 3.9. and 3.10.) [92]. Liposomes containing PCs were almost unable to fuse, which generalizes the findings of Braun *et al.* [7]. Additionally, liposomes containing ceramide, the neutral lipid with the smallest head group tested in this study, fused so effectively that liposomal concentration had to be reduced to minimize toxicity (Figure 3.10.) [92]. These results underline previous studies describing PEs, in general, and DOPE especially, as fusogenic lipids [11,71].

3.3.3. Importance of the aromatic component

Three different fluorophores were compared to elucidate the role of the chromophore. These were BODIPY FL-DHPE, a head labeled lipid, βBODIPY-C_{12}HPC, a chain labeled lipid, and DiR, a lipid analog, whom chromophore most likely resides in the lipid backbone range [176]. All three lipids were able to induce membrane fusion above a distinct concentration of 2.5 mol % (1/1/0.05 mol/mol). It could be that the chromophores caus high local instabilities in the lipid membrane. These instabilities in a membrane probably initiate the formation of intermediate fusion phases, e.g., inverted-hexagonal or cubic phases [45, 73, 74]. Still, neither the mere presence of phospholipids with conical effective molecular shape but without net positive charge, e.g., DOPE, in combination with the aromatic chromophore, nor the presence of a cyclic component without a π-electron system is sufficient for fusion induction (Figure 3.2. and Figure 3.7.). The hypothesis is that electrostatic interaction between the positively charged lipids and the highly polarizable π-electron system of the fluorophores serves as additional interaction to finally induce fusion. It is supported by the fact that molecules with aromatic character, but weak emissions in the ultraviolet or visible spectral range like resveratrol or other polyphenols [8] are also able to induce membrane fusion while missing delocalized electrons as in, e.g., biotin, results in barely fusogenic liposomes [92].

Chapter 4

4. Influence of environmental conditions on the fusion of cationic liposomes with living mammalian cells

After a systematic investigation of the composition of the liposomes and its influence on fusion induction and efficiency, the systematic study of the impact of the environmental conditions has been done. This chapter aims to provide information on the influence of temperature, osmolality, pH, and ionic strength of the buffers on the fusion between liposomes and cell membrane.

The major of this chapter is published in Kolasinac et al., *Influence of environmental conditions on the fusion of cationic liposomes with living mammalian cells,* Nanomaterials, 2019, *9*(7), 1025.

4.1. Introduction [93]

Natural vesicles are formed by a lipid bilayer that contains a high density of membrane proteins. In the organism, vesicles occur in many forms, e.g., lysosomes, endosomes, or exosomes, and incessantly fuse with and split off the membranes of cellular organelles. Particularly well-studied cases of such processes are intracellular traffic [4, 44], exo- and endocytosis, or viral infection [20]. In all of the examples, proteins within the lipid bilayer or linked to it are directly involved in membrane fusion induction and in processes that lead or follow membrane coalescence [80, 177-179]. However, the merging of two membranes is the main event during membrane fusion, and it is defined by the lipid matrix. Besides the factors like the presence of proteins and lipid composition, as described in chapter 3, environmental conditions determine fusion ability. Zimmerberg and co-workers found out that osmotic gradient drives membrane fusion in a living cell system [14]. Akimov et al. showed for a protein-free model system that changes of the environmental pH in the physiologically relevant range between 4.0 and 7.5 notably affected the membrane fusion rate [180].

Liposomes are regularly investigated because of a number of their applications in pharmacology, biotechnology, and medicine. They are extensively used as carrier particles for many compounds, for example, nucleic acids, anti-cancer therapeutics, and proteins [181, 182]. The delivery of cargo can be significantly improved using the vesicle carriers that can fuse with the plasma membrane that is the first cellular barrier. Until now, used viral membranes containing membrane-associated peptides [19, 21, 182], and peptide-free cationic liposomes showed comparably high fusion efficiency [181].

In the previous chapter, an investigation of liposomal composition influence on membrane fusion is given. In this chapter, the systematic study of the role of temperature, osmolality, pH, and ionic concentration of the buffer on fusion efficiency of cationic liposomes with the cell membrane *in vitro* is described. Chinese hamster ovary (CHO) cells were again used as a typical model for mammalian cells. The liposomes were containing either phosphoethanolamine (PE) or phosphocholine (PC) as neutral compounds, DOTAP as positively charged lipid and an aromatic molecule. The compositions of the liposomes used in the experiments described here are given in chapter 2.2.2. (Table 2.2.). A structural investigation of liposomes was done by small angle neutron scattering (SANS) to study the correlation of thermotropic lipid phases with membrane fusion events.

4.2. Results [93]

As shown in the previous chapter, the lipid composition strongly influences the fusion ability and efficiency of liposomes. Liposomes can be taken up by cells by endocytosis or via membrane fusion depending on the lipid composition. Here, both kinds of liposomes were compared for the experiments of varying environmental conditions. The used liposomes always enclosed the positively charged lipid DOTAP, a neutral lipid (PE or PC), and a fluorescent dye at the molar ratio of 1/1/0.1 mol/mol. The liposomes containing PC as a neutral lipid are called endocytic liposomes (ELs) because they are usually taken up by endocytosis. The PE-containing liposomes favor the membrane fusion, and therefore, are called fusogenic liposomes (FLs). The chain lengths and chain saturation of neutral lipids were also varied here, having sixteen and eighteen carbon atoms (C16 or C18) and with (1) or without (0) unsaturation in the fatty acid chains. As an aromatic component, the Bodipy derivatives TopFlour coupled at the head or chain region to PE (TFPE) or DiR were used for liposomal preparation in the experiments. The IUPAC names, structures, and molecular weights of all the components are given in chapters 2.1.2-2.1.4.

To identify the different fluorescence signal patterns belonging whether to membrane fusion or endocytosis 3D confocal imaging of CHO cells were carried out upon treatment with liposomes composed of DOPE/DOTAP/TopFluor-head (1/1/0.1 mol/mol) (FLs) or DOPC/DOTAP/TopFluor-head (1/1/0.1 mol/mol). As shown in Figure 4.1A, FLs homogeneously stained the whole cellular plasma membrane while ELs was localized mainly on the cell surface without distributing in the membrane (Figure 4.1B) or internalized in the cell cytoplasm.

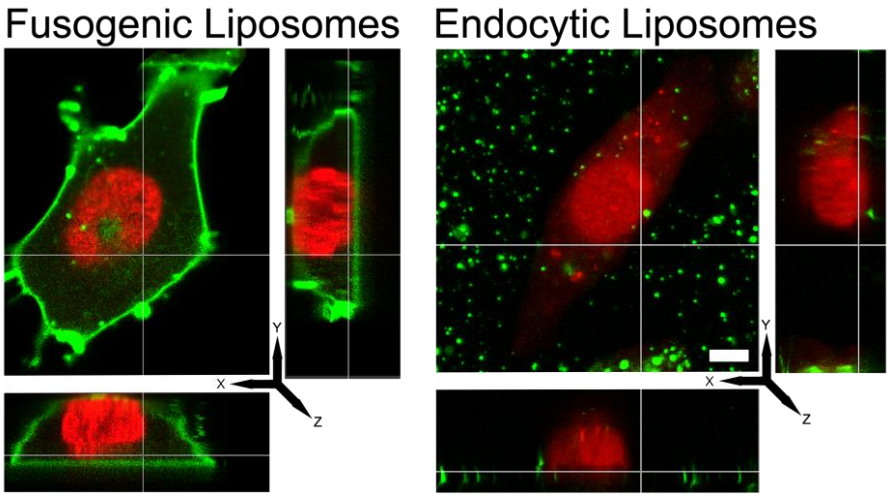

Figure 4.1. 3D-fluorescence micrograph of a CHO cell treated with fusogenic liposomes (FLs) DOPE/DOTAP/TFPE-head (1/1/0.1 mol/mol) (left), and endocytic liposomes (ELs) DOPC/DOTAP/TFPE-head (1/1/0.1 mol/mol) (right). Green: TFPE-head signal, red: nuclei staining with DRAQ5. Scale bar, 5 µm, applies to all [93].

4.2.1. Influence of temperature [93]

Liposomes with the composition described above were characterized by the physicochemical point of view, depending on the temperature. Here, fusogenic liposomes (FLs) showed a homogeneous population (see PDIs in Table 1) with a hydrodynamic diameter of about 115 nm and zeta potential of +50 mV without significant changes in the temperature range from 4°C to 37°C (Table 4.1). Within statistical significance, endocytic liposomes (ELs) gave similar results as FLs (Table 4.1).

Table 4.1. Temperature dependence of the hydrodynamic diameter, polydispersity index (PDI) and zeta potential of fusogenic (DOPE/DOTAP/TFPE-head 1/1/0.1 mol/mol) (FLs) and endocytic (DOPC/DOTAP/TFPE-head 1/1/0.1 mol/mol) (ELs) liposomes. Experiments are performed in a PBS buffer at physiological pH 7.4. Given are averages over three independent measurements and, in parentheses, their standard deviations [93].

Liposomal type	**Hydrodynamic diameter (nm) (s.d.)**			
	4 °C	**20 °C**	**30 °C**	**37 °C**
(FLs)	110 (13)	116 (13)	118 (16)	117 (13)
(ELs)	142 (42)	154 (68)	158 (71)	155 (72)
	PDI (s.d.)			
(FLs)	0.26 (0.06)	0.23 (0.02)	0.23 (0.02)	0.23 (0.02)
(ELs)	0.34 (0.12)	0.32 (0.11)	0.35 (0.11)	0.33 (0.11)
	Zeta potential (mV) (s.d.)			
(FLs)	59 (4)	48 (8)	51 (3)	43 (13)
(ELs)	68 (13)	64 (10)	56 (8)	58 (8)

Upon variation of temperature, two main trends were observed. Liposomes containing DOPE as neutral lipid homogenously stained the plasma membranes of CHO cells in the whole temperature range from 4 °C to 37 °C (see Figure 4.2A). Here, fusion efficiencies of above 80% were determined from fluorescent micrographs (Figure 4.2B). In contrast, liposomes containing a phosphocholine, here DOPC, as neutral lipid stuck to the cell surface resulting in an inhomogeneous dotted fluorescence pattern, and afterward were taken up by endocytosis. Internalization by endocytosis was detected in the whole temperature range from 4 °C to 37 °C (Figure 4.1B). Despite the temperature shock inherent in the procedure, no indications for cell stress were observed [93].

In all cases, the headgroup of the neutral lipid, PE, or PC, respectively, controlled fusion ability while chain length or saturation had much lower effects (Table 4.2). Moreover, the replacement of the head labeled lipid (TFPE-head) as the aromatic component with a chain labeled lipid (TFPE-chain) or a fluorescent lipid analog (DiR) did not significantly influence fusion efficiency of liposomes in the analyzed temperature range (Table 4.2) [93].

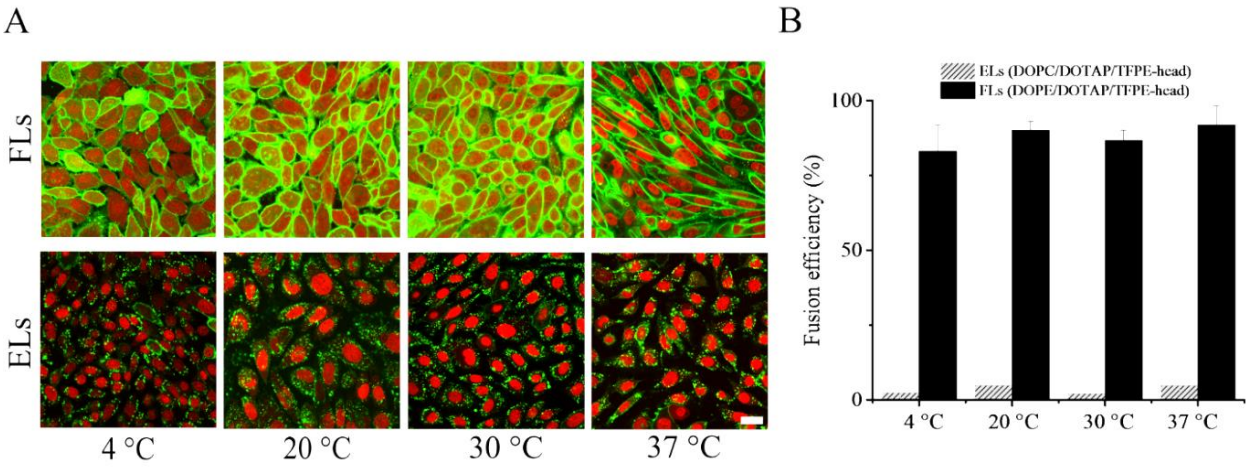

Figure 4.2. (**A**) Fluorescence micrographs of CHO cells treated with fusogenic liposomes (FLs) DOPE/DOTAP/TFPE-head (1/1/0.1 mol/mol), upper row, and endocytic liposomes (ELs) DOPC/DOTAP/TFPE-head (1/1/0.1 mol/mol), lower row. Green: TFPE-head signal, red: nuclei staining with DRAQ5. Scale bar, 20 µm, applies to all. Experiments were done in PBS buffer. (**B**) Fusion efficiencies. Whiskers indicate standard deviations of at least three independent experiments. In total, more than 1500 cells were analyzed at each condition [93].

4.2.2. Phase states of endocytic and fusogenic liposomes [93]

To find the reasons underlying the very different fusion behaviors of PC and PE containing cationic liposomes, small-angle neutron scattering (SANS) analyses were carried out at the physiologically most relevant temperature of 37 °C. As a cationic lipid DOTAP was used, and as a dye, BODIPY FL DHPE was incorporated. For these measurements, liposomes were formed in HEPES buffered heavy water (chapter 2.1.5.). With this method, multi-disperse, multilayered vesicles were formed. Experimental results and fits are shown in Figure 4.3 [93].

The scattering profile of DOPC containing liposomes was adequately modeled by a lamellar lipid phase, with a bilayer thickness of 42.7 Å. DOPE containing liposomes, however, displayed a different scattering pattern with a characteristic shoulder at Q=0.015 $Å^{-1}$. The latter indicated the presence of small scale features and could not be described by a lamellar phase alone. The best fit was achieved by a superposition of the scattering function of ellipsoid particles and a power law. The curve of DOPE containing liposomes could not be fitted with a cylinder model. This argues against the familiar hexagonal/inverted hexagonal phase of DOPE. Also, the combination of the cylinder model combined with ellipsoid failed to fit the curve [93].

Additionally, combinations of models (lamellar with ellipsoid and lamellar with power law) did not fit perfectly the specific region at Q=0.015 $Å^{-1}$. Apart from that part of the scattering curve, the lamellar model fitted nicely, which indicates the presence of bilayers. The observed power law contribution is a common occurrence if the probed length scale is smaller than the scattering object; it reflects local structures of the object [183]. Therefore, the good fit of this model combining a power law with an ellipsoid and separate fitting of most of the pattern by the lamellar model leads to the following hypothesis on the structure: We propose small micelle-like structures are embedded into the lipid bilayers. The best-fitting power-law exponent was 2.99, which can be attributed to large solid vesicles with a rough surface. The best-fitting ellipsoidal particles had a polar radius of 24.8 Å and an equatorial radius of 88.5 Å. The fitting functions are described in section 2.4.1.1 [93].

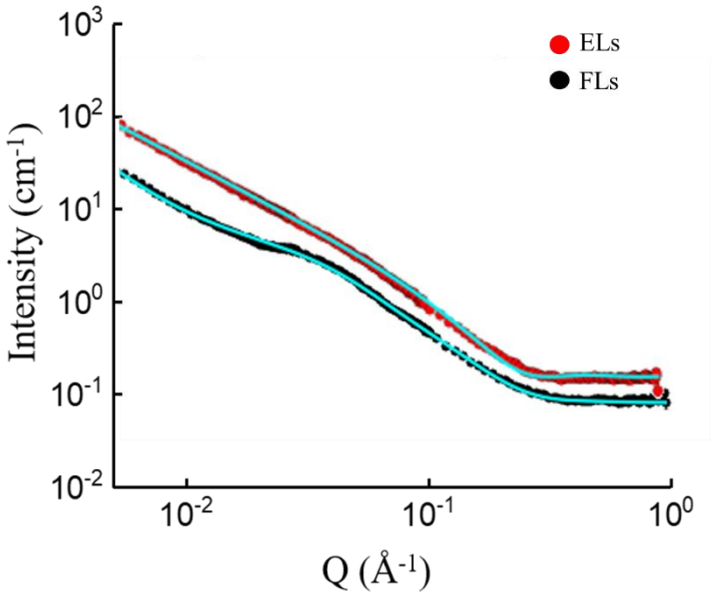

Figure 4.3. Scattering curves of DOPE/DOTAP/BODIPY FL DHPE (1/1/0.1 mol/mol) (black circles) liposomes and DOPC/DOTAP/BODIPY FL DHPE (1/1/0.1 mol/mol) (red circles) liposomes measured at 37 °C. Cyan lines indicate corresponding fits of a single measurement [93].

4.2.3. **Influence of ionic concentration** [93]

The influence of the surrounding ionic concentration was examined for various ionic strengths of the medium. For the purpose of these experiments, the lipid film was hydrated in ultrapure water instead of a buffer to avoid the presence of ions in the liposomal stock solution. Subsequently, liposomes were diluted in phosphate buffer (PB) at low total ion concentration (30 mM) or in phosphate buffer containing additional saline (PBS) at high total ion concentration (280 mM). The presence of ions drastically increased the hydrodynamic size of both types of liposomes (compare Tables 4.1 and 4.3) and reduced the liposomal homogeneity, as shown in Table 4.3. No significant differences were detected between FLs and ELs. The analysis of liposomal zeta potential showed a significant reduction in liposomal charges of both liposomes in the presence of PBS and a moderate decrease in PB buffer compared to glucose solutions [93].

Table 4.2. Temperature dependence of fusion efficiencies of liposomes containing the cationic lipid DOTAP, different neutral lipids, and TFPE-head as an aromatic molecule (1/1/0.1 mol/mol). Experiments are performed in a PBS buffer at physiological pH 7.4 and osmolality 280 mOsm/kg. Given are averages over three independent measurements and, in parentheses, their standard deviations [93].

Liposomal composition	**Fusion efficiency % (s.d.)**			
	4 °C	**20 °C**	**30 °C**	**37 °C**
C16(0)PE/DOTAP/TFPE-head	97 (1)	98 (2)	98 (1)	99 (1)
C16(0)PC/DOTAP/TFPE-head	0 (0)	0 (0)	0 (0)	0 (0)
C16(1)PE/DOTAP/TFPE-head	88 (11)	93 (6)	96 (3)	98 (2)
C16(1)PC/DOTAP/TFPE-head	13 (3)	16 (7)	14 (3)	17 (1)
C18(0)PE/DOTAP/TFPE-head	92 (6)	96 (1)	89 (9)	95 (5)
C18(0)PC/DOTAP/TFPE-head	37 (8)	38 (11)	47 (6)	62 (5)
C18(1)PE/DOTAP/TFPE-head	83 (9)	90 (3)	87 (4)	92 (6)
C18(1)PC/DOTAP/TFPE-head	3 (2)	5 (4)	2 (1)	4 (2)
C16(0)PE/DOTAP/TFPE-chain	84 (14)	93 (7)	99 (0)	97 (2)
C16(0)PC/DOTAP/TFPE-chain	4 (1)	0 (0)	0 (0)	0 (0)
C16(1)PE/DOTAP/TFPE-chain	84 (14)	94 (6)	99 (1)	97 (2)
C16(1)PC/DOTAP/TFPE-chain	15 (3)	14 (7)	13 (6)	15 (6)
C18(0)PE/DOTAP/TFPE-chain	97 (3)	89 (11)	98 (3)	93 (5)
C18(0)PC/DOTAP/TFPE-chain	53 (25)	59 (13)	69 (3)	55 (14)
C18(1)PE/DOTAP/TFPE-chain	81 (3)	83 (10)	94 (5)	90 (7)
C18(1)PC/DOTAP/TFPE-chain	3 (4)	0 (0)	3 (3)	0 (0)
C16(0)PE/DOTAP/DiR	86 (11)	94 (2)	92 (2)	97 (1)
C16(0)PC/DOTAP/DiR	7 (4)	3 (1)	9 (3)	5 (4)
C16(1)PE/DOTAP/DiR	95 (8)	86 (7)	97 (3)	97 (4)
C16(1)PC/DOTAP/DiR	4 (2)	5 (3)	1 (1)	1 (1)
C18(0)PE/DOTAP/DiR	95 (5)	98 (1)	85 (1)	94 (5)
C18(0)PC/DOTAP/DiR	16 (6)	17 (3)	12 (3)	13 (5)
C18(1)PE/DOTAP/DiR	80 (5)	98 (1)	99 (1)	94 (9)
C18(1)PC/DOTAP/DiR	4 (1)	1 (1)	8 (1)	2 (1)

Table 4.3. Ionic concentration and osmolarity dependence of the hydrodynamic diameter, polydispersity index (PDI) and zeta potential of fusogenic (DOPE/DOTAP/TFPE-head 1/1/0.1 mol/mol) (FLs) and endocytic (DOPC/DOTAP/TFPE-head 1/1/0.1 mol/mol) (ELs) liposomes. Given are averages over three independent measurements and, in parentheses, their standard deviations [93].

Liposomal type	**Hydrodynamic diameter (nm) (s.d.)**			
	PB (30 mOsm/kg)	**PBS (290 mOsm/kg)**	**Glucose (30 mOsm/kg)**	**Glucose (290 mOsm/kg)**
(FLs)	568 (145)	567 (102)	537 (71)	493 (157)
(ELs)	460 (277)	551 (357)	524 (296)	515 (357)
	PDI (s.d.)			
(FLs)	0.25 (0.05)	0.36 (0.13)	0.41 (0.09)	0.32 (0.01)
(ELs)	0.34 (0.07)	0.32 (0.11)	0.35 (0.11)	0.33 (0.11)
	Zeta potential (mV) (s.d.)			
(FLs)	36 (6)	28 (4)	72 (3)	69 (11)
(ELs)	62 (1)	36 (1)	78 (3)	73 (7)

The fusion efficiency of CHO cells with the same liposomes were also determined. Liposomes containing DOPE as neutral lipid diluted in PB buffer showed homogeneous membrane staining with high fusion efficiencies of approximately 90%. When the same liposomes were diluted in PBS buffer, they remained fusogenic with similar or slightly higher efficiencies (Figure 4.4). However, when DOPE was replaced with DOPC as a neutral component, liposomes displayed different behaviors depending on ionic strength. In PB, they fused with CHO cells with high efficiencies, while no significant fusion was detected in PBS (Figure 4.4). During the treatment with low ionic strength, buffer cells reacted to these hypo-osmotic conditions by membrane blebbing. Nevertheless, cells recovered immediately after the treatment without any signs of damage. The same trends were observed in the case of all investigated PE or PC containing liposomes irrespective of chain length or unsaturation of the neutral component or exchange of the aromatic component (Table 4.4) [93].

4.2.4. **Influence of osmolality** [93]

To test if the remarkably different behavior of DOPC containing liposomes in PB and PBS originated from electrostatic or osmotic effects, we varied osmolality by an uncharged solute. To this end, liposomes were prepared as previously described and diluted subsequently in a low (30 mOsm/kg) or a high (290 mOsm/kg) osmolality glucose solution without any addition of salts. Liposomes containing DOPE as neutral lipid diluted in 30 mOsm/kg or 290 mOsm/kg glucose solutions fused with the cell membrane of CHO cells with similar high efficiencies of approximately 80%. In contrast, liposomes containing DOPC as neutral

component again showed fusion efficiencies that depended on osmolality. If such liposomes were diluted in 30 mOsm/kg glucose solution, significant fusion (approx. 50% efficiency) was detected, while almost no fusion events were observed in 290 mOsm glucose solution (Figure 4.4 and Table 4.4) [93].

During the treatment with low osmolality buffer, cells reacted to hypo-osmotic conditions by membrane blebbing. Nevertheless, after the treatment, cells recovered immediately without any apparent damage. Upon exchange of neutral lipids with various chain lengths and saturation, our results indicated a universal trend valid for liposomes containing PE or PC neutral lipids, as shown in Table 4.4. PE-containing liposomes fused very efficiently with the plasma membrane of CHO cells independent of chain length, saturation, or the aromatic component (Table 4.4), while the fusion efficiency of PC containing liposomes strongly depended on buffer osmolality [93].

4.2.5. Influence of pH [93]

Both types of liposomes, fusogenic and endocytic, were characterized in the pH range of buffer between 5 and 9. Even though the PBS buffer capacity was not ideal in the whole range, all experiments were carried out in a PBS buffer, where the pH was adjusted to the appropriate value. FLs (DOPE/DOTAP/TFPE-head 1/1/0.1 mol/mol) as well as ELs (DOPC/DOTAP/TFPE-head 1/1/0.1 mol/mol) became less homogeneous with larger particles formed at higher pH values. Zeta potential of FLs was reduced when pH was increased while ELs did not show any pH-dependent changes (see Table 4.5) [93].

We also analyzed the pH dependence of membrane fusion of cationic liposomes with CHO cells at 37 °C. Liposomes containing phosphoethanolamine, here DOPE, as neutral lipid homogenously stained the cellular plasma membrane of CHO cells at all pH values in the range from 5 to 9. Throughout the whole range, tested fusion, efficiency exceeded 75% (Figure 4.5). In contrast, liposomes containing phosphocholine, here DOPC, as neutral lipid adhered to the cell surface, which resulted in an inhomogeneous speckled fluorescence pattern. In the whole pH range from 5 to 9, internalization by endocytosis was detected with a fusion efficiency rarely above 1% (Figure 4.5) [93].

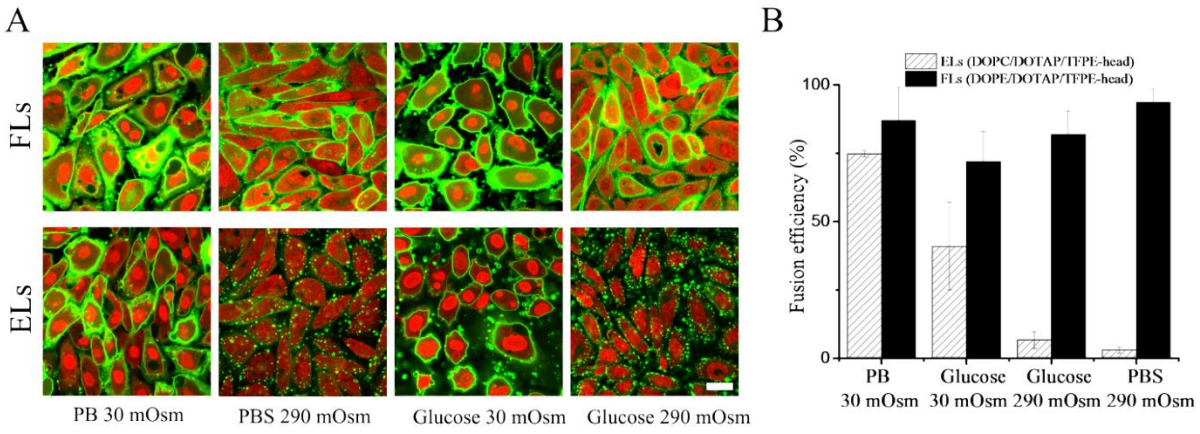

Figure 4.4. (**A**) Fluorescence micrographs of CHO cells after treatment with fusogenic (DOPE/DOTAP/TFPE-head 1/1/0.1 mol/mol) upper row, and endocytic liposomes, (DOPC/DOTAP/TFPE-head 1/1/0.1 mol/mol) lower row. Green: TFPE-head signal, red: nucleic staining with DRAQ5. Scale bar, 20 µm, applies to all. (**B**) Fusion efficiencies. Whiskers indicate standard deviations of at least three independent experiments [93].

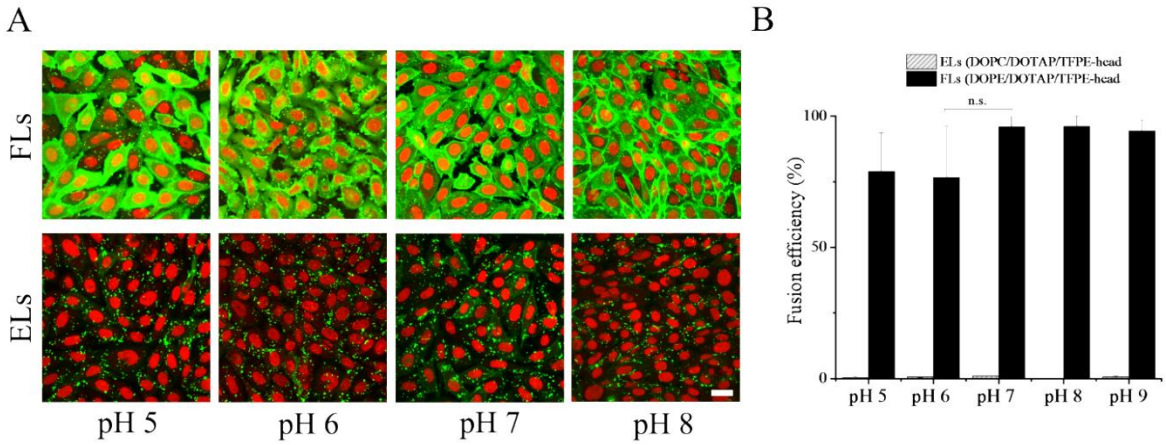

Figure 4.5. (**A**) Fluorescence micrographs of CHO cells after treatment with fusogenic (DOPE/DOTAP/TFPE-head, 1/1/0.1 mol/mol), upper row, and endocytic liposomes (DOPC/DOTAP/TFPE-head, 1/1/0.1 mol/mol), lower row, at different pH values. Green: TFPE-head signal, red: nucleic staining with DRAQ5. Scale bar, 20 µm, applies to all. (**B**) Fusion efficiencies. Whiskers indicate standard deviations of at least three independent experiments [93].

Table 4.4. Fusion efficiencies of liposomes containing the cationic lipid DOTAP, different helper lipids, and TFPE-head as a dye molecule (1/1/0.1 mol/mol) depending on the osmolality of the solution at 37°C. Average values of three independent experiments and their standard deviations are given [93].

Liposomal composition	**Fusion efficiency % (s.d.)**			
	PB (30 mOsm/kg)	**PBS (290 mOsm/kg)**	**Glucose (30 mOsm/kg)**	**Glucose (290 mOsm/kg)**
C16(0)PE/DOTAP/TFPE-head	98 (1)	85 (5)	95 (4)	79 (2)
C16(0)PC/DOTAP/TFPE-head	93 (6)	3 (3)	66 (2)	5 (4)
C16(1)PE/DOTAP/TFPE-head	86 (4)	99 (1)	98 (1)	99 (1)
C16(1)PC/DOTAP/TFPE-head	33 (3)	0 (0)	27 (7)	10 (2)
C18(0)PE/DOTAP/TFPE-head	76 (9)	89 (2)	82 (12)	98 (2)
C18(0)PC/DOTAP/TFPE-head	89 (3)	51 (1)	64 (8)	65 (8)
C18(1)PE/DOTAP/TFPE-head	87 (12)	94 (5)	72 (11)	82 (8)
C18(1)PC/DOTAP/TFPE-head	75 (1)	3 (1)	41 (16)	7 (3)
C16(0)PE/DOTAP/TFPE-chain	84 (13)	89 (10)	96 (2)	99 (1)
C16(0)PC/DOTAP/TFPE-chain	83 (5)	1 (0)	97 (3)	3 (2)
C16(1)PE/DOTAP/TFPE-chain	60 (16)	95 (8)	83 (2)	99 (1)
C16(1)PC/DOTAP/TFPE-chain	84 (8)	5 (2)	44 (22)	5 (1)
C18(0)PE/DOTAP/TFPE-chain	49 (9)	75 (13)	86 (9)	65 (10)
C18(0)PC/DOTAP/TFPE-chain	70 (16)	52 (6)	62 (5)	56 (6)
C18(1)PE/DOTAP/TFPE-chain	87 (12)	89 (5)	89 (6)	99 (1)
C18(1)PC/DOTAP/TFPE-chain	59 (3)	3 (1)	56 (3)	7 (3)
C16(0)PE/DOTAP/DiR	87 (10)	91 (9)	65 (12)	91 (7)
C16(0)PC/DOTAP/DiR	39 (10)	7 (2)	30 (8)	16 (2)
C16(1)PE/DOTAP/DiR	71 (29)	97 (3)	76 (20)	97 (2)
C16(1)PC/DOTAP/DiR	66 (13)	8 (6)	31 (13)	3 (2)
C18(0)PE/DOTAP/DiR	70 (5)	89 (5)	97 (1)	98 (1)
C18(0)PC/DOTAP/DiR	68 (12)	30 (8)	66 (8)	68 (11)
C18(1)PE/DOTAP/DiR	90 (5)	97 (3)	87 (1)	70 (9)
C18(1)PC/DOTAP/DiR	83 (2)	2 (1)	49 (5)	0 (0)

Table 4.5. pH dependence of the hydrodynamic diameter, polydispersity index (PDI) and zeta potential of fusogenic (DOPE/DOTAP/TFPE-head 1/1/0.1 mol/mol) (FLs) and endocytic (DOPC/DOTAP/TFPE-head 1/1/0.1 mol/mol) (ELs) liposomes. Experiments were performed in a PBS buffer titrated to the indicated pH. Given are averages over three independent measurements and, in parentheses, their standard deviations [93].

Liposomal type		**Hydrodynamic diameter (nm) (s.d.)**			
	pH 5	**pH 6**	**pH 7**	**pH 8**	**pH 9**
(FLs)	221 (193)	179 (124)	177 (36)	276 (52)	333 (117)
(ELs)	118 (24)	117 (19)	108 (23)	186 (22)	197 (16)
		PDI (s.d.)			
(FLs)	0.30 (0.10)	0.30 (0.11)	0.35 (0.11)	0.31 (0.21)	0.35 (0.21)
(ELs)	0.21 (0.03)	0.22 (0.02)	0.19 (0.02)	0.23 (0.09)	0.32 (0.18)
		Zeta potential (mV) (s.d.)			
(FLs)	42 (7)	39 (2)	36 (4)	26 (4)	15 (5)
(ELs)	35 (4)	36 (3)	38 (3)	35 (3)	38 (5)

4.3. Discussion [93]

The occurrence of membrane fusion in the absence of fusogenic peptides or proteins follows the steps described in Chapter 1.3, Figure 1.7. First, the membranes have to establish close contact, which requires the removal of firmly bound hydration water. Second, the locally disrupted outer membrane leaflets melt together and form hemifusion intermediate structures called membrane stalks. Third, the inner monolayers of lipids reorganize, which leads to pore opening and full membrane content mixing. All of the intermediate states are characterized by a well-defined free enthalpy that together defines the activation energy barrier for fusion. Some chemical compounds like ions, drugs, or specific lipids, as well as environmental conditions like temperature, pH, or osmolality of the buffer, can alter this barrier [184, 185]. In this chapter, the experiments studying the effect of environmental conditions were described [93].

Changes of the factors such as ionic concentration, pH, or buffer osmolality influence mostly the first step in the fusion process. The reduction of the water interface between the two membranes is essential for overcoming the first barrier. For example, ions bound to the membrane (Ca^{2+}, Na^{+}, and K^{+}) can modify their surface polarities, which in turn reduces the hydration-dependent intermembrane repulsion [186-189]. Nevertheless, the results presented here showed that in the case of FLs, fusion efficiency was not influenced by the ionic composition of the surrounding buffer suggesting the presence of another factor that is more important for the fusion process than the electrostatic interaction. Additionally, even though no differences were observed between size or zeta potential of fusogenic and endocytic liposomes, both types of liposomes were taken up by very different cellular pathways. Also, model membrane experiments by other groups demonstrated that a mixture of giant unilamellar vesicles (GUVs) with opposite surface charge (e.g., DOTAP containing liposomes and DOPS containing liposomes) aggregate readily and the lipid mixing efficiency does not change with increasing ionic strength [190, 191]. In the case of ELs, however, the ionic environment played a crucial role in membrane fusion induction. Here, an increased fusion efficiency was detected only at a low salt concentration (30 mOsm/kg). At physiological salt concentration (280 mOsm/kg), the fusion efficiency was reduced again. Additionally, the same trend was observed when buffer osmolality was changed from low to high (from 30 mOsm/kg to 280 mOsm/kg) by adding sugar instead of salt [93].

The only exception of PC containing liposomes showing elevated fusion capacity were liposomes with DSPC. This abnormal fusion behavior can be explained most likely by the special phase state of DSPC in the presence of phospholipids with notably different properties. For example, DSPC mixed with DMPC forms a non-ideal mixture with a broad gel-fluid coexisting region [192, 193]. It could be that such a phase coexistence, present in a DOTAP/DSPC mixture as well, is favorable for the fusion intermediates formation. Despite their extraordinary fusion ability, liposomes containing DSPC as neutral lipid showed the same trend of higher fusion efficiency at low osmolality and ionic strength buffer compared to the physiological conditions [93].

So, the increased membrane fusion can be caused by osmotic destabilization of CHO cells rather than by the ionic interaction between the liposomal and the cellular membrane. In this context, the following recent observation is of interest. Middel et al. showed that the repair of membrane lesions in skeletal muscle is accompanied by transiently increased concentrations of negatively charged phosphatidylserine lipids [194]. A similar mechanism might cause enhanced electrostatic attraction in osmotically stressed cell membranes [93].

When a close contact between the membranes is established, a transient disturbance of the bilayers structure and subsequent reorganization is required to overcome the energy barrier of the different steps and form hemifusion intermediates [194]. It has been proposed that the phase transition between a lamellar (L) and an inverted hexagonal (H_{II}) phase is essential for the formation of such intermediate structures [162, 196]. Several molecules have been described as initiators for the H_{II} phase, such as drugs, surfactants, and lipids, e.g., PEs. However, for the fusogenic lipid mixture containing DOPE, SANS measurements are not compatible with a H_{II} phase (Figure 4.3) but rather suggest a mixture of lamellar membranes with membrane compartments of high curvature (with polar radii of 24.8 Å and an equatorial radius of 88.5 Å, see Figure 4.3). Bulavin and Lebovka reported similar fitting models for rough interfaces of microcapsules carrying five or eight polymer bilayers [183]. The hypothesis, determined from these results, is that membrane fusion is facilitated by the observed micelle-like inclusions in the membranes. As they exhibit curvatures of similar magnitude than lipid H_{II} phases, we expect an effect of comparable size. Because the fusogenic lipid mixture studied here can fuse with any biological membrane [9] without the influence of environmental conditions, it is possible that the observed structures generally occur for this lipid mixture and induce the fusion. The lamellar phase, found for endocytic liposomes is considered as non-fusogenic [93].

For further understanding of the following steps of the membrane fusion, the molecular shapes of the lipids forming membranes have to be taken into respect [45]. Lipids with an effective cylindrical shape (e.g., PC) form bilayers with zero spontaneous curvature. Lipids obtaining inverted conical shapes lead to positive membrane curvature, while lipids with conical effective molecular shape (e.g., PE) form membrane structures with negative curvature. Such membranes are postulated as more fusogenic [197, 198]. The results obtained in the experiments presented in Chapter 3 support this hypothesis. In this study, liposomes containing PE were called fusogenic, and liposomes containing PC non-fusogenic or endocytic liposomes. Analogous behavior was found for the PE and PC containing liposomes when they were incubated with erythrocytes [199]. The fact that such fusogenic liposomes do not show any considerable differences in fusion efficiency with cells depending on the temperature, osmolality or ionic concentration of the buffer indicates that the presence of a 3D lipid phase formed by spherical membrane structures with high curvatures lowers the energy barrier for fusion significantly and thus efficiently facilitates membrane fusion. In this context, the additional structures within the vesicle lamellae can be considered a pre-formation of the intermediate structures that are necessary for the lamellar fusion. Since they are already present, they do not need to be formed during the fusion process and, therefore, lower the barrier for the occurrence of fusion [93].

Chapter 5

5. Understanding the Phase Behavior of Fusogenic Liposomes and its Correlation with the Fusion Ability

This chapter aims to report the specific phase behavior of fusogenic liposomes in comparison to commonly used endocytic liposomes. A probable lipid phase assigned to fusogenic liposomes and the hypothetical mechanism of fusion are presented.

5.1. Introduction

Vesicles are created through the self-assembly of amphiphilic lipid molecules that contain a hydrophilic headgroup and a hydrophobic hydrocarbon chain region. The forces governing the self-assembly of amphiphiles originate from the hydrophobic effect. These forces lead to the minimization of contact between lipid chains and hydration of hydrophilic head groups [69, 200, 201]. Upon addition of water, lipid molecules form spherically closed bilayers with long-range order, so-called vesicles, or liposomes. Changes in water content or temperature, lead to different molecular arrangements, called lyotropic and thermotropic mesomorphism, respectively. Among the degree of hydration and temperature, other environmental parameters such as pressure, ionic strength, and pH of the buffer or the lipid concentration itself can also strongly influence lipid polymorphism [202]. The term introduced here “liposomes” does not fully apply to the investigated so-called fusogenic liposomes presented in the thesis. The term is more applicable to endocytic liposomes.

The orientational order parameter of lipid chains or heads can attain several preferred values with various components [203]. Examples for this are the transition between phases with different hydrocarbon tilt angles. The molecular director may be arranged in distinct one-, two- or three- dimensional (1D, 2D, 3D) patterns. These patterns can be, for example, arranged in "ferroelectric" or "antiferroelectric" manner, have a herring-bone or ribbon-like appearance, etcetera [203]. Hence, even for a single class of (hydrated) lipids dozens of phases may exist, e.g., 1D lamellar phase with different sub-phases like liquid-crystalline phase, gel phase, or crystalline phase, the 2D hexagonal and inverted hexagonal phases, bicontinuous phase, and solution phases, and the 3D cubic and rhombohedral phases. The different phases can transform into each other via phase transition when some of the environmental conditions change. For example, when the temperature increases, the tails of the lipid molecules in the membrane bilayer become more disordered, inducing higher membrane fluidity. A decrease in temperature makes lipid tails more ordered and the membrane more rigid [204]. Such a phase transition is frequently called lipid melting or main transition [54, 55, 74, 184, 204-207].

Upon phase transitions, different intermediate membrane structures can form to reach the final molecular organization at the end. Siegel and colleagues showed that during the transformations from a 1D lamellar phase into a 3D inverted hexagonal, or bicontinuous cubic phase, intermediate membrane structures appear to be the same as those forming during the fusion of two lipid membranes [91, 185, 208, 209]. Therefore, the membrane fusion ability of a distinct membrane correlates with the fraction of the inverted phase-forming lipids.

The membrane composition, in general, is one of the most important factors influencing the phase behavior of lipid membranes and biological processes governed by lipid polymorphism. For example, in biological membranes composed of several hundreds of lipids, membrane segments with high curvature are prerequisites for processes such as membrane fusion, cell budding, or endosomes formation. Model membrane studies imposing curvature on a three-component lipid membrane have concluded that lipid heterogeneities are formed in the membrane, and they are centered around regions with curvatures that are energetically favorable [210-212]. Moreover, distinct lipid molecules with a conical molecular shape, (e.g. phosphatidylethanolamines) favor the formation of lipid phases with negative membrane curvatures, e.g. cubic phase or hexagonal phase facilitating membrane fusion as it has been shown in Chapter 3.

In this chapter, we are investigating liposomes with special ability for membrane fusion. As it was shown earlier, this so-called fusogenic liposomes (FLs) need cationic and neutral lipids with inverted conical molecular shapes and aromatic components at a distinct concentration for the best fusion induction. Additionally, the influence of some environmental parameters such as temperature, buffer composition, and its ionic strength, and the buffer osmolarity on the membrane fusion efficiency of those liposomes with biological membranes were also investigated. It has been shown in Chapter 4 that none of the parameters influenced the fusion ability of FLs significantly.

Hence, the identification of the mesomorphic phase of FLs was a logical step forward, understanding the extraordinary high fusion ability of those liposomes with the cellular membrane. Additionally, the phase behavior of conventional cationic liposomes taken up via endocytosis was also analyzed and compared to that of FLs. For this purpose, fluorescence microscopy, solid-state nuclear magnetic resonance (SSNMR), small-angle neutron scattering (SANS), freeze-fracture combined with scanning transmission electron microscopy (FF/STEM), cryo-transmission electron microscopy (cryo-TEM), and falling ball viscosimetry were used.

5.2. Results

5.2.1. Investigation of the phase transition of fusogenic liposomes by DSC

In order to understand the thermotropic behavior of fusogenic liposomes, differential scanning calorimetry (DSC) was applied. The technique measures heat flow related to transitions in materials as a function of temperature, as described in section Materials and Methods. Here, liposomes consisting of the neutral lipid DOPE or DOPC, the positively charged lipid DOTAP, and TFPE-head labeled as a dye (for IUPAC names of the lipids see sections 2.1.2-2.1.4) in a molar ratio of 1/1/0.1 (mol/mol) were investigated. The phosphocholine (PC) containing liposomes were called endocytic liposomes (ELs) due to their cellular uptake pathway, while the phosphoethanolamine (PE) containing liposomes were designated as fusogenic liposomes (FLs) based on their high membrane fusion ability. As a control sample with known phase transitions at 35 °C and 41 °C, DPPC liposomes were prepared. As shown in figure 5.1., neither FLs nor ELs showed a detectable change in Gibbs free enthalpy, or the transitions (if any) were broad and therefore DSC could not detect them in the tested temperature range between 5 °C and 65 °C while DPPC liposomes showed both the pre- as well as the main phase transitions at 35 °C and 41 °C, respectively.

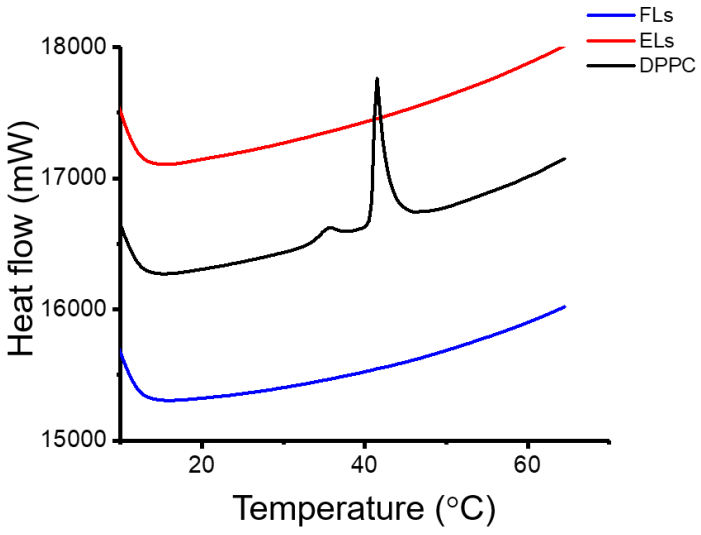

Figure 5.1. First heating curves of fusogenic and endocytic liposomes in the temperature range from 5°C to 65 °C. Neither FLs nor ELs had a phase transition detectable within the tested temperature range, or the associated enthalpy of transition is vanishingly small. DPPC liposomes, used as a control sample, showed both pre-transition at 35 °C and the main transition at 41 °C.

5.2.2. Investigation of the lipid phase behavior of fusogenic liposomes using solid-state NMR (SSNMR)

In this study, the SSNMR technique was applied to investigate the thermotropic phases of liposomes. Measurements were performed by **Dr. Erik Strandberg**, KIT, Karlsruhe (Germany). The composition of the liposomes is given in chapter 2.2.3 and table 2.4. A detailed description of the experiments' performance is given in section 2.9.2. The IUPAC names and structures of lipids used here are given in chapters 2.1.2-2.14. Samples, consisting of DOPC or DOPE as neutral lipid and DOTAP as cationic lipid and DiR, TFPE-head, or TFPE-chain as aromatic dyes, were tested in the temperature range from 4 °C to 60 °C.

As expected, DOPC liposomes showed a lamellar while DOPE liposomes a hexagonal phase lineshape throughout the temperature range (Figure 5.3.). The addition of one of the dyes (TFPE-head, TFPE-chain, or DiR) had a minor effect on phase formation in these two-component systems. The observed lipid phases of the DOPE/TFPE-head liposomes and DOPE/TFPE-chain liposomes showed a mixture of an isotropic/lamellar phase lineshape, and lamellar phase, at 4 °C, respectively. At higher temperatures, all the DOPE/dye liposomes showed hexagonal phase, and this behavior was mostly reversible by temperature changes. Both neutral lipids (DOPE and DOPC), in combination with the cationic lipid DOTAP at a molar ratio of 1/1, exhibited a lamellar phase lineshape (Figure 5.3).

In this study, liposomes made of DOPE/DOTAP/dye at the molar ratio of 1/1/0.1 mol/mol were reported as fusogenic (FLs), while liposomes containing DOPC instead of DOPE at the same molar ratio were described as endocytic liposomes (ELs). TFPE-head, TFPE-chain, and DiR (for IUPAC names and structures see chapter 2.1.4) were used as aromatic dye molecules. Figure 5.5 shows that FLs containing TFPE-head as a dye had a mixture of an isotropic and a lamellar phase lineshape at lower temperatures. The isotropic peak (narrow peak at 0 ppm) was dominant at higher temperatures in two out of three measurements.

Similar behavior was observed for DOPE/DOTAP containing DiR as an aromatic component. There, either the coexistence of a lamellar and an isotropic phase or pure lamellar or pure isotropic phase were observed (Figure 5.6). On another hand, the same lipid mixture having TFPE-chain as an aromatic component showed only the lamellar phase in the whole temperature range (Figure 5.7).

Additionally, SSNMR was performed to identify the lipid phase of liposomes lacking on an aromatic compound but containing a cyclic molecule coupled to a phospholipid, here Biotinylcap-PE. DOPE liposomes with Biotinylcap-PE showed hexagonal phase typical for PE

lipids. When DOTAP was added together with Biotinylcap-PE, both DOPC and DOPE liposomes (now three-component systems) showed a lamellar phase lineshape (Figure 5.4).

Liposomes consisting of DOPE/DOPC (3/1 mol/mol %) mixture have been described by Siegel and co-workers as fusogenic with an isotropic phase as a characteristic phase [220]. Therefore, this two-component system was also tested by SSNMR. At low temperatures around 10 °C, a lamellar phase was observed, with a small amount of isotropic phase. Up to 30 °C, the fraction of the isotropic phase increased. At 35 °C and higher temperatures, the lamellar phase disappeared, while traces of the hexagonal phase appeared. When the temperature was reduced again, the hexagonal phase faded, and the isotropic phase remained, showing irreversibility in the phase behavior. As shown in Figure 5.8, SSNMR confirmed the isotropic phase lineshape. However, these liposomes did not fuse with the cell membrane of CHO cells even if the fusogenic concentration of the dye (TFPE-head, 5 mol%, Figure 5.9) was added.

When instead of DOPE as a neutral lipid, DOPC was used (endocytic liposomes, ELs) the characteristic lineshape of the lamellar phase was mainly observed independently on the used dye (Figures 5.10-5.12) except in the case of TFPE-head, where an isotropic peak appeared in coexistence with the dominant lamellar phase (Figure 5.10). The summary of the appearing phases corresponding to the liposomal composition is given in Table 5.1. The striking observation of the irreproducibility of the measurements is typical for such liposomal systems, and it will be discussed in the discussion part of this chapter.

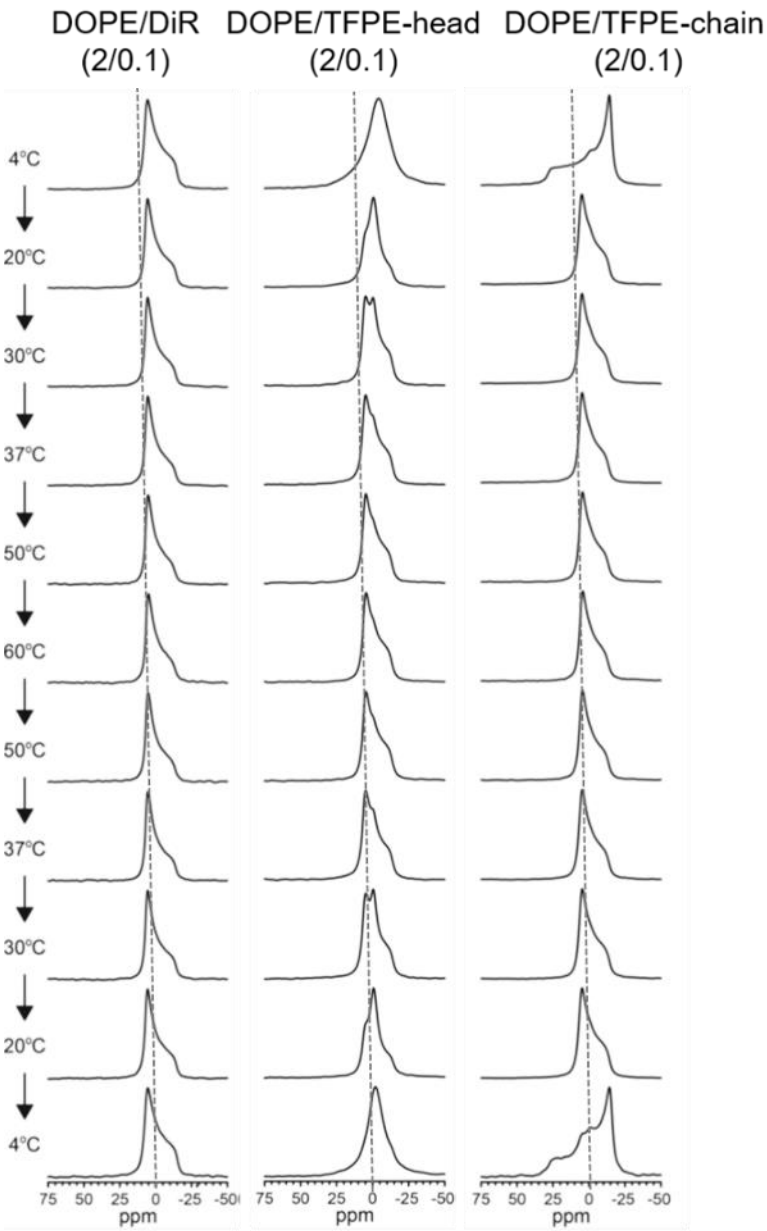

Figure 5.2. ^{31}P-NMR spectra at temperatures between 4 °C and 60 °C. DOPE/DiR (2/0.1) liposomes showed hexagonal phase at all temperatures. DOPE/TFPE-head (2/0.1) showed a broad isotropic peak at 4 °C; a mixture of isotropic and hexagonal phase is observed at 20 °C and 30 °C and above 50 °C a hexagonal phase. The isotropic peak returned upon cooling. In the DOPE/TFPE-chain sample, a lamellar/hexagonal phase mixture was observed at 4 °C. Above 20 °C, only a hexagonal phase was detected. The lamellar phase returned upon cooling to 4 °C. The dotted line indicates the position of the isotropic peak.

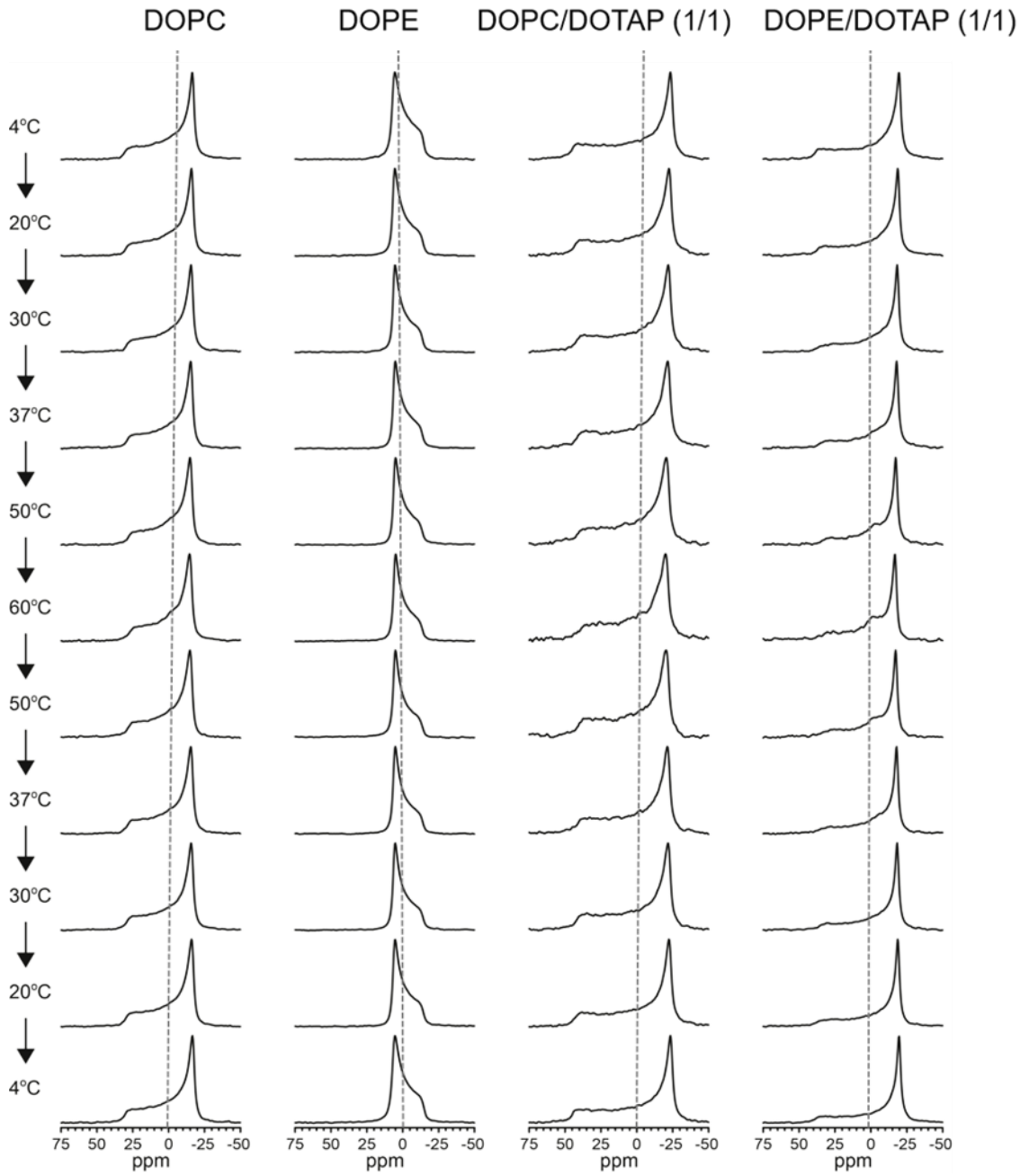

Figure 5.3. ^{31}P-NMR spectra of liposomes without any dye, at temperatures between 4 °C and 60 °C. DOPC forms a lamellar phase, while DOPE forms a hexagonal phase at all temperatures. The addition of the cationic lipid DOTAP (DOPC/DOTAP and DOPE/DOTAP (1/1 mol/mol)) induced the formation of a lamellar phase at all temperatures. The dotted line indicates the position of the isotropic peak.

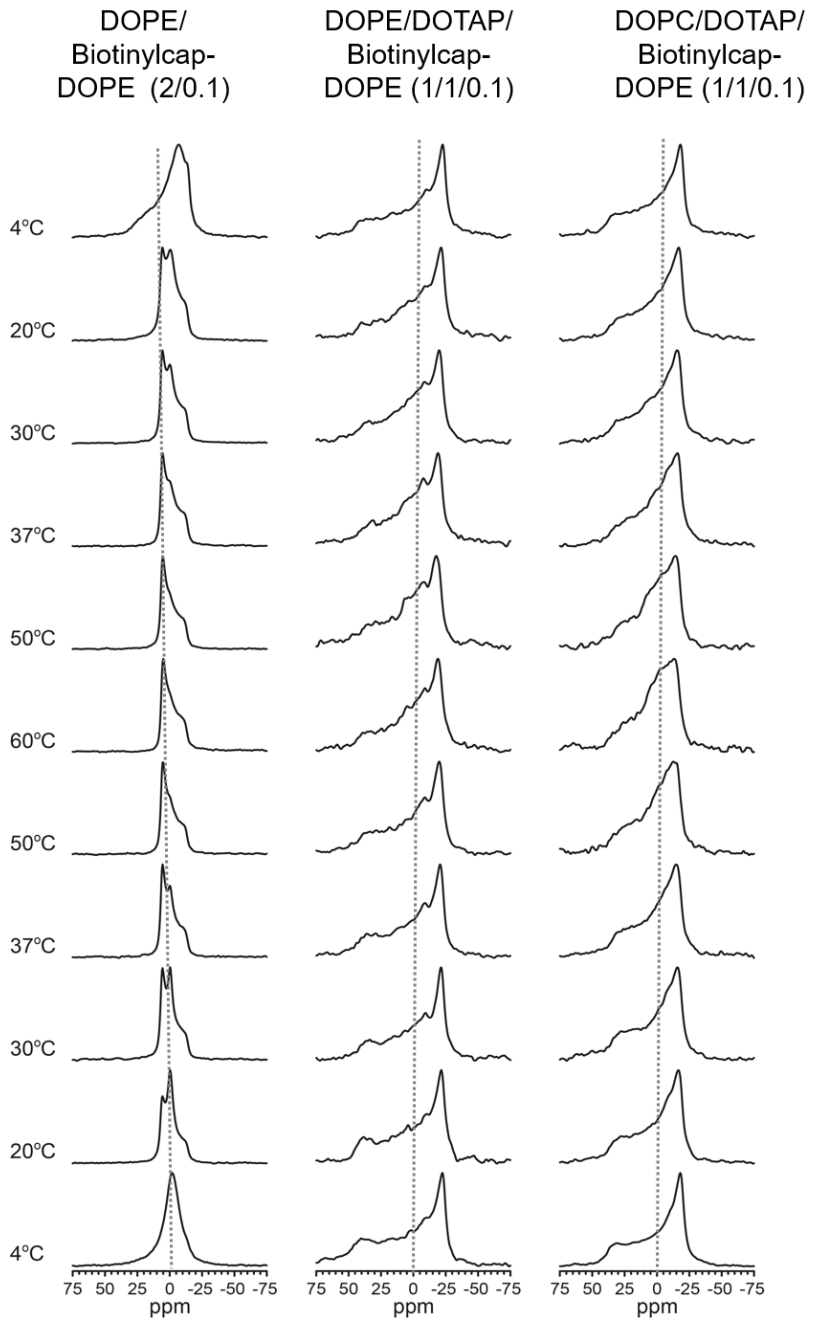

Figure 5.4. ^{31}P-NMR spectra of liposomes containing Biotinylcap-DOPE instead of a dye, at temperatures between 4 °C and 60 °C. DOPE/Biotinylcap-DOPE (2/0.1 mol/mol) formed a mixture of lamellar and isotropic phase at 4 °C. At 20 °C and higher temperatures, a hexagonal phase mixed with isotropic phase (narrow peak at 0 ppm) was observed, which disappears above 50 °C. DOPC/DOTAP/Biotinylcap-DOPE (1/1/0.1 mol/mol) and DOPE/DOTAP/Biotinylcap-DOPE (1/1/0.1) formed lamellar phase at all temperatures. The dotted line indicates the position of the isotropic peak.

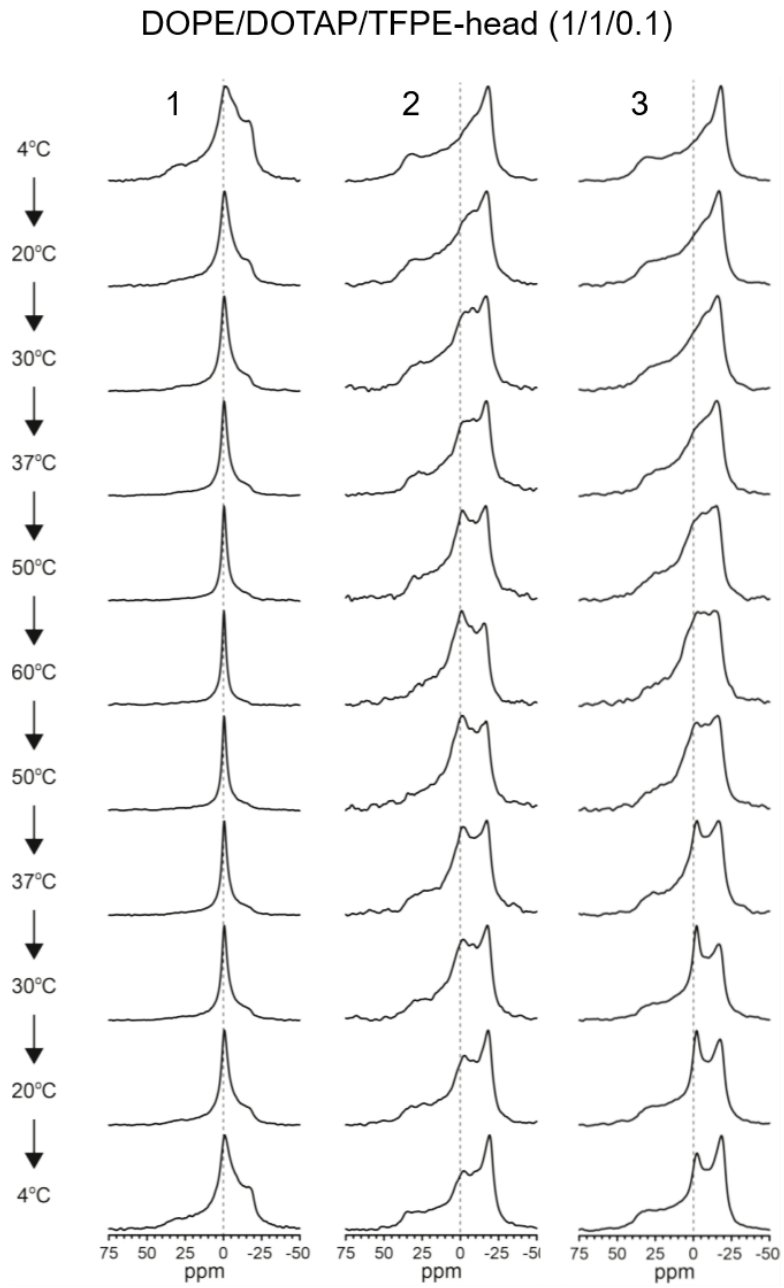

Figure 5.5. ^{31}P-NMR spectra of DOPE/DOTAP/TFPE-head (1/1/0.1 mol/mol) liposomes at temperatures between 4 °C and 60 °C. The figure shows three repetitions of the same sample prepared independently. The first repetition showed the simultaneous presence of a lamellar phase and an isotropic phase at 4 °C. From 20 °C on, the isotropic phase dominated the spectrum. This phase behavior was reversible. The second repetition revealed the coexistence of a lamellar phase, dominant at lower temperatures, and the isotropic phase, dominant at higher temperatures. The third repetition showed the presence of a lamellar phase at lower temperatures. At 50 °C, an isotropic phase appeared and remained upon cooling. The dotted lines mark the isotropic peak position.

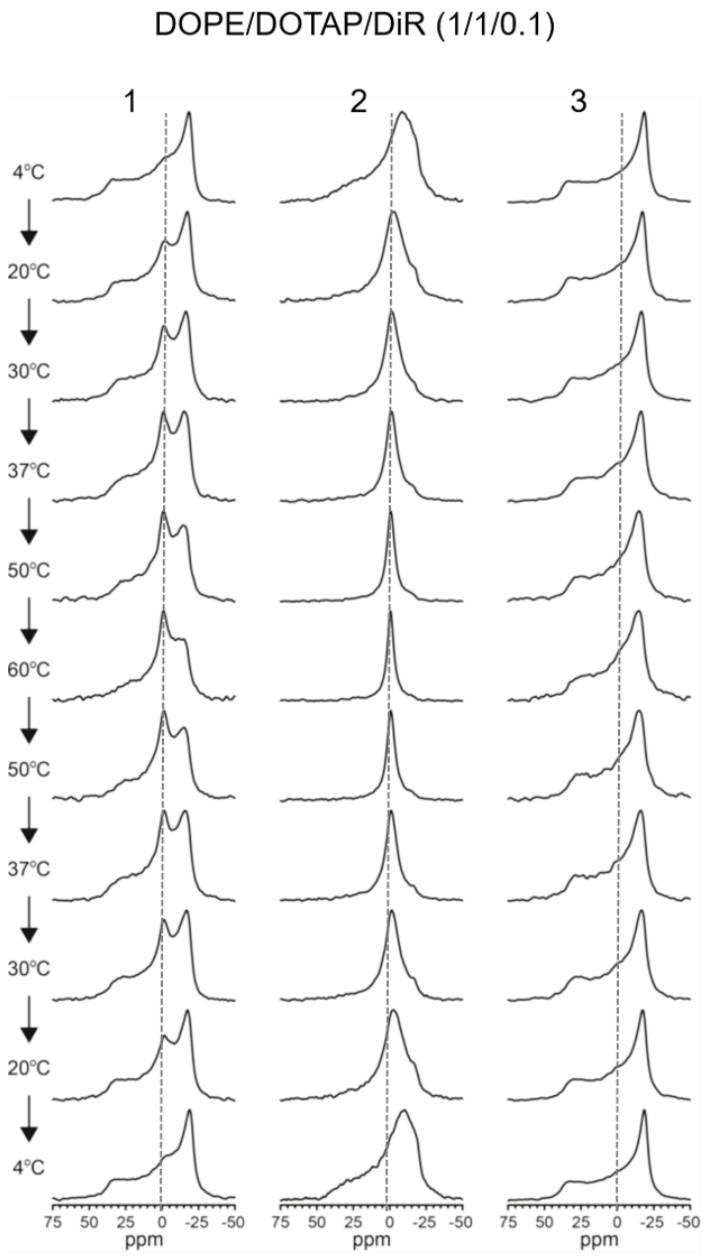

Figure 5.6. ^{31}P-NMR spectra of DOPE/DOTAP/DiR (1/1/0.1 mol/mol) at temperatures between 4 °C and 60 °C. The figure shows three repetitions of the same sample prepared independently. The first repetition indicated a lamellar phase at 4 °C. An isotropic phase appeared at 20 °C, its presence increased with increasing temperature and decreased again at lower temperatures. The second repetition showed a lamellar phase at 4 °C, but an isotropic phase appeared at 20 °C and dominated the spectrum at higher temperatures. The third repetition revealed only a lamellar phase at all temperatures. The dotted line indicates the position of the isotropic peak.

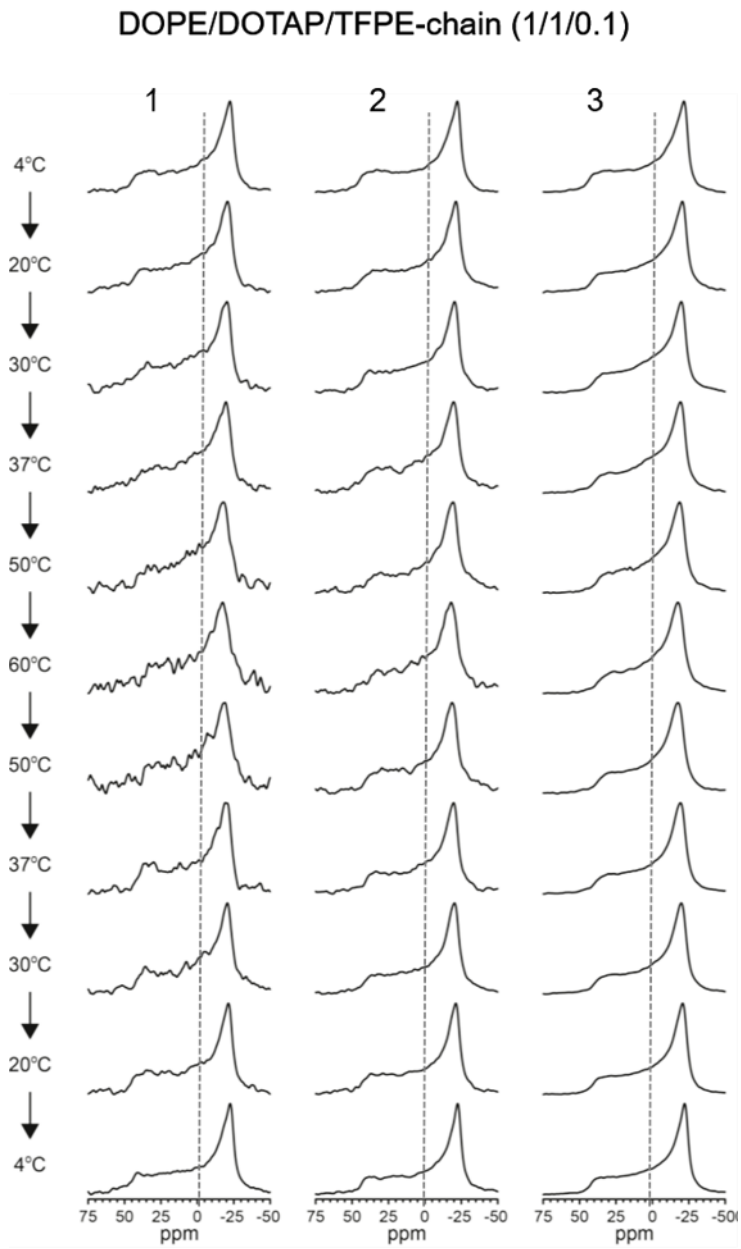

Figure 5.7. ^{31}P-NMR spectra of DOPE/DOTAP/TFPE-chain (1/1/0.1 mol/mol) liposomes at temperatures between 4 °C and 60 °C. The figure shows three repetitions of the same sample prepared independently. A lamellar phase was observed in all repetitions at all temperatures. The signal to noise ratio of the first measurement was lower compared to that of the following measurements because of a low number of collected scans. The dotted line indicates the position of the isotropic peak.

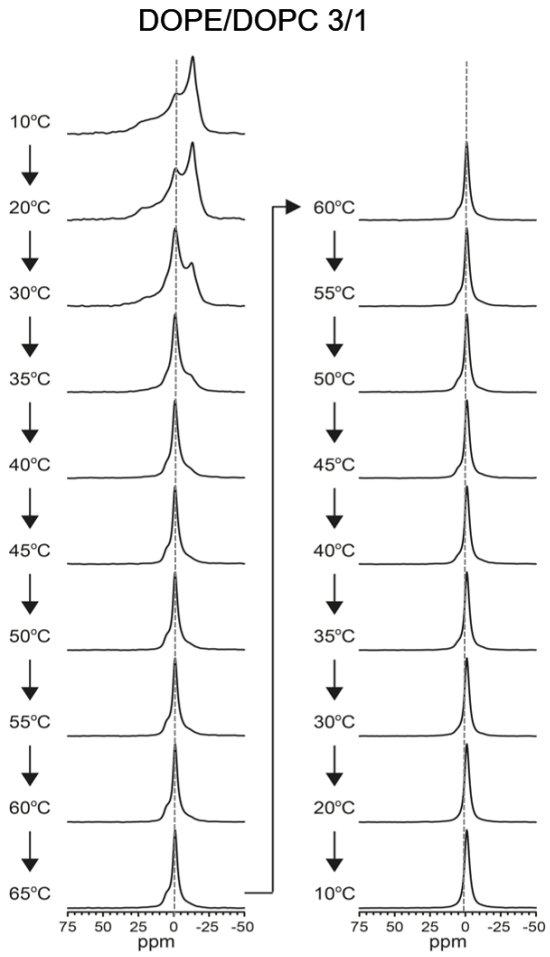

Figure 5.8. ^{31}P-NMR spectra of DOPE/DOPC (3/1 mol/mol %) liposomes at temperatures between 10 °C and 65 °C. At 10 °C, a lamellar phase was observed, with a small amount of isotropic phase. Up to 30 °C, the fraction of the isotropic phase increased. At 35 °C and higher temperatures, the lamellar phase disappeared, while traces of the hexagonal phase appeared. When the temperature was reduced again, the hexagonal phase faded, and the isotropic phase (dotted line) remained.

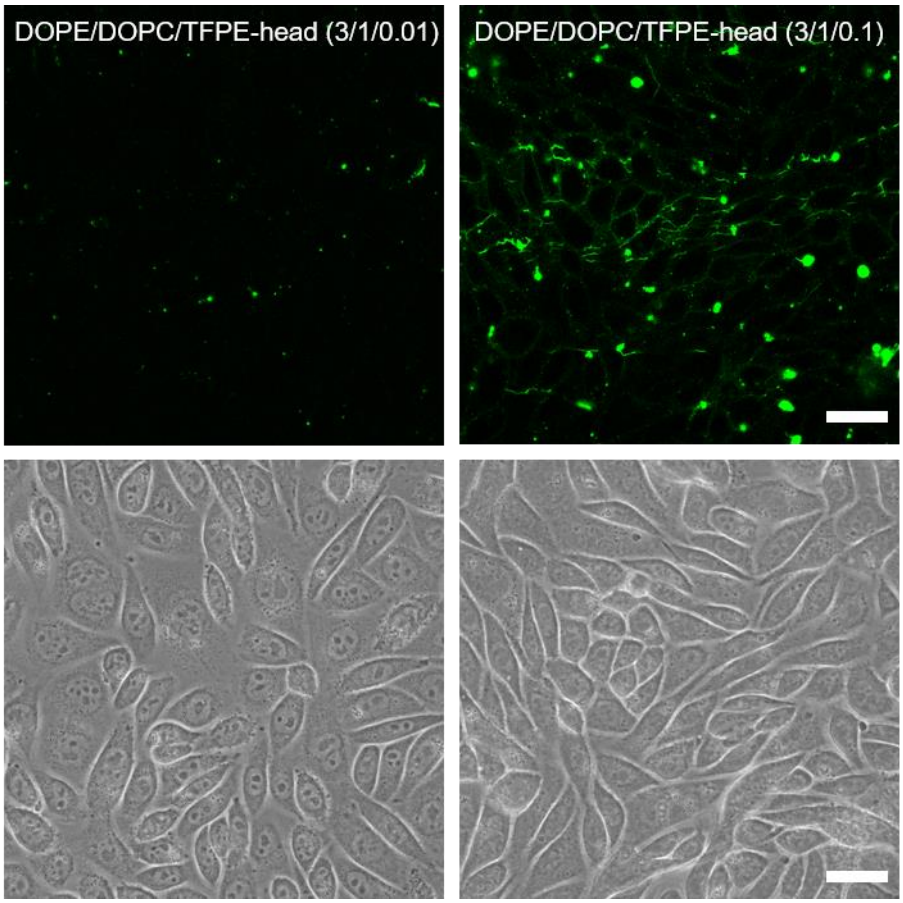

Figure 5.9. Fluorescence micrographs of CHO cells after treatment with DOPE/DOPC/TFPE-head liposomes at molar ratio 3/1/0.01 (left) and 3/1/0.1 (right). Green fluorescent channels (upper raw), as well as phase contrast (lower raw), are shown. Scale bars, 20 μm, applies to all micrographs.

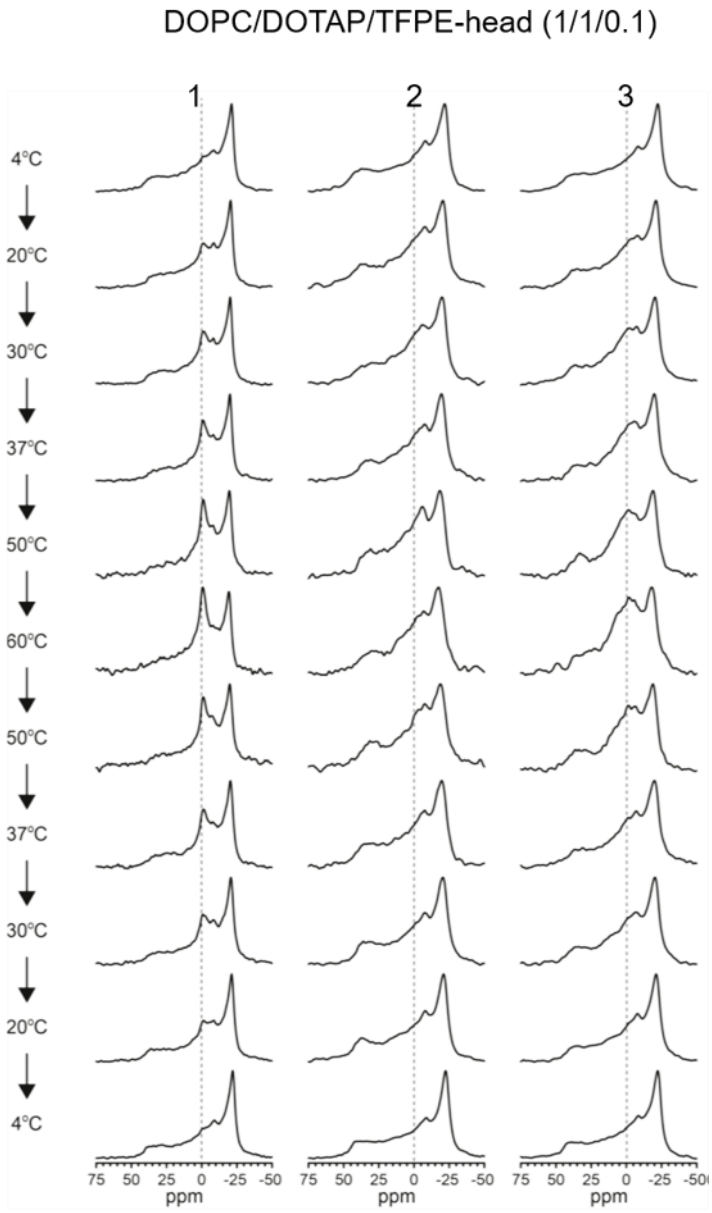

Figure 5.10. ^{31}P-NMR spectra of DOPC/DOTAP/ TFPE-head (1/1/0.1 mol/mol) at temperatures between 4 °C and 60 °C. The figure shows three repetitions of the same sample prepared independently. The first repetition revealed a lamellar phase with a small amount of isotropic phase, which increased with temperature and vanished upon cooling. The second measurement indicated only the lamellar phase at all temperatures with a small peak around 8 ppm. The third experiment showed mostly the lamellar phase with the simultaneous presence of the isotropic phase and a minor peak at 8 ppm. The dotted lines mark the isotropic peak position.

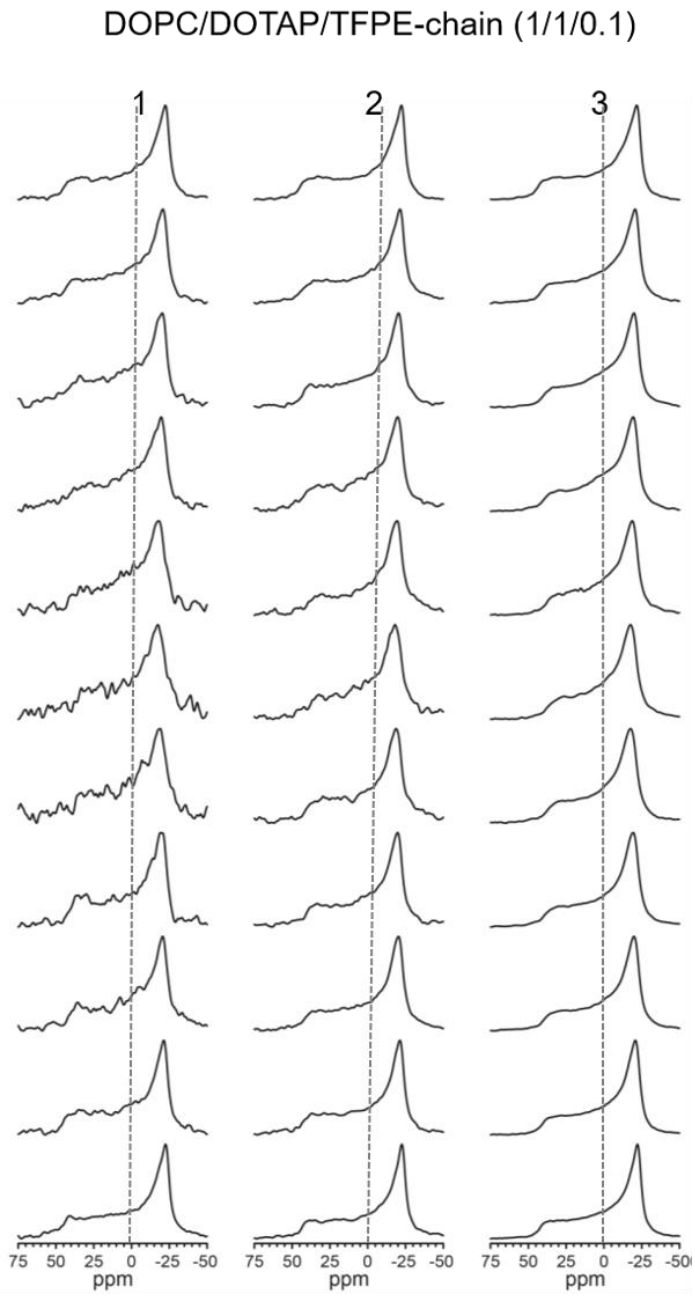

Figure 5.11. ^{31}P-NMR spectra of DOPC/DOTAP/ TFPE-chain (1/1/0.1 mol/mol) liposomes at temperatures between 4 °C and 60 °C. The figure shows three repetitions of the same sample prepared independently. A lamellar phase was observed in all repetitions at all temperatures. The signal to noise ratio of the first measurement was lower in comparison to the following measurements because of the lower number of collected scans. The dotted line indicates the position of the isotropic peak.

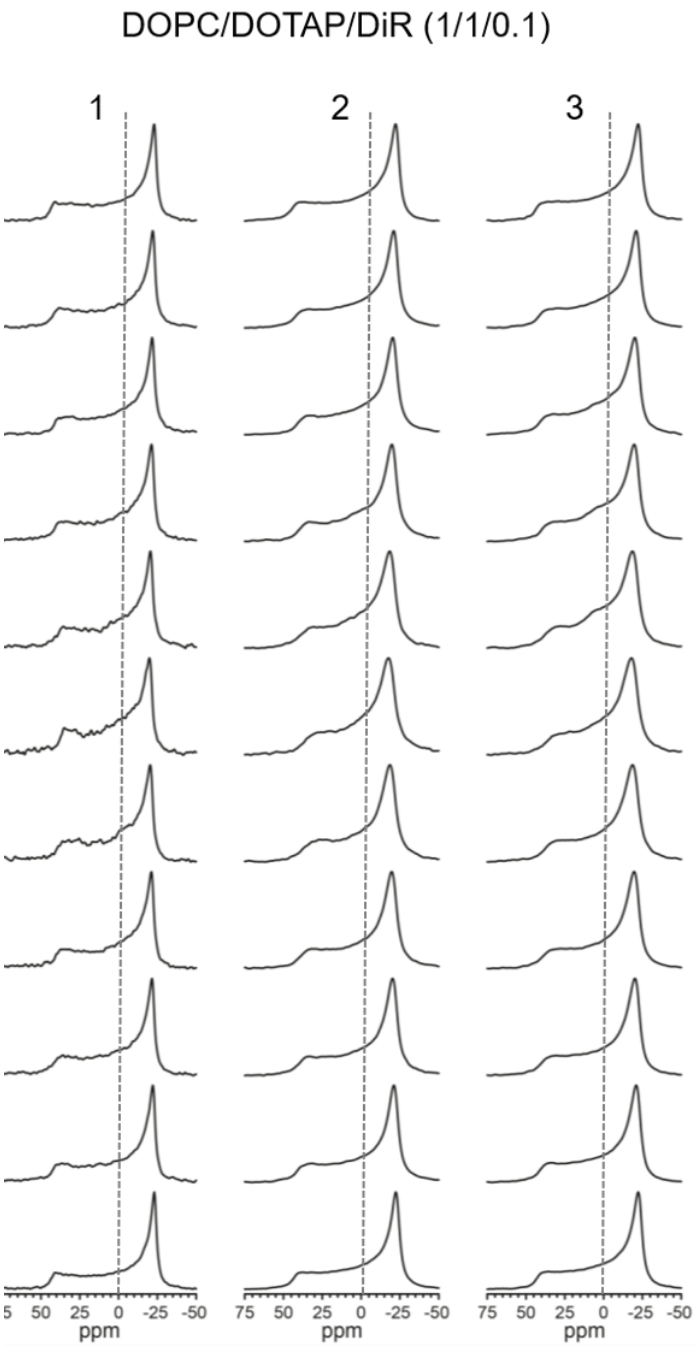

Figure 5.12. ^{31}P-NMR spectra of DOPC/DOTAP/ DiR (1/1/0.1 mol/mol) at temperatures between 4 °C and 60 °C. The figure shows three repetitions of the same sample prepared independently. A lamellar phase was observed in all repetitions at all temperatures. The dotted line indicates the position of the isotropic peak.

Table 5.1. Summary of liposomal phases seen by SSNMR and the correlation of phases with liposomal fusogenicity with the cell membrane.

Liposomal mixture	Fusogenic on CHOs	Phase, indicated by SSNMR	Repeatability	Reversibility
DOPE/DiR (2/0.1)	No	Hexagonal	Not tested	Yes
DOPE/TFPE-head (2/0.1)	No	Hexagonal/isotropic	Yes	Yes
DOPE/TFPE-chain (2/0.1)	No	Hexagonal/lamellar	Yes	Yes
DOPC	No	Lamellar	Not tested	Yes
DOPE	No	Hexagonal	Not tested	Yes
DOPC/DOTAP (1/1)	No	Lamellar	Not tested	Yes
DOPE/DOTAP (1/1)	No	Lamellar	Not tested	Yes
DOPE/Biotynil (2/0.1)	No	Lamellar/Isotropic	Not tested	No
DOPE/DOTAP/Biotynil (1/1/0.1)	No	Lamellar	Not tested	Yes
DOPC/DOTAP/Biotynil	No	Lamellar	Not tested	Yes
DOPE/DOTAP/TFPE-head (1/1/0.1)	Yes	Isotropic/Lamellar	No	Yes
DOPE/DOTAP/DiR (1/1/0.1)	Yes	Isotropic/Lamellar	No	Yes
DOPE/DOTAP/TFPE-chain (1/1/0.1)	Yes	Lamellar	Yes	Yes
DOPE/DOPC (3/1)	No	Isotropic	Not tested	No
DOPC/DOTAP/TFPE-head (1/1/0.1)	No	Lamellar/Isotropic	Yes	Yes
DOPC/DOTAP/TFPE-chain (1/1/0.1)	No	Lamellar	Yes	Yes
DOPC/DOTAP/DiR (1/1/0.1)	No	Lamellar	Yes	Yes

5.2.3. Investigation of the lipid phase and phase transition via small-angle neutron scattering (SANS)

Fusogenic and endocytic liposomes were also investigated using small-angle neutron scattering (SANS). The experiments were performed by **Dr. Sebastian Jaksch** and **Dr. Marie-Sousai Appavou**, instrument scientists at KWS-2 (MLZ, JCNS, Research Center Juelich) in Garching, Germany. For the detailed sample composition and preparation, see chapter 2.2.3 and table 2.3.

As described in previous sections, liposomes containing DOPE as a neutral lipid are called fusogenic liposomes (FLs), whereas liposomes with incorporated DOPC instead are named endocytic liposomes (ELs). Moreover, DiR, TFPE-head, TFPE-chain were used as aromatic dyes. The DOTAP as a cationic lipid was a constant component of the liposomes. The measurements were performed in the temperature range from 4 °C to 37 °C.

FLs containing TFPE-head as aromatic compound were investigated at 5, 20, 30, and 37 °C. As shown in Figure 5.12A, the same scattering pattern was detected at all of the temperatures indicating no phase transition in the investigated temperature range. The single scattering curves had typically three shoulders at around Q=0.015 $Å^{-1,}$ indicating inhomogeneity in the sample. A model containing only the lamellar phase (equation 2.10) was not sufficient for the best fit. The best fit was defined from a priori knowledge of what is in the sample, what structures are likely to be present, and what is physically reasonable. The best model was found using the combination of the scattering function of ellipsoid particles (equation 2.11), and a power law (equation 2.12) with an exponent of 2.96 typical for vesicles with a rough surface. The model indicated the presence of small micelle-like compartments with a rough surface, a polar radius of 1.92 nm, and an equatorial radius of 8.68 nm. The ellipsoid-like structures were embedded in lipid bilayers.

The scattering profile of endocytic liposomes containing the same aromatic molecule of TFPE was well modeled by a lamellar lipid phase (equation 2.10) with a bilayer thickness of 4.55 nm. In this case, there was no phase transition detected, and the same scattering pattern was obtained at all tested temperatures (Figure 5.12B).

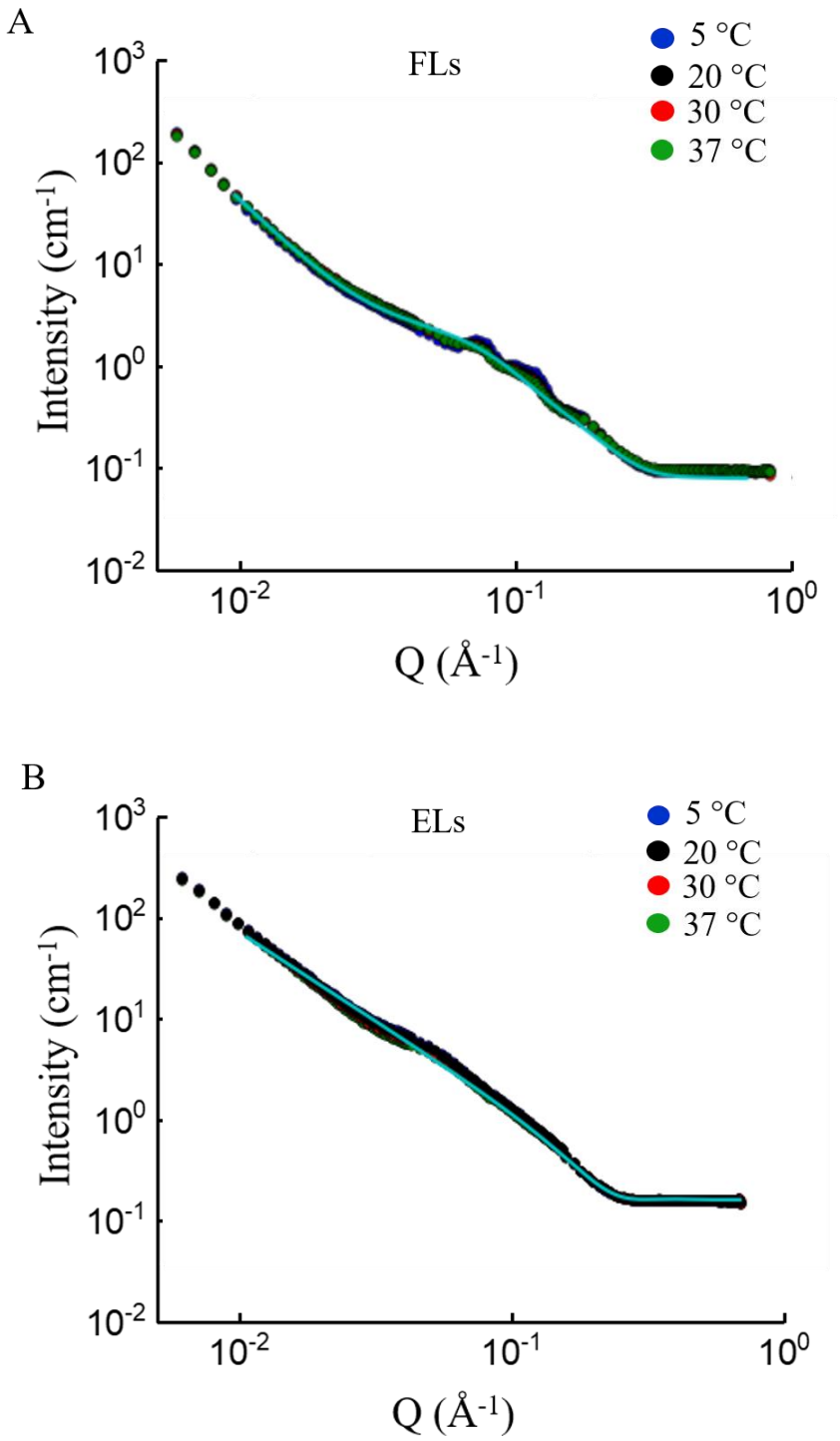

Figure 5.12. (A) Scattering curves of FLs (DOPE/DOTAP/TFPE-head (1/1/0.1 mol/mol)) and (B) ELs (DOPC/DOTAP/TFPE-head (1/1/0.1 mol/mol)) measured at four different temperatures (color code for the lines is given in the upper right corner of the plot). The scattering curves of individual temperature experiments strongly overlapped in both cases. Therefore cyan line indicates corresponding fits of a single measurement at all temperatures.

The investigation of FLs having TFPE-chain as aromatic compound yielded a scattering pattern with a characteristic shoulder at around Q=0.015 $Å^{-1}$ at all temperatures in the range of 4 °C to 37 °C (Figure 5.13A). The same fitting model (equation 2.11) was applied as before. In this case, the best-fitting power-law exponent (equation 2.12) was 3.02, which was attributed to vesicles with a rough surface. The best-fitting ellipsoidal particles (equation 2.11) had a polar radius of 1.80 nm and an equatorial radius of 9.82 nm. The scattering profile of ELs containing TFPE-chain was also successfully modeled by a lamellar lipid phase (equation 2.10), with a bilayer thickness of 4.07 nm (Figure 5.12B). No phase transition was detected in any of the samples.

A comparable scattering curve pattern was determined for FLs containing DiR as aromatic compound as before (Figure 5.14A), and the already established fitting model was applied. For this sample, the best fit power-law exponent (equation 2.12) was 3.0, and the best fitting ellipsoidal particles (equation 2.11) had a polar radius of 2.15 nm and an equatorial radius of 113.4 Å. The scattering data of ELs containing DiR was again modeled by a lamellar lipid phase (equation 2.10), with a lipid bilayer thickness of 4.30 nm (Figure 5.14 B). Also, here, no phase transition was detected in any of the measured liposomes.

The summaries of the structural parameters for all measured samples are given in Tables 5.2 and 5.3.

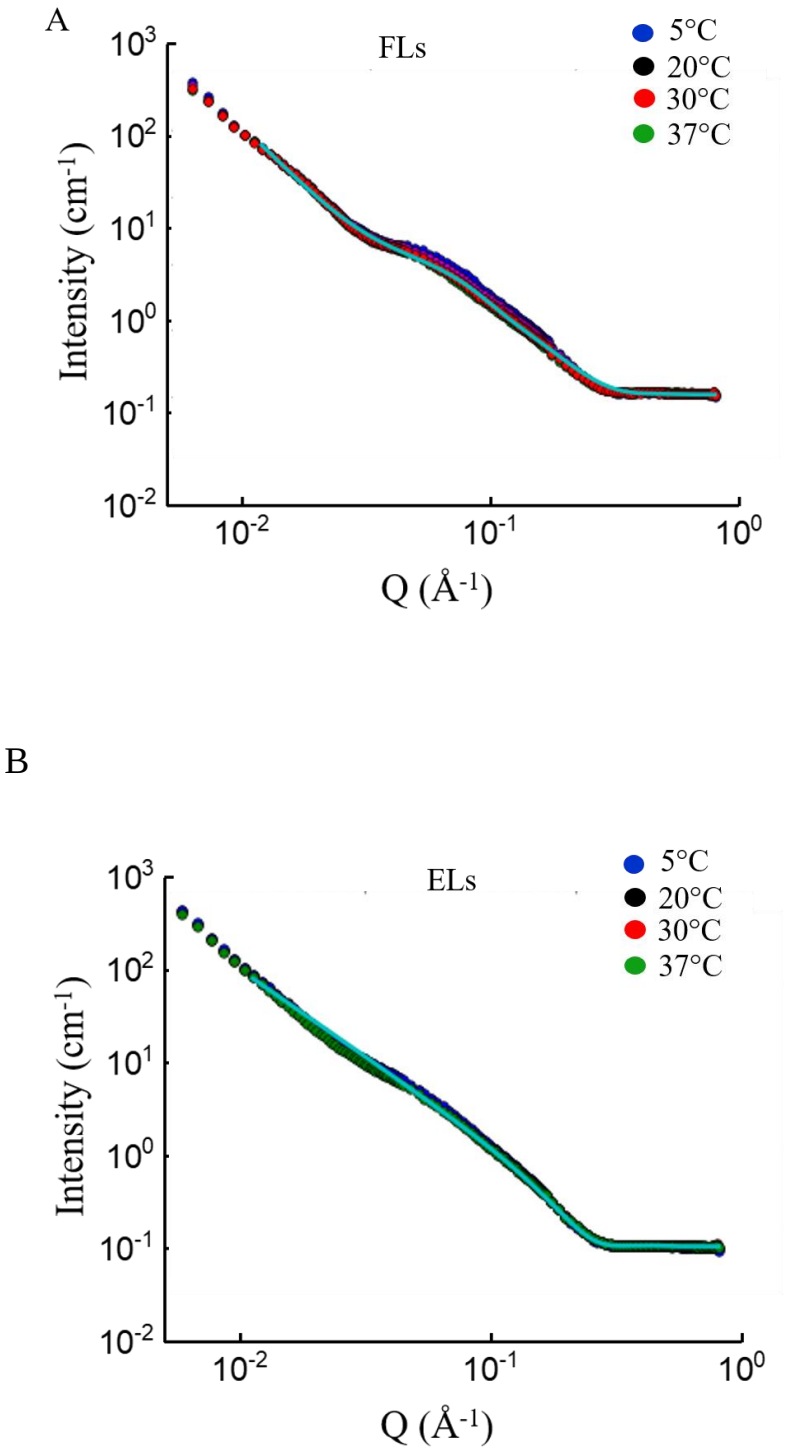

Figure 5.13. (A) Scattering curves of FLs (DOPE/DOTAP/TFPE-chain (1/1/0.1 mol/mol)) and (B) ELs (DOPC/DOTAP/TFPE-chain (1/1/0.1 mol/mol)) measured at four different temperatures (color code for the lines is given in the upper right corner of the plot). The scattering curves of individual temperature experiments strongly overlapped in both cases. Therefore cyan line indicates corresponding fits of a single measurement at all temperatures.

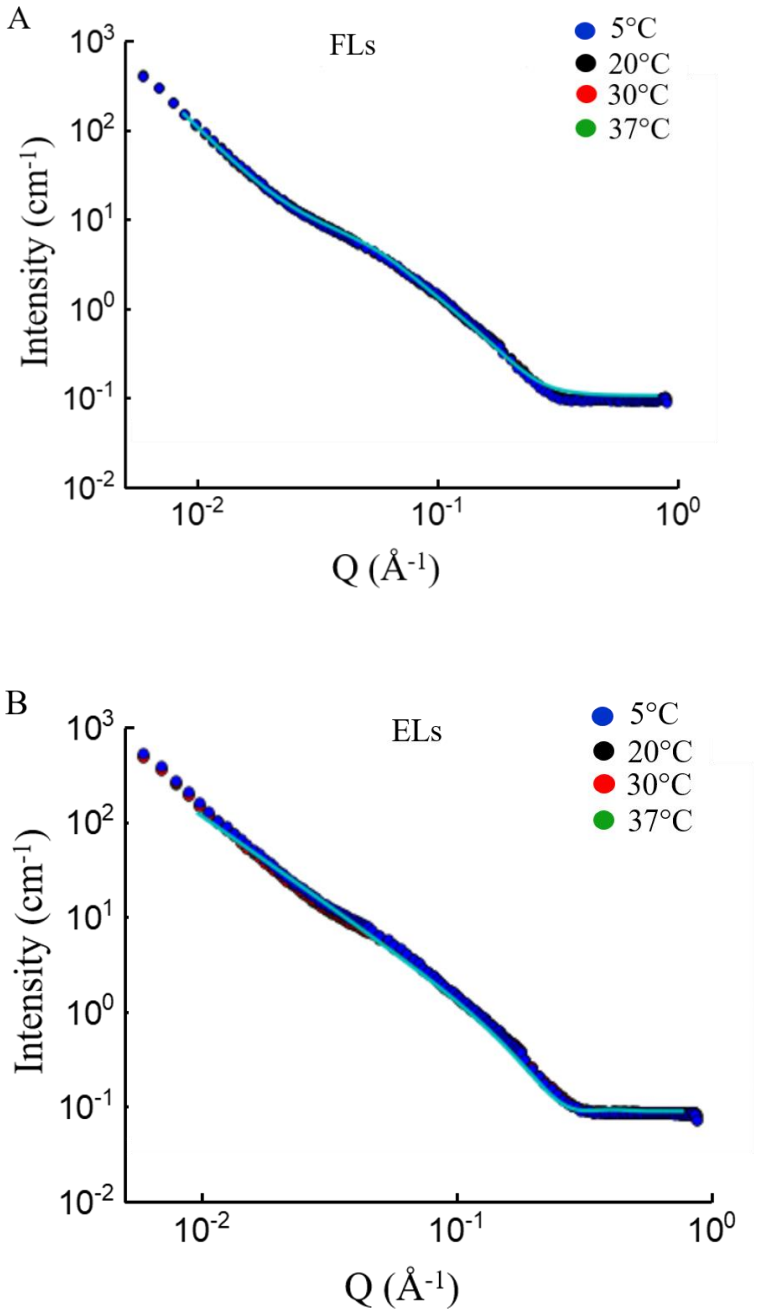

Figure 5.14. (A) Scattering curves of FLs (DOPE/DOTAP/DiR (1/1/0.1 mol/mol)) and (B) ELs (DOPC/DOTAP/DiR (1/1/0.1 mol/mol)) measured at four different temperatures (color code for the lines is given in the upper right corner of the plot). The scattering curves of individual temperature experiments strongly overlapped in both cases. Therefore cyan line indicates corresponding fits of a single measurement at all temperatures.

Table 5.2. Summary of the structural parameters of tested fusogenic liposomes obtained from the fitting of recorded scattering curves. The obtained parameters did not differ from each other at different temperature measurements, and only one measurement per distinct temperature has been done.

Sample / Parameter	**Power law exponent**	**Equatorial radius**	**Polar radius**
FLs-TFPE-head	2.96	8.68 nm	1.92 nm
FLs-TFPE-chain	3.02	9.82 nm	1.80 nm
ELs-DiR	3.00	11.34 nm	2.15 nm

Table 5.3. Summary of the structural parameters of tested endocytic liposomes obtained from the fitting of recorded scattering curves. The obtained parameters did not differ from each other at different temperature measurements, and only one measurement per distinct temperature has been done.

Sample	**Bilayer thickness**
ELs -TFPE-head	4.55 nm
ELs - TFPE-chain	4.07 nm
ELs -DiR	4.30 nm

5.2.4. Investigation of the lipid phase via freeze-fracture/STEM and Cryo-TEM

Freeze-fracture technique combined with scanning transmission electron microscopy (FF-STEM) and cryo-transmission electron microscopy (Cryo-TEM) were used to visualize single liposomes, their internal as well as surface structures. The experiments were performed by **Dr. Sabine Dieluweit** (ICS-7 at Forschungszentrum Jülich GmbH) and **Dr. Marie-Sousai Appavou** (MLZ, Münich, Germany), respectively. The liposomal composition and description of preparation are given in chapters 2.2.3. b) and c). The sample preparations and experimental procedures are thoroughly described in chapter 2.6.3.

In the case of ELs (DOPC/DOTAP/dye), the application of both techniques, FF-STEM and Cryo-TEM, confirmed the results obtained by previously described techniques, SANS and SSNMR. As shown in figure 5.15., liposomes formed either unilamellar or multilamellar vesicles. When Fast Fourier Transformation (FFT) was applied to the bilayer structure, an ordered line pattern was observed (Figure 5.15 A) confirming layered structures (lamellar phase).

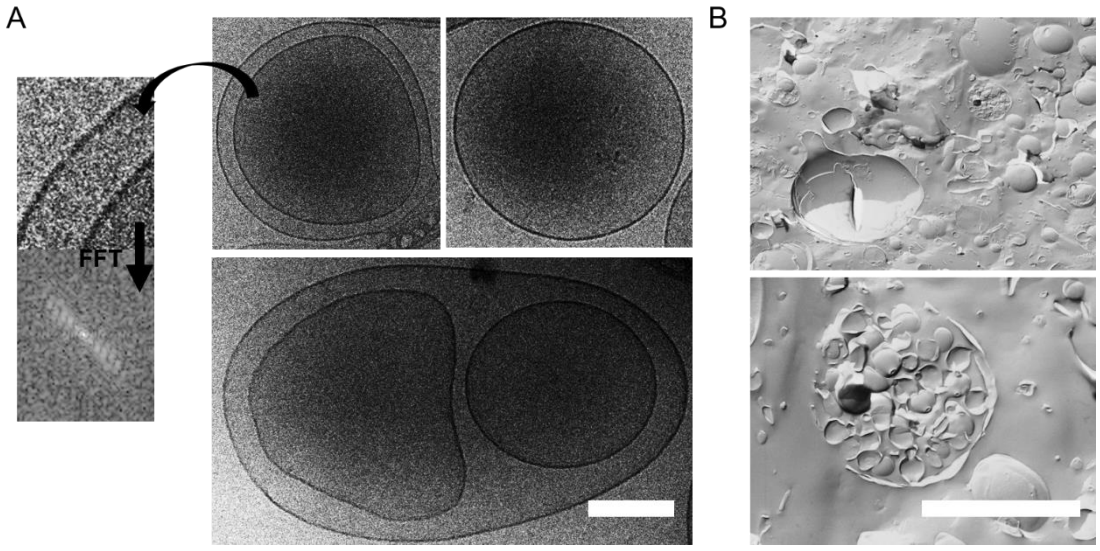

Figure 5.15. Typical **(A)** Cryo-TEM and **(B)** Freeze-fracture/STEM micrographs of endocytic liposomes forming unilamellar vesicles (upper row) or multilamellar/multivesicular liposomes (lower row). On the left side, a line pattern obtained by Fast Fourier Transformation (FFT) of the raw micrograph is shown. Typical distances calculated from the Cryo-TEM micrographs are 38,73 +/- 5,10 nm for the double layer, 5,11+/- 0,67 nm and 5,20+/- 0,78 nm for the inner and outer layer respectively. Scale bars, 100 nm (A), and 2 µm (B).

The imaging of single fusogenic liposomes resulted in the simultaneous presence of different phases. As shown in figure 5.16., small roundish structures were recorded on the multilamellar vesicle surface (B-C) with an average diameter of around 50 nm. In some cases, the liposomal surface pattern reminded of the sponge lipid phase (Figure 5.16A). In cryo-TEM micrographs (Figure 5.17), liposomal surface regions were recorded, indicating the simultaneous presence of hexagonal, cubic, and lamellar phases (A-C). The Fast Fourier Transformation (FFT) resulted in patterns specific for hexagonal phase (Figure 5.17A), close-packed hexagons characteristic for cubic phases (Figure 5.17B), and lamellar phase (Figure 5.17C).

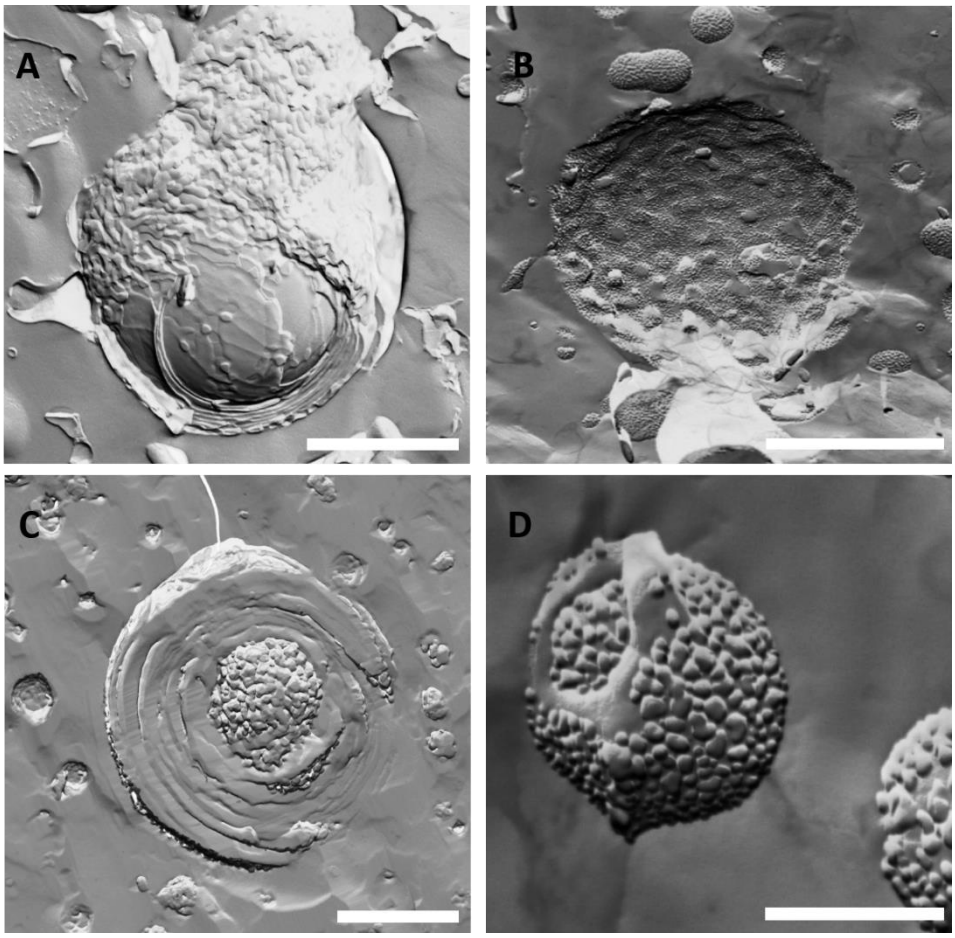

Figure 5.16. Typical freeze-fracture/STEM micrographs of fusogenic liposomes. **(A)** Liposomal surface with sponge-like lipid phase, **(B)** Concave section of the liposomes showing presence of small roundish structures, **(C)** Top view of multilamellar liposome with the small micelle-like structure embedded within the lipid bilayer, **(D)** Close view of liposome having small structures making the liposomal surface rough. Scale bars, A-C = 1 μm, D = 300 nm.

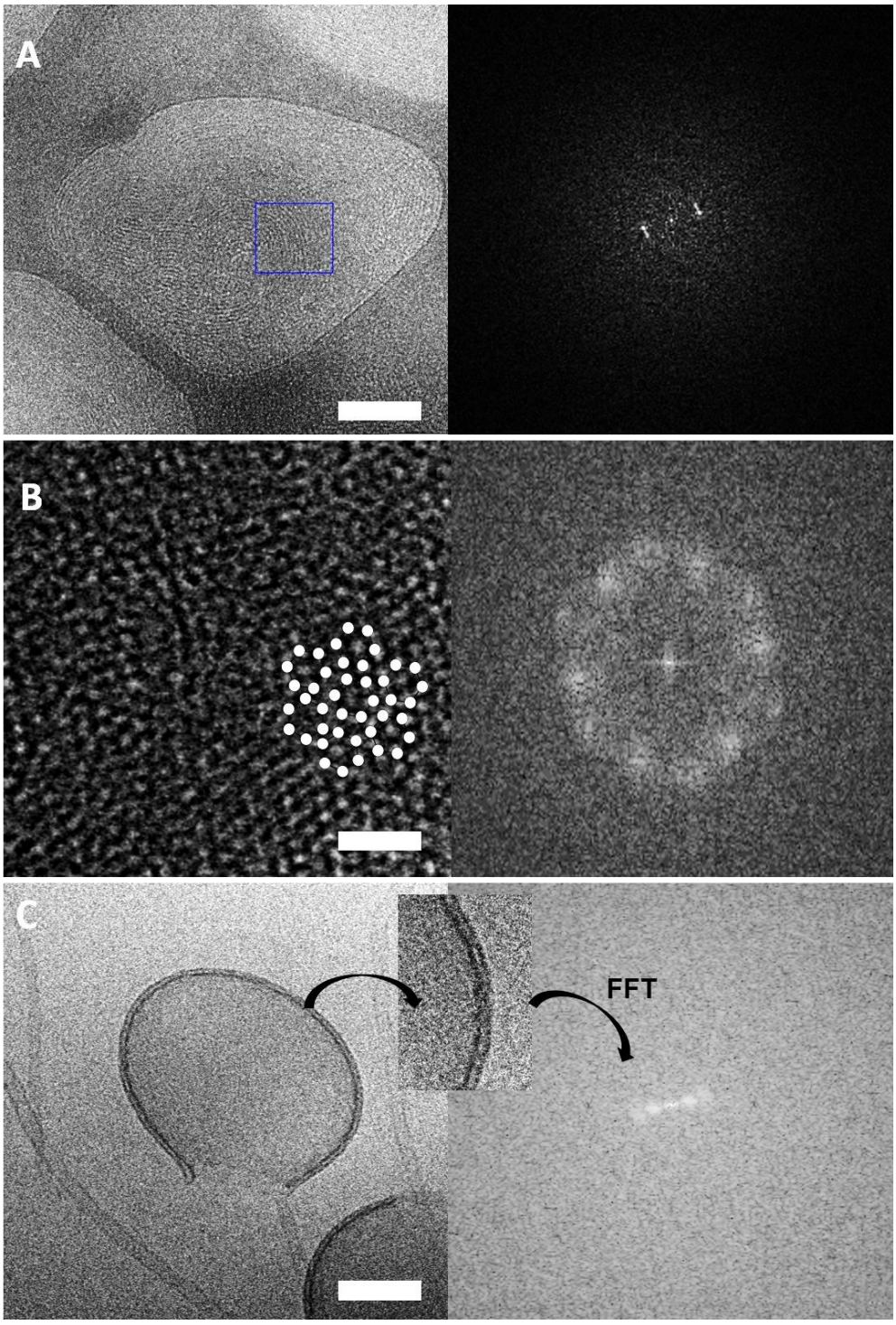

Figure 5.17. Typical Cryo-TEM micrographs of fusogenic liposomes (left) with the corresponding Fast Fourier Transformation (FFT) patterns (right): **(A)** Fingerprint-like arrangement of liposomes (distance between the lines determined by FFT is 7,0 +/- 1,0 nm) **(B)** Liposomal close hexagonal packing (cubic) with the corresponding FFT pattern showing two overlapped hexagons, the distance between centered and side dot determined by FFT is 1.2 nm/cycle. **(C)** A disrupted lipid bilayer (lamellar). The measured distances are 10,92 +/- 1,08 nm for the double layer, 4,80+/- 0,43 nm and 4,38+/- 0,88 nm for the inner and outer layer respectively. Scale bars, 100 nm.

5.2.5. Investigation of the liposomal viscosity via falling-sphere viscosimetry

In order to achieve a better understanding of different phase behavior of the studied liposomes, their dynamic viscosity was tested by falling-sphere viscosimetry between 4 °C and 37 °C. The detailed explanation of the experimental procedure and sample preparation is given in chapter 2.8.2 (see also Figure 2.8). The liposomal compositions are described in chapter 2.2.3 (e).

Results showed that the solution of endocytic liposomes (ELs) was less viscous than fusogenic liposomes (FLs) solutions. There was almost no difference between the sphere velocity of endocytic liposomes with varying aromatic components. FLs with TFPE-head as a dye showed the lowest sphere velocity indicating the highest viscosity of the sample in comparison to the other samples. Sample inhomogeneity became obvious based on the inhomogeneous sphere velocity during fall. The TFPE-chain containing FLs were not as viscous, but more viscous in comparison to DiR-FLs that had almost the same sphere velocity as for tested endocytic liposomes. The velocities of the fallings sphere for FLs and ELs containing different dye are presented in figure 5.18.

As shown in figure 5.18, the viscosity of the tested FLs could be qualitatively described as following: FLs (TFPE-head) > FLs (TFPE-chain) > FLs (DiR)

and for ELs: ELs (TFPE-head) ≈ ELs (TFPE-chain) ≈ ELs (DiR)

Two different behaviors of the liposomes tested in this study were also observed from their viscosity. The viscosity did not change much with the temperature. However, the velocity of the falling ball differed in the case of the FLs depending on the incorporated aromatic component (Figure 5.18). In this case, the observed inhomogeneities in the FLs solution could indicate the coexistence of several lipid phases.

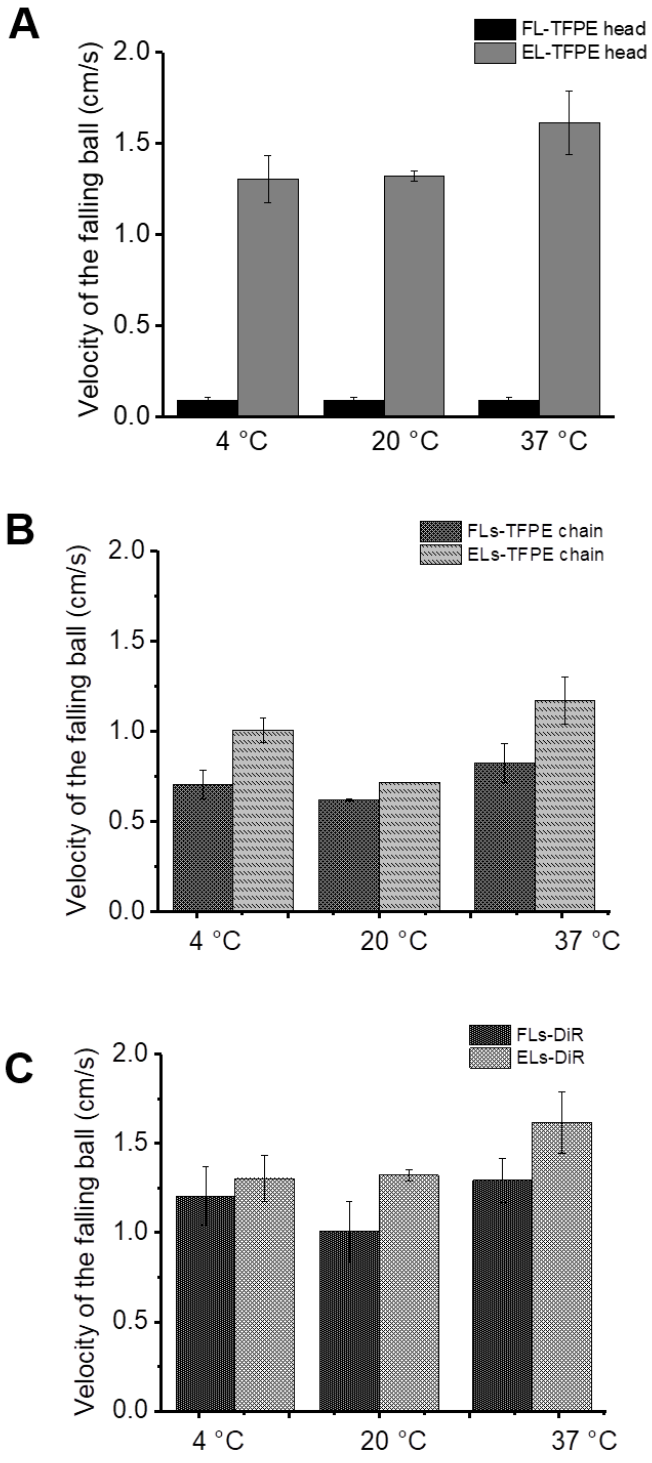

Figure 5.18. The velocities of the fallings sphere for liposomal solutions of fusogenic (FLs) and endocytic liposomes (ELs) containing different dye: TFPE-head (A), TFPE-chain (B), and DiR (C) are presented.

5.3. Discussion

In the current study, lipid polymorphism of the fusogenic liposomes (FLs) was investigated in comparison with endocytic liposomes (ELs) using several complementary techniques such as Solid-State Nuclear Magnetic resonance (SSNMR), Small Angle Neutron Scattering (SANS), calorimetry, or electron microscopy.

Lamellar and hexagonal phases have been clear to identify using SSNMR based on their characteristic lineshapes (see Chapter 2.9.1, Figure 2.9). What is more challenging to elucidate is the isotropic ^{31}P peak characteristic for cubic lipid phases, as well as micelles and small vesicles [213, 214]. In both cases, the fast lateral diffusion of lipids over the highly curved surface of the membrane reveals a narrow peak in SSNMR at the isotropic frequency [215]. However, Yang and colleagues showed via simulation that ^{31}P T_2 relaxation times of isotropic micelles and cubic-phase membranes differ significantly [215]. Lipids in the cubic-phase exhibit a two-orders of magnitude shorter relaxation time than the micelles-forming lipids. This difference could be explained by the different timescales of lipid lateral diffusion on the cubic-phase surface versus the timescales of micelle tumbling [215]. The presence of an isotropic peak indicates the existence of small micelles being possibly responsible for fusion occurrence. Its appearance in the SSNMR spectra of FLs was in good correlation with the data collected by neutron scattering (SANS). In this case, the best fitting model indicated the presence of small micelle-like structures within the lipid bilayer (Figure 5.19). Some fusogenic lipid mixtures, e.g., FLs-TFPE-chain or, in some cases, FLs-DiR, showed no isotropic peak in the SSNMR spectra. However, SANS technique revealed the presence of micelles within the bilayer in all cases.

After a closer look at the results, it is hypothesized that in the case of FLs containing lens-shaped micelles due to the molecular packing of dyes, such as FLs-TFPEchain or FLs-DiR, the lipid motion cannot be classified as isotropic anymore, which is based on the elongated horizontal axis of the micelles resulting in a non-isotropic peak in the SSNMR spectra. The reproducibility of performed experiments is requiring, but that is the art of a puzzle, as these systems are known to be irreproducible in the behavior, they are tricky to handle and strongly depended on the sample treatment and preparation as shown before [216]. Winter and his colleagues postulated that for a series of lipid molecules also non-lamellar lyotropic phases are observed as thermodynamically stable phases or as long-lived metastable phases after special sample treatment [216]. The results obtained by SSNMR and freeze-fracture/cryo-electron microscopy indicate that the intermediates could be a long-living metastable phase rather than

as millisecond transient structures. Similar intermediate long-living metastable structures were observed by Angelov *et al*., suggested to correspond to the growth and order of a three-dimensional bicontinuous nanochannel network into a cubic phase [217]. They proposed that the intermediate state is a swollen cubic phase precursor, still lacking a long-range crystalline order [217]. The development of an ordered cubic structure from sponge-like (melted) cubic precursor domains is rather a slow process, while melting of the cubic phase to a homogeneous fluid, represents a fast process [217].

SANS data could not be fitted with the models for lamellar, nor with any of the following: hexagonal, bicontinuous cubic phases, and the combination of them, indicating the co-existence of many phases. A combination of lamellar and isotropic phase was also shown by SSNMR and (S)TEM (Figures 5.16 and 5.17). The presence of small vesicles (or areas of cubic phase) embedded in multilamellar liposomes with a raspberry-like rough surface in (FL-TFPE-head) was also verified by freeze-fracture-STEM (FF-STEM). The diameter of the small "dots" on the liposomal surface was ~ 50 nm, confirming the diameter calculated from SANS data of FLs. Such coexistence of phases is particularly described for heterogeneous liposomes, or PEG-ylated liposomes [218]. The lipid phase coexistence (e.g., gel phase and liquid phase) usually occurs when lipids with low melting point mix with high melting point lipids. In this case, the former will persist in the liquid phase at temperatures where the latter would be in the gel phase. Van Meer postulated that the membrane phases do not exist at equilibrium, but instead exist at a steady state with quasi-equilibrium. Such a state describes the local patches of a membrane in which compositions of components remain for longer times, which is, for example, the time taken for vesicle fusion [15]. However, if there are co-existing phases, they have to be in the thermodynamic equilibrium.

In figure 5.17A, regions similar to those known from literature for so-called hexosomes [120, 135, 219-221] are shown. This finding indicates the possible formation of cylindrical micelles simultaneously with multilamellar liposomes. After FFT of micrographs of FLs, a pattern of overlapping hexagons in the different z-position could be seen, indicating the formation of the rhombohedral phase, which was reported as an intermediate state of fusion [59-61, 222]. The description of rhombohedral phase [223], reported by Koynova, is in good agreement with the presence of small micelles within the lipid bilayer, characteristic for FLs. However, there is no indication of a clear hexagonal/cubic phase alone, even though some of the STEM micrographs revealed cubic phases found in other studies [121, 135, 219-221, 224, 225]. The hypothesis here is that in the fusogenic liposomes, lamellar phases coexist with the

several fluid isotropic phases (solution 3D phases), particularly inverted micelles (L_2), which leads to the formation of membrane segments with high curvatures and therefore increased fusion ability (Figure 5.19).

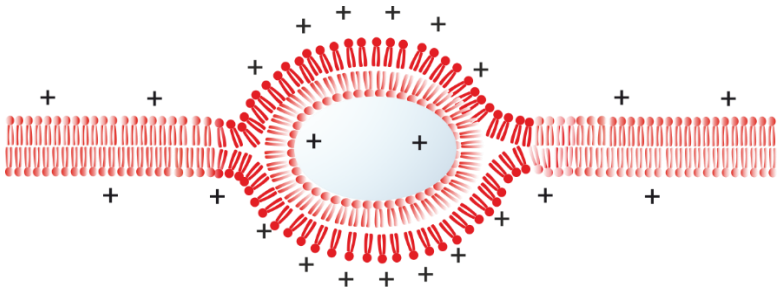

Figure 5.19. The schematic representation of inverted micelle-like structures embedded into the lipid bilayer.

The coexistence of the rhombohedral phase with lamellar is possible, but as there is no suitable model for fitting this phase, further investigation via compatible techniques (e.g., SAXS, or X-ray and neutron diffraction) is necessary. Investigation via of amphiphile/water system via X-ray diffraction has shown the existence of two different paths between lamellar and hexagonal phases upon heating and cooling with different heating and cooling rates [226]. The same group reported that the decrease in curvature from lamellar to hexagonal via rhombohedral phase is a natural sequence to be followed what indicated that the rhombohedral phase is kinetically favored metastable structure [226]. Although here investigated FLs did not show any detectable phase transition at the given scan rate (see DSC results, chapter 5.1), it could be that the rhombohedral metastable phase is present in FLs. The changes in cross-sectional area and curvature of the structures observed previously [226] should also happen with lipid membranes during biological processes such as membrane fusion. Therefore, the presence of rhombohedral or some other alike phase is very probable. Funari and Rapp also proposed that the disruption of lamellar domains (lipid membrane) and the formation of hydrophobic rods together with their change from 2D to 3D network represent a convenient pathway for the formation of the transient states [226]. Meyer *et al*. have defined a novel lipid phase of DMPC and DPPC, formed below the pre- and main transition at a temperature of about 4 °C [227]. The reported phase is less hydrated than the crystalline phase (Lc) and is denoted as Pcc according to its peculiar convex-concave bilayer curvatures similar to the rough raspberry-like surface of FLs seen in the micrographs shown in Figure 5.16, although FLs do not consist of PC lipids.

The phase behavior of lipids is dominated by the main (order-disorder, T_m) phase transition. Above the T_m, lipids can obtain different liquid crystalline mesomorphic structures with lamellar and non-lamellar symmetry, and below the T_m, a basic equilibrium structure is the subgel (crystalline) L_c phase (see chapter 1.2). Besides, a large number of intermediate stable, metastable, and transient lamellar gel structures are adopted by different lipids. Tenchov and co-workers found new-ordered metastable phases between the gel and subgel phases in hydrated phospholipids [228]. The PE and PC low-temperature metastable phases denoted L_{R1} and SGII, respectively, having different packing of lipids within the phases. The chains arranged in an orthorhombic lattice of four-nearest-neighbor type characterize L_{R1} phase [228]. The orthorhombic lattice is also characteristic of the rhombohedral phase, which might also appear in FLs investigated here. The phase-transition dynamics of liposomes, consisting of mixtures of DLPE and DLPG, revealing a metastable liquid crystalline-to-stable crystalline phase transition upon cooling from 60 °C to 37 °C was described by Jacoby and colleagues [229]. Molecular dynamics simulations discovered "the dynamic appearance and disappearance of spatially related nanometer-sized thick ordered and thin interdigitating domains in a fluid-like bilayer close to the phase transition temperature (T_m)" [230]. The reported structures are probably metastable precursors of the ripple phase extinction at high temperatures. The same group showed that bilayer stability is reduced, leading to the pore formation occurring in the metastable parts of a membrane, for temperatures close to T_m when an external electric field is applied [230]. Such precursors, or metastable phases, can be denoted to the FLs lipid phase, having in mind inverted micelles embedded into the lipid bilayer. It was shown that pore metastability depends on the lipid packing (CPP, see chapter 1.2.2 and figure 1.6) within the membrane.

Two theoretical methods consistently suggest that metastable pre-pores are formed by lipids with a larger head-group region or shorter saturated tails while unstable pre-pores are formed by the smaller head-group volume fraction or longer unsaturated tails [231]. This finding is in good agreement with results from Chapter 3 where was proved that FLs need lipid molecules with a conical effective shape (small heads and long unsaturated tails) for efficient fusion. Interestingly, it was shown that the particular lamellar phase could be metastable and eventually relaxes, either in time or by perturbation of the sample by centrifugation, into aligned multi-bilayer stacks of single orientation [232]. The metastability of the lamellar phase was also shown by Matsuki et al., where they reported the metastable phase between crystalline and fluid lamellar phase [233-235]. Theoretically, FLs could also form a metastable lamellar phase with other 3D phases, and formation of unstable pre-pores could be a reason for fusion events.

Based on the obtained results, a theoretical mechanism of membrane fusion between FLs and cellular membranes can be proposed. The presence of the positively charged lipid (e.g., DOTAP) is essential for establishing contact between the liposomal and the cell membrane. The role of the neutral lipid, especially phosphoethanolamine (PE), becomes evident if its molecular shape is taken into consideration. In contrast to phosphocholines (PCs), PE lipids (e.g., DOPE) tend to form hexagonal phases and micelles (or inverted micelles) due to their conical molecular shape. Therefore, it is hypothesized here that the inverted micelles embedded into the liposomal bilayers are mainly formed by PE lipids. Because of missing indications of a complete lipid separation, only the enrichment of DOPE is presented in Figure 5.20. The lipid bilayer enclosing inverted micelles has a high positive membrane curvature, which is especially favorable for the positively charged lipid molecules. The electrostatic repulsive forces acting between the cationic lipid head groups decrease with increasing molecular distances and stabilize the membrane.

On the other hand, the high density of membrane segments with extreme membrane curvature [44, 45, 81, 187, 236] makes it energetically unstable. Such curvature stress usually promotes fusion-stalk formation [22, 73, 74, 78, 79, 82-84, 88]. After micelle-stalks are formed and the energy barriers are crossed, the monolayers and the micelle tend to merge governed by the hydrophobic effect. This step leads to the breakage of the micelle and formation of the fusion pore; thus, the membrane fusion occurs. The stalk-formation and subsequent membrane fusion have previously been described by Siegel and co-workers and known in the literature as stalk-mechanism [73,79, 82-84, 209, 237-240]. However, it turned out, that liposomes denoted by Siegel as fusogenic (DOPE/DOPC 3/1 mol/mol) do not fuse with the plasma membrane of mammalian cells. Csiszar and colleagues discovered that the positively charged lipid, DOTAP, is essential for the fusion of fusogenic liposomes with the cellular plasma membrane [9, 241]. The structure of DOTAP is similar to that of DOPE as they both have small head groups and unsaturated long hydrocarbon chains. Therefore, the theory of Siegel [73] can be applied to DOTAP as it has the conical molecular shape, which promotes a phase transition into the H_{II} phase and thus the stalk mechanism, or modified form of the mechanism of membrane fusion.

The role of the aromatic component in membrane fusion induction is poorly investigated. It was shown in Chapter 3, that the presence of cationic lipids, as well as aromatic compounds, is mandatory for efficient fusion induction. There is undoubtedly the attraction between the positively charged lipids and aromatic moieties, and it probably opposes the tendency of lipids to mix homogeneously. Hence, the enrichment of the cationic lipids in the outer membrane leaflets, as well as the polarized π-electrons in the aromatic rings, reduce the energy barrier required for membrane contacts, and it is more a local effect within the membrane. An aromatic molecule might also play a role by disturbing the phase of the liposomes, and together with different effects present, like opposing charge effects, have positive effects on membrane fusion induction. Similar to this, some virus-mediated fusion events occur due to the aromatic part of the peptides or proteins, like fusogenic domains found in F-protein [242] or tryptophan part in different membrane peptides [243].

Moreover, the molecular shape of the used dye could influence the formation of membrane segments with high curvatures. It is known that one of the essential factors for lipid phase formation is the critical packing parameter. Tran et al. reported that the CPP of lamellar, cubic, and hexagonal phases are values ranging from 1.27 to 1.31, and about 1.7, respectively [221]. High CPP corresponds to high negative curvature of membrane surfaces. De Campo et al. reported that with increasing temperature, the internal structure of membranes goes through a transition from cubic via hexagonal to fluid isotropic phase [244].

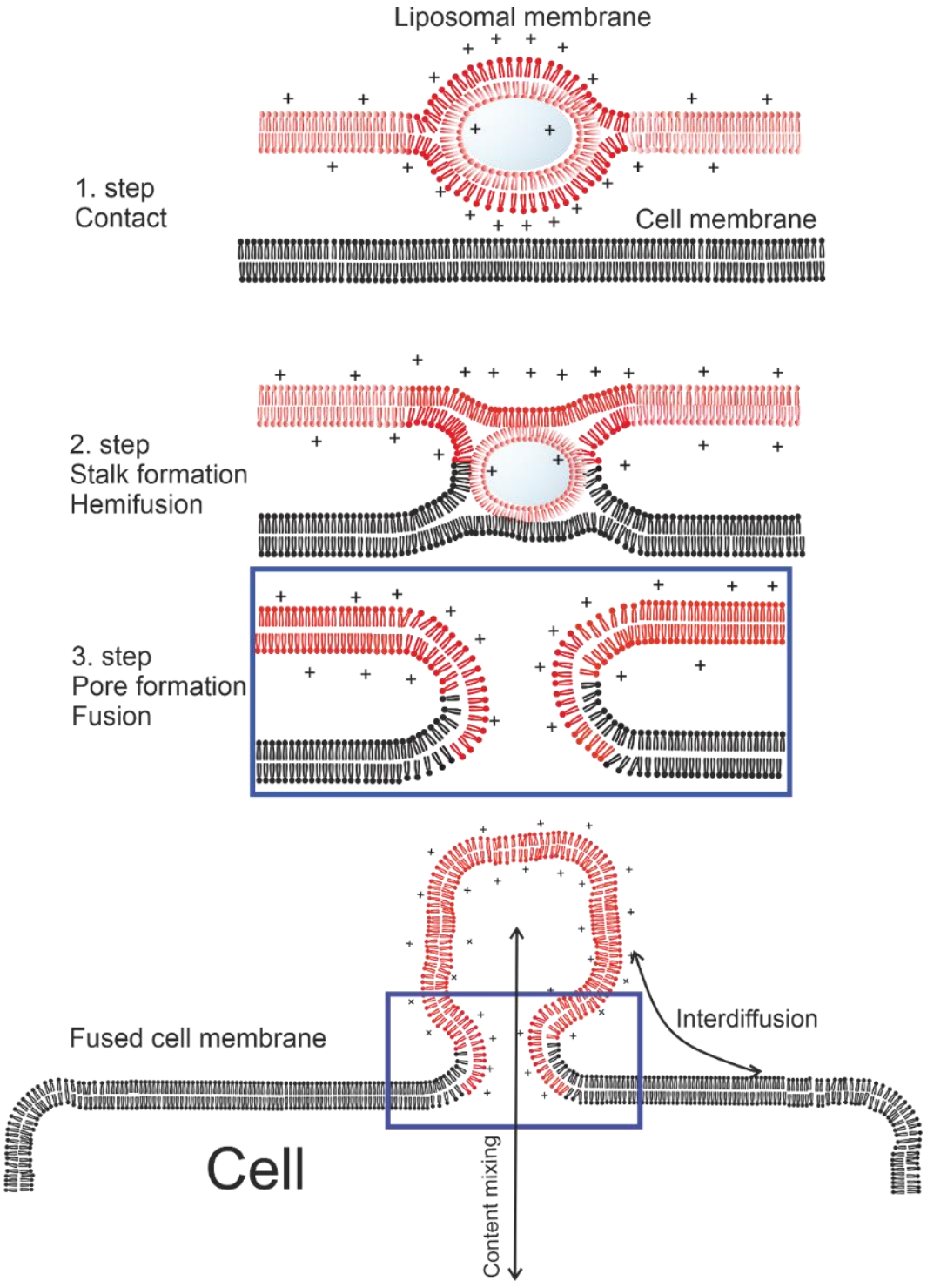

Figure 5.20. The schematic representation of the modified stalk mechanism of membrane fusion. The first step presents the necessary contact between liposomal and cell membranes. After the contact is established and membranes start to hemifuse, inverted micelles that were embedded within the liposomal membrane collapse and join the pore formation and fusion process. The hypothesis of the fusion mechanism was reached on the bases of the findings of this thesis.

The investigation of endocytic liposomes, here cationic liposomes containing an aromatic molecule and a phosphocholine (PC) as neutral lipid, revealed the presence of a lamellar phase independently from the measurement technique. The differences in the bilayer thicknesses, calculated from SANS data, can be interpreted as a consequence of the insertion of the dye molecule within the bilayer. Bilayer thickness increased if lipid molecule with aromatic rings poking out of the membrane surface was embedded into the bilayer, while aromatic rings coupled to the acyl chain did not significantly influence the membrane thickness.

Even though the theoretical fusion mechanism of FLs could be established based on the data obtained in this study, the exact lipid phase obligatory for fusion induction with cellular membranes remains to be elucidated. Small-angle X-ray scattering (SAXS) and X-ray diffraction would be the most suitable techniques to resolve the riddle of the co-existing phases and metastable intermediates. In general, the Bragg diffraction peaks of lipid membranes are relatively sharp; therefore, the correct peak position can be evaluated directly from the slit-smeared data. The structure of the lyotropic liquid crystalline phases can be determined from the relative positions of the SAXS diffraction peaks. For the lamellar (smectic) and hexagonal (cylindrical assemblies crystallized in a two-dimensional hexagonal lattice) structures, the position of the peaks should obey the relationships 1:2:3:4...and 1:√3:2: √7:3..., respectively.

These findings open new avenues for further investigation of the lipid phase of fusogenic liposomes, their metastability and corresponding relaxation times, and even controlled fusion for better application of those liposomes.

Chapter 6

6. Delivery of the Radionuclide ^{131}I to Cancer Cells using Fusogenic Liposomes as Nanocarriers

This chapter represents the application part of the thesis wherein the fusogenic liposomes are used for the delivery of ^{131}I into cancer cells. The effectiveness of the fusogenic liposomes to deliver radionuclide into cancer cells makes them suitable for potential use in nuclear medicine.

The major of this chapter is submitted as Kolasinac et al., *Delivery of the Radionuclide ^{131}I to Cancer Cells using Fusogenic Liposomes as Nanocarriers*, International Journal of Nanomedicine, 2019.

6.1. Introduction

Liposomes are widely used in the pharmacology as carrier particles [30, 245]. They are highly biocompatible, biodegradable, and non-immunogenic lipid-based vehicles, suitable for solubilization of hydrophobic as well as hydrophilic substances. Such drug carriers improve therapeutic efficacy by minimizing the rapid degradation of the cargo and increasing its adsorption [246, 247]. Liposomes are well established in cancer chemotherapy [248, 249] and gene therapy [245]. In addition, since the late 1990s, they have found more and more applications in nuclear medicine and diagnostics. Especially image-guided drug delivery uses the benefits of liposomal carriers. Due to the negative charge of natural phospholipids, liposomes intended for theranostic use usually intercalate metal-based radionuclides, e.g., ^{64}Cu, ^{99}mTc, ^{188}Re, ^{89}Zr [250, 251]. To increase loading efficiency, click labeling and surface chelation have been established [252]. Coupling of the radionuclide to liposomes containing pharmacologically active compounds enabled the tracking of the liposomes, their transport, accumulation as well as cleavage from the organism. As the most potent non-invasive imaging methods positron emission tomography (PET), single photon emission computed tomography (SPECT), and magnetic resonance imaging (MRI) were applied [250, 251, 253].

Radiolabeling of liposomes with a neutral or negative surface charge was extensively investigated over the last decades; however, cationic liposomal carriers are less established in nuclear medicine. Such liposomes are rather popular in therapeutic gene delivery where the cargo DNA or mRNA build stable complexes with the carrier particles due to attractive electrostatic interactions. Cationic liposomes are usually made of the classical lipid mixture of the neutral lipid DOPE and the cationic lipid DOTAP (for IUPAC names and structures please see chapter 2.1.1). As earlier research showed, the addition of an aromatic molecules to the classical mixture at a concentration of 5 mol% or above renders the cationic liposomes fusogenic [9]. They are also able to directly fuse with the cellular plasma membrane. As a consequence their cargo is delivered into the cytoplasm of the mammalian cells with high efficiency bypassing cargo degradation in the endosomes [11, 12] referred as the main liposomal uptake route. Due to their extraordinary high fusion ability they are called fusogenic liposomes (FLs).

Using such liposomes as carrier particles, best cargo delivery was achieved when cargo internalization was based on the attractive interaction between the positively charged liposomal surface and the negatively charged cargo, e.g., proteins, peptides [81] or RNA molecules [51].

Hence, it appears highly likely that such liposomes are also able to efficiently bind radioactive anions, e.g., [^{131}I]I^-, [^{120}I]I^-, or [^{76}Br]Br^- and to deliver them to mammalian tissues and cells of interest. Free iodine without any carrier particles predominantly accumulates in the thyroid [254-256], while liposomes are mainly enriched in tumor tissues due to their high metabolic activities [257].

Therefore, the present study aimed to formulate and characterize cationic liposomes radiolabeled by ^{131}I for potential use in cancer therapy. The epithelial human breast cancer cell line MDA-MB-231 was used as a model for invasive cancer cells, incorporation of liposomal [^{131}I]I^- was monitored *in vitro*, and delivery efficiency was examined. Moreover, given possible intravenous use, delivery to human blood cells was examined as well.

6.2. Results

6.2.1. Characterization of liposomes containing iodine as cargo

The detailed description of liposomal preparation is given in chapter 2.2.4. The experiments with radionuclide ^{131}I were performed at the Institute of Neuroscience and Medicine-5: Nuclear Chemistry (INM5, Research Center Juelich, Germany). Fusogenic liposomes (FL) were consisting of DOPE/DOTAP/DiR at 1/1.2/0.3 molar ratio, while endocytic liposomes (EL) had DOPC/DiR at 2/0.05 molar ratio and were used as a control sample. The lipid mixture was rehydrated in the iodine solution at high lipid concentration without any additional homogenization steps except vigorous mixing (see Figure 2.4). The radionuclide ^{131}I was replaced by the non-radioactive isotope ^{127}I for characterization purposes, assuming that both isotopes interact with the liposomal membranes in the same manner.

The formed multilamellar liposomes had an average diameter of 456 (51) nm slightly bigger than liposomes without cargo (376 (5) nm). The polydispersity indexes (PDI) in both cases indicated relatively similar size distributions (see Table 6.1). The small size of spontaneously formed liposomes was presumably stabilized by the strong electrostatic repulsion between the charged liposomes. Zeta potentials, characteristic for the electrostatic properties of the membrane surface of both, ^{127}I loaded and empty, liposomes were +89(3) mV, and +88(5) mV, respectively, without any significant difference.

Due to the neutral zeta potential of the control liposomes (-2.5 mV), they formed large liposomes and liposomal aggregates with an average size of ca. 2 μm and very high polydispersity (see Table 6.1). While iodine internalization decreased the sample polydispersity, the zeta potential of the complexes remained unchanged.

Table 6.1. Average hydrodynamic diameter (d), polydispersity index (PDI), and zeta potential (ς) of fusogenic (FL) and endocytic (EL) liposomes with and without ^{127}I cargo.

Sample	d (s.d.) (nm)	PDI	ζ (s.d.) (mV)
FL	376 (5)	0.4	88 (5)
FL/^{127}I	456 (51)	0.5	89 (3)
EL	2221 (1860)	1.0	-2 (1)
EL/^{127}I	2616 (429)	0.6	-6 (6)

To determine iodine incorporation efficiency, liposomes intercalating the radionuclide ^{131}I were prepared, and the cargo loaded particles were first separated from the buffer by centrifugation (Figure 2.4). Iodide activities were determined in the pellet (FLp and ELp), and the supernatant (FLs and ELs) as characteristic for its concentration and intercalation efficiencies were calculated. As shown in Figure 6.1A, cationic liposomes were able to incorporate 29 (13)% and control liposomes 38 (14)% of the used ^{131}I. Therefore an additional control sample at 25% of the original iodide concentration was also applied in the *in vitro* experiments.

6.2.2. Cancer cell treatment using iodine loaded cationic fusogenic liposomes

These experiments were done at INM-5. Iodine transfer efficiency was tested on the human epithelial breast cancer cell line MDA-MB-231 using FL and EL as carrier particles. The cargo loaded liposomes were separated from the free iodine via centrifugation. Although EL were able to incorporate ^{131}I, their delivery efficiency to the cancer cells remained only one half of that reached by FL (5.1% (2.9) and 9.35 (3.4), respectively, n=3 in both cases) (Figure 6.1B). The uptake efficiency of free $[^{131}I]I^-$ was determined using two different iodide concentrations, the initial one ($[^{131}I]I^-$) and one-fourth of it ($[^{131}I]I^-/4$) which was approximately identical with the intercalated iodine amount in FLs. The activity of free iodide from liposomal supernatants was analyzed, as well. In all cases, iodide uptake was less effective compared to liposomal delivery and remained below 4% (Figure 6.1B). The delivery efficiency was calculated as the percentage of delivered iodine in comparison to the total amount of iodide within the liposomes measured before cell treatment. This result corresponds with other reports about the minimal accumulation of ^{131}I in non-thyroidal tissues.

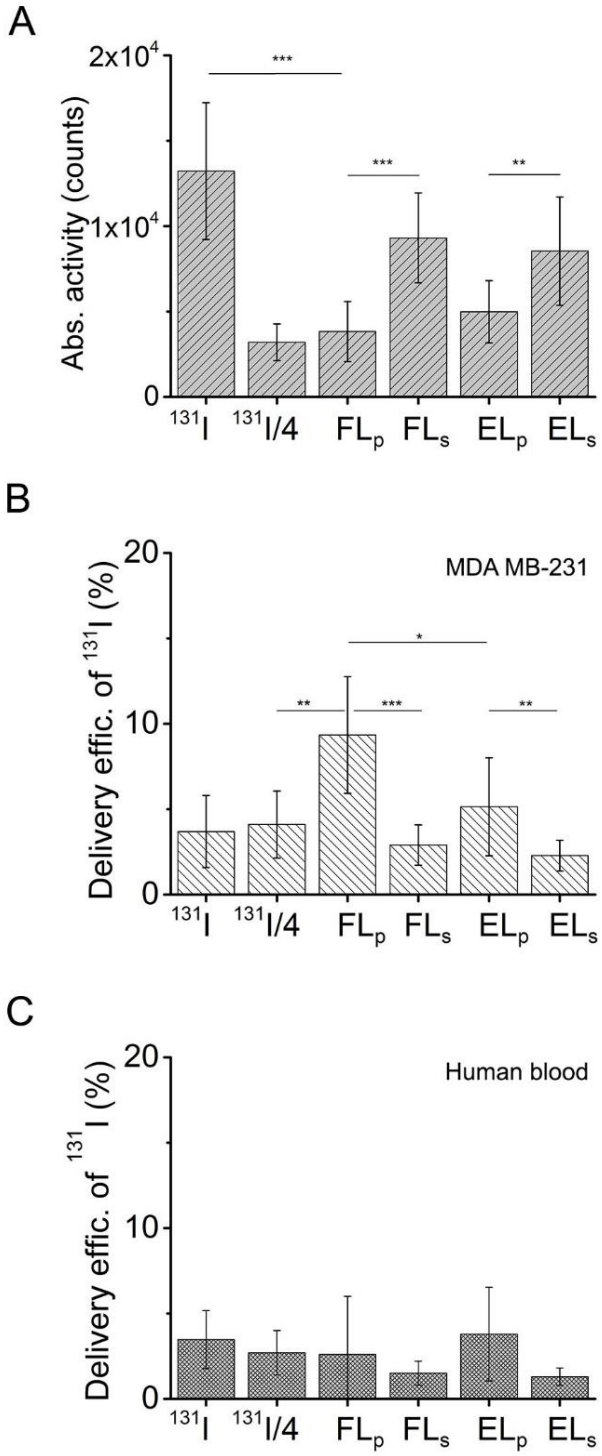

Figure 6.1. A) The absolute activity of free ^{131}I radionuclide solution, as well as the activity of ^{131}I, intercalated into fusogenic (FLp) and endocytic liposomes (ELp) and the activity of the non-liposomal ^{131}I in the supernatant (FLs, and ELs, respectively). B) Delivery efficiencies of ^{131}I using the same liposomes as carrier particles and the free ^{131}I radionuclide as a control to MDA MB-231 cancer cell line and C) to human red blood cells.

The radionuclide ^{131}I was replaced by the non-radioactive isotope ^{127}I, assuming that both isotopes interact with the liposomal membranes in the same manner, in order to test the fusion efficiency of iodine-intercalated liposomes. The best fusion efficiency and, therefore, cargo delivery efficiency was reached using FL as nanocarriers. We assumed that this high value could be achieved due to the different uptake mechanism of those liposomes compared to control. To test our hypothesis, cellular uptakes of FL and control liposomes were visualized using confocal microscopy by following the fluorescence signal of the liposomal membrane tracer DiR. Cells were identified upon DAPI staining of the cell nuclei. As shown in Figure 6.2, DiR fluorescence was located mainly in the plasma membrane of MDA- MB-231 cells upon treatment with FL, indicating that fusion and delivery efficiency reached 90%. Compared to this, only some dot-like signal of the lipid tracer DiR was detected on the cell surfaces treated with EL.

In the case of *in vivo* application of liposomes loaded with radioactive tracers, the complexes are directly injected into the bloodstream. Therefore we analyzed ^{131}I delivery to human blood cells as well. To this end human blood samples were incubated with free and liposomal ^{131}I at the same concentration as used on cancer cells, and the cellular iodine activities were determined. As shown in Figures 6.1C, 6.2, and 6.3 iodine delivery efficiencies remained comparably low (~ 3% (2)) in all cases independent from the treatment strategy. These results are especially surprising in the case of FL. Even though FL directly interact with almost any kind of mammalian cells upon contact and fuse with their plasma membrane, serum proteins seem to block the fusion process between liposomes and blood cells. Some earlier results of the experiments performed at the home institute showed that membrane fusion successfully occurred between purified and serum-free red blood cells and fusogenic liposomes [258].

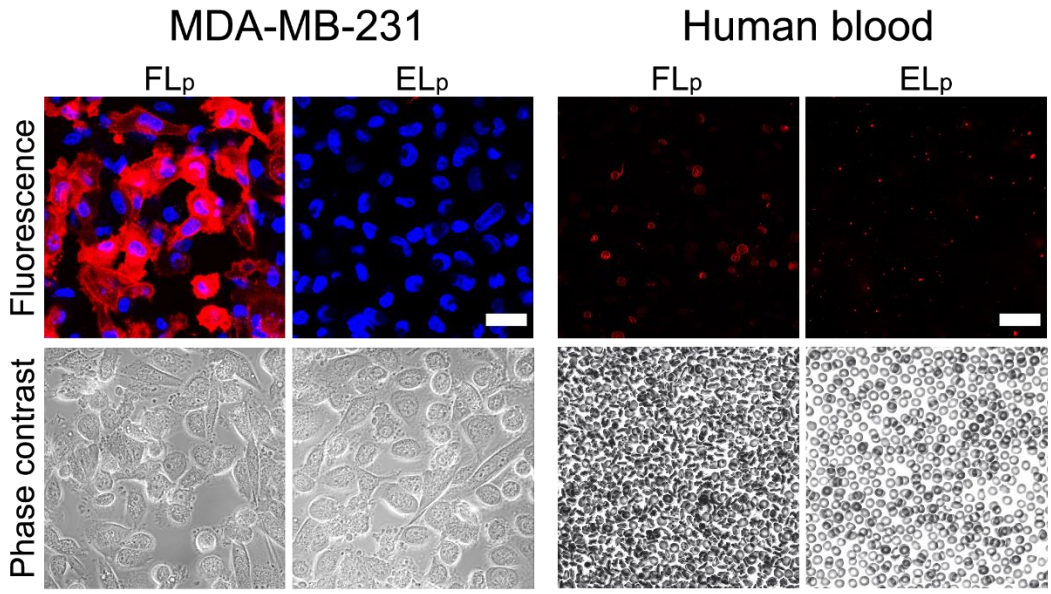

Figure 6.2. Monitoring the incorporation of fusogenic and endocytic liposomes pellets (FLp and ELp) containing ^{127}I into MDA MB-231 cancer cells by microscopy. The fluorescence signal of the lipid tracer DiR (red) and the cell nuclei staining DAPI (blue) are shown in overlays. Phase-contrast images reveal healthy cell morphologies. Scale bars, 20 µm

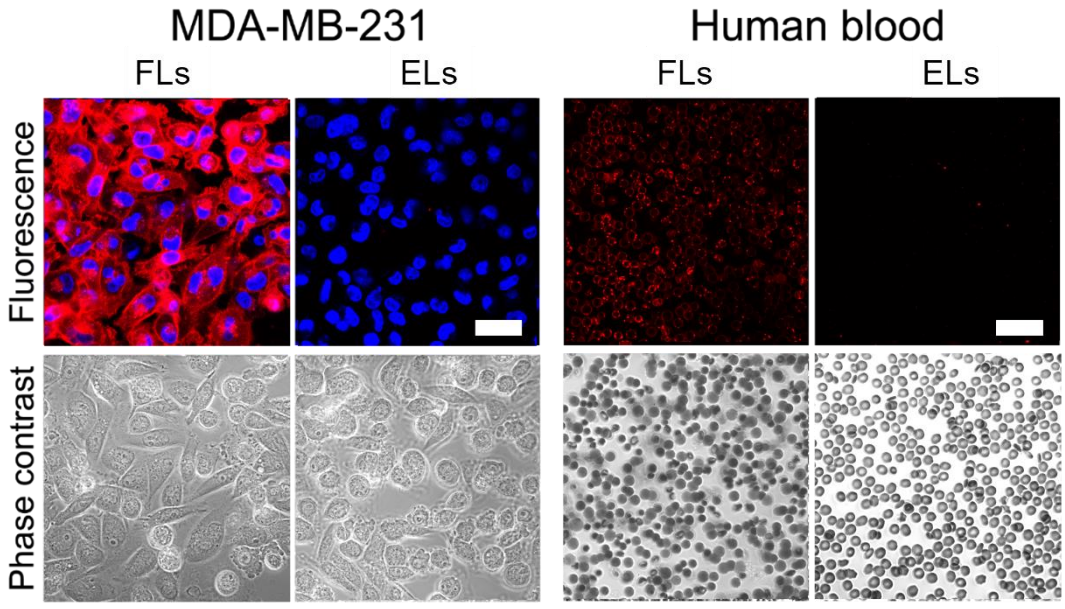

Figure 6.2. Monitoring the incorporation of fusogenic and endocytic liposomes supernatant (FLs and ELs) containing ^{127}I into MDA MB-231 cancer cells by microscopy. The fluorescence signal of the lipid tracer DiR (red) and the cell nuclei staining DAPI (blue) are shown in overlaps. The fluorescence signal comes from the liposomes remained in the supernatant, which fused with the cell membrane. Phase-contrast images reveal healthy cell morphologies. Scale bars, 20 µm.

6.3. Discussion

Cationic liposomes are mainly used for nucleic acids transport into living cells [259, 260]. Here, a special type of them, so-called fusogenic liposomes (FL), were used for the incorporation of the ^{131}I isotopes into cancer cells *in vitro* to test their application potential not only in gene therapy but also in nuclear treatments.

The preparation method of liposomes, the rehydration of the dry lipid film in a buffered solution containing iodide, as well as the separation of the cargo loaded liposomes from the free solution by centrifugation are well established and described in the literature [257]. Surprisingly, cationic FL cannot be separated from the supernatant by centrifugation at room temperature. A decrease in temperature from 20 °C to 4 °C resulted in efficient separation of the liposomes from the free buffer due to the formation of the lamellar lipid phase at low temperatures. Due to the high positive charge of the lipids, a stable liposomal suspension with an average particle size of 400 nm was formed [261] with a moderate iodide encapsulation efficiency of 29%. As a control, liposomes with neutral charge were used (EL). This high incorporation efficiency of EL (38%) can be traced to the high amount of iodide-containing buffer intercalated between the lamellas of the µm-sized liposomes. Compared to this, FL were found to be 4-5 times smaller (see Table 6.1), probably build up from much fewer altering lipid/water layers. As shown in Chapter 4, such liposomes have only partially lamellar structures [93]. Three-dimensional (3D) lipid phases, in general, contain less water than a two-dimensional lamellar phase. As a consequence, the amount of cargo dissolved in buffer is reduced.

The cationic FL have been successfully tested on the triple resistant breast cancer cell line MDA MB-231. Namely, the best ^{131}I delivery efficiency was reached using such liposomes as nanocarriers. In all other cases, iodine uptake remained neglectable (Figure 6.1B). This result agrees with other reports about the very low accumulation of ^{131}I in non-thyroidal tissues [262]. It could be that the high delivery efficiency reached by FL was achieved due to the different uptake mechanism of those liposomes compared to control EL. As shown earlier, cationic liposomes containing aromatic molecules in sufficient amounts are able to fuse with the plasma membrane of mammalian cells whereby they deliver their cargo with high efficiency directly into the cell interior [12]. Here, the best loading efficiencies were achieved using negatively charged cargos due to the attractive electrostatic forces between cargo and carrier particles.

Negatively charged proteins, e.g., eGFP or phycoerythrine [12], as well as nucleic acids (e.g. mRNA, siRNA) [51], have been successfully tested.

As our results showed, the anionic [^{131}I]I$^-$ can also be efficiently delivered by fusogenic liposomes. We assume that similar to proteins and RNA mentioned above, the negatively charged iodide ions are also bound to the cationic liposomal surface and are directly transported to the cancer cells via membrane fusion reaching high delivery efficiencies.

In the case of therapeutic applications, liposomes are usually directly injected into the bloodstream and are transported to different organs and tissues [263]. Their direct absorption by the blood cells is unwanted, with exceptions of some special blood treatments [264, 265]. Therefore we analyzed ^{131}I delivery to human blood cells as well. As shown in Figures 6.1C, 6.2, and 6.3. , iodine delivery efficiencies remained comparably low (ca. 3 (2)%) in all cases independent of treatment strategy. These results are especially surprising in the case of FL because these directly interact with almost any kind of mammalian cells, including purified red blood cells [258], upon contact and fuse with their plasma membranes. According to our hypothesis, serum proteins might be able to block the fusion process between liposomes and blood cells [266] (Figures 6.2, and 6.3). In this case, FL remain also adhered to the plasma membrane, similar to EL, and are intercalated by endocytosis instead of membrane fusion. As already shown, this uptake route is less beneficial for molecular delivery applications [51]. As our earlier results showed, the complex formation of FL with serum proteins is a temporal process. Liposomes became released from the complex reaching the endothelium of blood vessels and were able to fuse with these cells.

7. General conclusion and outlook

Fusogenic liposomes are proven as a versatile and effective tool for the delivery of various cargo. They can fuse with the cell membrane within minutes without inducers such as peptides or viruses. The main motive of this work was to understand the fusion mechanism of examined fusogenic liposomes. In order to understand more physicochemical properties of the fusogenic liposomes and to get close to the elucidation of the mechanism, the questions of liposomal composition, environmental conditions, and existing lipid phases of fusogenic liposomes were investigated.

Even though the fusogenic liposomes can fuse with the mammalian cell membranes without any external fusion inducer, no systematic investigation of the composition influence on fusion events has been done until now. In this study, the primary components were varied for a better understanding of how and why these liposomes fuse with the cell membrane. Here, the comparison of two lipids of similar chemical structure but different charge (DOTAP and DODAP) shown that the presence of cationic lipid is necessary for fusion induction. Further investigation of the influence of DOTAP concentration made known that even at low concentrations (~ 25%), the fusion occurs. Variation of different cationic lipids with different molecular shapes revealed that not only the positive charge is essential, but the molecular shape plays a vital role as well. Thus, cationic lipids with conical shape (DOTAP, DOTMA) make the liposomes highly fusogenic, unlike the lipids with cylindrical (DMTAP, DOEPC), round (DC-Cholesterol) or inverted conical (MVL5) where the fusion events are at low or none occurrence at all.

This study showed that another crucial component for fusion induction is an aromatic component, often fluorophores. Three different dyes placed within three different positions in the liposomes (lipid head or chain part or in the backbone) were tested. The experiments showed that from the distinct molar concentration of dye in the liposomes, fusion happens. This concentration is specific for each dye, and below it, only endocytosis was observed. The role of the aromatic component (presence of the π-electron system) needs to be investigated further with the particular analysis of electrostatic interactions and molecular polarizability. Because the fusion can already happen if the liposomes are made of positively charged lipid and a dye, the neutral lipid, as the third fundamental component of fusogenic liposomes, was varied here to understand its role in fusion events better.

The head group, chain length, and saturation of neutral lipids were changed. The lipids with phosphoethanolamine (PE) as a head group and long, unsaturated chains favor the fusion, while lipids with phosphocholine (PC) as a head group reverse the fusion back to endocytosis despite the chain length and saturation. The conclusion is that the presence of neutral lipid is not mandatory. However, its presence can strongly influence the fusion.

Furthermore, the influence of external factors like temperature, buffer osmolality, and ionic strength, as well as pH on membrane fusion, was examined. Liposomes consisting of DOTAP as cationic lipid, different neutral lipid, and a dye at a molar ratio of 1/1/0.1 mol/mol were used. Neutral lipids varied in chain length and saturation, and they were classified as PE-containing liposomes if they had PE as a head group (fusogenic liposomes, FLs) or PC-containing liposomes when a head group was PC (endocytic liposomes, ELs).

For a lipid formulation that fuses very efficiently with cell membranes, here a structure characterized by the concurrent existence of lipid bilayers and small micelle-like structures with high surface curvatures was found. This atypical structure is shown to be present at all tested conditions and increases fusion efficiency. In contrast, endocytic liposomes having lipids mostly organized in a lamellar phase, like the liposomes analyzed in this study, low osmolality and ionic strength of buffer strongly influence membrane fusion. However, under physiological conditions and in a broad range of pH changes, they remained endocytic. Further investigation of the liposomes via several techniques combined (solid-state NMR, small-angle neutron scattering, freeze-fracture, and Cryo-(S)TEM) confirmed the presence of small micelle-like structures with high curvatures. Moreover, such a systematic investigation revealed that these liposomes could co-exist in different lipid phases that can become slightly more mobile and invigorated with increasing temperature, and yet metastable. Based on these findings, a so-called modified stalk mechanism of fusion was proposed. Nevertheless, these results need further investigation with compatible techniques like small-angle X-ray scattering (SAXS) that can confirm and elucidate the lipid phases present in fusogenic liposomes in more detail. Moreover, the systematic study on the critical packing parameter of the lipids forming fusogenic liposomes should be done. Having pure lamellar phase as non-fusogenic and yet liposomes with combined lamellar/isotropic phases or pure isotropic phases as fusogenic set a question to be resolved: is the fusogenic phase any other phase except lamellar? Isotropic phases are shown to be more fluid and to have higher curvatures in comparison to the lamellar phase, which is proven as rigid and with fewer curvatures formed. Maybe, that is the reason why cell membranes do not fuse with each other, which is the consequence of the evolution of lipid

phases. Other lipids within the cell membrane make it more rigid so that it protects the cell and yet remain permeable enough to maintain the cell vitality.

Additionally, a new application of fusogenic liposomes was established. It was shown that cationic liposomes with high fusion ability were successfully used as carrier particles for the delivery of the radionuclide ^{131}I into mammalian breast cancer cells *in vitro*. Their high delivery efficiency and low interaction with human blood cells, especially erythrocytes, make them a suitable tool for application in nuclear medicine.

Bibliography:

1. Gadella, B.M. and Evans, J.P., *Membrane Fusions During Mammalian Fertilization.* Advances in experimental medicine and biology, 2011. **713**: p. 65-80.
2. Denesvre, C. and Malhotra, V., *Membrane fusion in organelle biogenesis.* Current opinion in cell biology, 1996. **8**(4): p. 519-523.
3. Patel, S.K., et al., *Organelle membrane fusion: a novel function for the syntaxin homolog Ufe1p in ER membrane fusion.* Cell, 1998. **92**(5): p. 611-620.
4. Wickner, W. and Schekman, R., *Membrane fusion.* Nature structural & molecular biology, 2008. **15**(7): p. 658-664.
5. Lentz, B.R. and Lee, J., *Poly(ethylene glycol) (PEG)-mediated fusion between pure lipid bilayers: a mechanism in common with viral fusion and secretory vesicle release?* Molecular Membrane Biology, 1999. **16**(4): p. 279-296
6. Ma, M. and Bong, D., *Controlled fusion of synthetic lipid membrane vesicles.* Accounts of Chemical Research, 2013. **46**(12): p. 2988-2997.
7. Braun, T., et al., *A bioanalytical assay to distinguish cellular uptake routes for liposomes.* Cytometry 2016. **89**(3): p. 301-308.
8. Csiszar, A., et al., *Resveratrol encapsulated in novel fusogenic liposomes activates Nrf2 and attenuates oxidative stress in cerebromicrovascular endothelial cells from aged rats.* The journals of gerontology. Series A, 2015. **70**(3): p. 303-313.
9. Csiszar, A., et al., *Novel fusogenic liposomes for fluorescent cell labeling and membrane modification.* Bioconjugate chemistry, 2010. **21**(3): p. 537-543.
10. Hersch, N., et al., *Biotin-conjugated fusogenic liposomes for high-quality cell purification.* Journal of biomaterials applications, 2016. **30**(6): p. 846-856.
11. Kleusch, C., et al., *Fluorescent lipids: functional parts of fusogenic liposomes and tools for cell membrane labeling and visualization.* Molecules, 2012. **17**(1): p. 1055-1073.
12. Kube, S., et al., *Fusogenic liposomes as nanocarriers for the delivery of intracellular proteins.* Langmuir, 2017. **33**(4): p. 1051-1059.
13. Yeagle, P.L., *Membrane Fusion*, in *The Membranes of Cells* P.L. Yeagle, Editor. 2016, Academic Press: Boston. p. 379-399.
14. Zimmerberg, J. and Whitaker, M., *Irreversible swelling of secretory granules during exocytosis caused by calcium.* Nature, 1985. **315**(6020): p. 581-584.
15. van Meer, G., Voelker, D.R. and Feigenson, G.W., *Membrane lipids: where they are and how they behave.* Nature reviews. Molecular cell biology, 2008. **9**(2): p. 112-124.
16. Segev, N., Avinoam, O. and Podbilewicz, B., *Fusogens.* Current Biology, 2018. **28**(8): p. R378- R380.
17. Ungermann, C. and Langosch, D., *Functions of SNAREs in intracellular membrane fusion and lipid bilayer mixing.* Journal of Cell Science, 2005. **118**(17): p. 3819-3828.
18. Bilek, G., et al., *Liposomal nanocontainers as models for viral infection: monitoring viral genomic RNA transfer through lipid membranes.* Journal of virology, 2011. **85**(16): p. 8368- 8375.
19. Donald, J.E., et al., *Transmembrane orientation and possible role of the fusogenic peptide from parainfluenza virus 5 (PIV5) in promoting fusion.* Proceedings of the National Academy of Sciences, 2011. **108**(10): p. 3958-3963.
20. Harrison, S.C., *Viral membrane fusion.* Virology, 2015. **479-480**: p. 498-507.

21. Shmulevitz, M., et al., *Structural and functional properties of an unusual internal fusion peptide in a nonenveloped virus membrane fusion protein.* Journal of virology, 2004. **78**(6): p. 2808- 2818.
22. Jahn, R. and T.C. Sudhof, *Membrane fusion and exocytosis.* Annual review of biochemistry, 1999. **68**: p. 863-911.
23. Tareste, D., et al., *SNAREpin/Munc18 promotes adhesion and fusion of large vesicles to giant membranes.* Proceedings of the National Academy of Sciences of the United States of America, 2008. **105**(7): p. 2380-2385.
24. Marsden, H.R., Tomatsu, I. and Kros, A., *Model systems for membrane fusion.* Chemical society reviews, 2011. **40**(3): p. 1572-1585.
25. Smirnova, Y.G., Risselada, H.J. and Müller, M., *Thermodynamically reversible paths of the first fusion intermediate reveal an important role for membrane anchors of fusion proteins.* Proceedings of the National Academy of Sciences, 2019. **116**(7): p. 2571-2576.
26. Chernomordik, L.V., Zimmerberg, J. and Kozlov, M.M., *Membranes of the world unite!* Journal of cell biology, 2006. **175**(2): p. 201-207.
27. Kerbel, R.S., et al., *Spontaneous fusion in vivo between normal host and tumor cells: possible contribution to tumor progression and metastasis studied with a lectin-resistant mutant tumor.* Molecular and Cellular Biology, 1983. **3**(4): p. 523-538.
28. Lasic, D.D., *Application of liposomes*, in *Handbook of biological physics*, R. Lipowsky and E. Sachnann, Editors. 1995, Elsevier: Menlo Park, California, USA.
29. Wagner, A. and Vorauer-Uhl, K., *Liposome technology for industrial purposes.* Journal of Drug Delivery, 2011. **2011:** 9 pages.
30. Bozzuto, G. and Molinari, A., *Liposomes as nanomedical devices.* International Journal of Nanomedicine, 2015. **10**: p. 975-999.
31. Ulrich, A.S., *Biophysical Aspects of Using Liposomes as Delivery Vehicles.* Bioscience reports, 2002. **22**(2): p. 129-150.
32. Akbarzadeh, A., et al., *Liposome: classification, preparation, and applications.* Nanoscale research letters, 2013. **8**(1): p. 102-107.
33. Gabizon, A., et al., *Development of liposomal anthracyclines: from basics to clinical applications.* Journal of controlled release, 1998. **53**(1-3): p. 275-279.
34. Hofheinz, R.D., et al., *Liposomal encapsulated anti-cancer drugs.* Anticancer drugs, 2005. **16**(7): p. 691-707.
35. Lipowsky, R., *The conformation of membranes.* Nature, 1991. **349**(6309): p. 475-481.
36. Edidin, M., *Lipids on the frontier: a century of cell-membrane bilayers.* Nature Reviews. Molecular Cell Biology, 2003. **4**: p. 414-418.
37. Cornelius, F., *Functional reconstitution of the sodium pump. Kinetics of exchange reactions performed by reconstituted Na/K-ATPase.* Biochimica et Biophysica Acta, 1991. **1071**(1): p. 19- 66.
38. Caracciolo, G., et al., *The liposome–protein corona in mice and humans and its implications for in vivo delivery.* Journal of Materials Chemistry B, 2014. **2**(42): p. 7419-7428.
39. Chatin, B., et al., *Liposome-based formulation for intracellular delivery of functional proteins.* Molecular Therapy - Nucleic Acids, 2015. **4**: p. e244-254.
40. Lasic, D.D., *Kinetic and thermodynamic effect on the structure and formation of phosphatidylcholine vesicles.* Hepatology, 1991. **13**(5): p. 1010-1013.
41. Sakaguchi, N., et al., *The correlation between fusion capability and transfection activity in hybrid complexes of lipoplexes and pH-sensitive liposomes.* Biomaterials, 2008. **29**(29): p. 4029- 4036.

42. Kobayashi, S., et al., *Cytosolic targeting of macromolecules using a pH-dependent fusogenic peptide in combination with cationic liposomes.* Bioconjugate chemistry, 2009. **20**(5): p. 953- 959.
43. Banóczi, Z., et al., *Synthesis of cell-penetrating conjugates of calpain activator peptides.* Bioconjugate chemistry, 2007. **18**(1): p. 130-137.
44. Jahn, R., T. Lang, and Sudhof, T.C., *Membrane fusion.* Cell, 2003. **112**(4): p. 519-533.
45. Chernomordik, L.V. and Kozlov, M.M., *Mechanics of membrane fusion.* Nature Structural & Molecular Biology, 2008. **15**: p. 675-683.
46. Swaminathan, J. and Ehrhardt, C., *Liposomal delivery of proteins and peptides.* Expert Opinion on Drug Delivery, 2012. **9**(12): p. 1489-1503.
47. Terasaki, M., et al., *Fluorescent staining of subcellular organelles: ER, Golgi complex, and mitochondria.* Current protocols in cell biology, 2001. **0**(1): p. 4.4.1-4.4.18.
48. Kolter, T. and K. Sandhoff, *Lysosomal degradation of membrane lipids.* FEBS letters, 2010. **584**(9): p. 1700-1712.
49. Münter, R., et al., *Dissociation of fluorescently labeled lipids from liposomes in biological environments challenges the interpretation of uptake studies.* Nanoscale, 2018. **10**(48): p. 22720-22724.
50. Naumovska, E., et al., *Plasma membrane functionalization using highly fusogenic immune activator liposomes.* Acta biomaterialia, 2014. **10**(3): p. 1403-11.
51. Hoffmann, M., et al., *Changing the way of entrance: highly efficient transfer of mRNA and siRNA via fusogenic nano-carriers*. Journal of biomedical nanotechnology, 2019. **15**: p. 170- 183.
52. Cullis, P.R., Hope, M.J. and Tilcock, C.P.S., *Lipid polymorphism and the roles of lipids in membranes.* Chemistry and Physics of Lipids, 1986. **40**(2): p. 127-144.
53. Luzzati, V., Tardieu, A. and Gulik-Krzywicki, T. *Polymorphism of lipids.* Nature, 1968. **217**(5133): p. 1028-1030.
54. Tilcock, C.P.S., *Lipid polymorphism.* Chemistry and Physics of Lipids, 1986. **40**(2): p. 109-125.
55. Cevc, G., Allen, T.M. and Neidleman, S.L., *Phospholipids handbook*. 1993.
56. Seddon, J.M. and Templer, R.H., *Polymorphism of lipid-water systems*, in *Handbook of Biological Physics*, R. Lipowsky and E. Sackmann, Editors. 1995, Elsevier Science London.
57. Garti, N., Libster, D. and Aserin, A., *Lipid polymorphism in lyotropic liquid crystals for triggered release of bioactives.* Food & Function, 2012. **3**(7): p. 700-713.
58. Figueiredo, N.A.M. and Salinas, S.R.A., *The physics of lyotropic liquid crystals phase transitions and structural properties*. 2007, Oxford; Toronto: Oxford University Press.
59. Yang, L. and Huang, H.W., *A rhombohedral phase of lipid containing a membrane fusion intermediate structure.* Biophysical Journal, 2003. **84**(3): p. 1808-1817.
60. Ding, L., et al., *Distorted hexagonal phase studied by neutron diffraction: lipid components demixed in a bent monolayer*. Langmuir, 2005. **21**(1): p. 203-210.
61. Yang, L., Ding, L. and Huang, H.W., *New phases of phospholipids and implications to the membrane fusion problem.* Biochemistry, 2003. **42**(22): p. 6631-6635.
62. Hyde, S., *Identification of lyotropic liquid crystalline mesophases*, in *Handbook of Applied Surface and Colloid Chemistry*, K. Holmberg, Editor. 2001, John Wiley & Sons Inc: Chichester, England. p. 299-332.
63. Strey, R., et al., *Freeze fracture electron microscopy of dilute lamellar and anomalous isotropic (L3) phases.* Langmuir, 1990. **6**(11): p. 1635-1639.
64. Kulkarni, C.V., *Lipid crystallization: from self-assembly to hierarchical and biological ordering.* Nanoscale, 2012. **4**(19): p. 5779-5791.

65. Lewis, R.N., Mannock, D.A. and McElhaney, R.N., *Differential scanning calorimetry in the study of lipid phase transitions in model and biological membranes: practical considerations.* Methods in molecular biology, 2007. **400**: p. 171-195.
66. Smith, E.A. and Dea, P.K., *Differential scanning calorimetry studies of phospholipid membranes: the Interdigitated gel phase*, in *Applications of Calorimetry in a Wide Context - Differential Scanning Calorimetry, Isothermal Titration Calorimetry and Microcalorimetry*. 2013.
67. Bolean, M., et al., *The effect of cholesterol on the reconstitution of alkaline phosphatase into liposomes*. Biophysical Chemistry, 2010. **152**(1-3): p. 74-79.
68. Biltonen, R.L. and Lichtenberg, D., *The use of differential scanning calorimetry as a tool to characterize liposome preparations.* Chemistry and physics of lipids, 1993. **64**(1): p. 129-142.
69. Tanford, C., *The Hydrophobic Effect: Formation Of Micelles and Biological Membranes*. Vol. 1. 1980, New York: Wiley-Interscience.
70. Israelachvili, J.N., *Intermolecular and Surface Forces*. 2010, Saint Louis, USA: Elsevier Science & Technology.
71. Israelachvili, J.N., Mitchell, D.J. and Ninham, B.W., *Theory of self-assembly of hydrocarbon amphiphiles into micelles and bilayers.* Journal of the Chemical Society, Faraday Transactions 2: Molecular and Chemical Physics, 1976. **72**(0): p. 1525-1568.
72. Becher, P., *Hydrophile-lipophile balance: history and recent developments Langmuir lecture.* Journal of dispersion science and technology, 1983. **5**(1): p. 81–96.
73. Siegel, D.P., *The modified stalk mechanism of lamellar/inverted phase transitions and its implications for membrane fusion.* Biophysical journal, 1999. **76**(1): p. 291-313.
74. Siegel, D.P. and Epand, R.M., *The mechanism of lamellar-to-inverted hexagonal phase transitions in phosphatidylethanolamine: implications for membrane fusion mechanisms.* Biophysical journal, 1997. **73**(6): p. 3089-3111.
75. Ellens, H., Bentz, J. and Szoka, F.C., *Fusion of phosphatidylethanolamine-containing liposomes and mechanism of L.alpha.-HII phase transition.* Biochemistry, 1986. **25**(14): p. 4141-4147.
76. Siegel, D.P., et al., *Physiological levels of diacylglycerols in phospholipid membranes induce membrane fusion and stabilize inverted phases.* Biochemistry, 1989. **28**(9): p. 3703-3709.
77. Jouhet, J., *Importance of the hexagonal lipid phase in biological membrane organization.* Frontiers in Plant Science, 2013. **4**(494): 5 pages.
78. Fuhrmans, M., et al., *Mechanics of membrane fusion/pore formation.* Chemistry and Physics of Lipids, 2015. **185**: p. 109-128.
79. Siegel, D.P. and Kozlov, M.M., *The gaussian curvature elastic modulus of N-monomethylated dioleoylphosphatidylethanolamine: relevance to membrane fusion and lipid phase behavior.* Biophysical journal, 2004. **87**(1): p. 366-374.
80. Chernomordik, L.V. and Kozlov, M.M., *Protein-lipid interplay in fusion and fission of biological membranes.* Annual review of biochemistry, 2003. **72**: p. 175-207.
81. Chernomordik, L.V. and Kozlov, M.M. *Membrane hemifusion: crossing a chasm in two leaps.* Cell, 2005. **123**(3): p. 375-382.
82. Kozlov, M.M., et al., *Stalk mechanism of vesicle fusion.* European Biophysics Journal, 1989. **17**(3): p. 121-129.
83. Markin, V.S. and Albanesi, J.P., *Membrane fusion: stalk model revisited.* Biophysical journal, 2002. **82**(2): p. 693-712.
84. Markin, V.S., Kozlov, M.M. and Borovjagin, V.L., *On the theory of membrane fusion. The stalk mechanism.* General physiology and biophysics, 1984. **3**(5): p. 361-377.

85. Shillcock, J. and R. Lipowsky, *The computational route from bilayer membranes to vesicle fusion.* Journal of physics. Condensed matter : an Institute of physics journal, 2006. **18**: p. S1191-219.
86. Grafmüller, A., Shillcock, J. and Lipowsky, R., *The fusion of membranes and vesicles: pathway and energy barriers from dissipative particle dynamics.* Biophysical journal, 2009. **96**(7): p. 2658-2675.
87. François-Martin, C., Rothman, J.E. and Pincet, F., *Low energy cost for optimal speed and control of membrane fusion.* Proceedings of the National Academy of Sciences, 2017. **114**(6): p. 1238- 1241.
88. Kawamoto, S. and Shinoda, W., *Free energy analysis along the stalk mechanism of membrane fusion.* Soft Matter, 2014. **10**(17): p. 3048-3054.
89. Ryham, R.J., et al., *Calculating transition energy barriers and characterizing activation states for steps of fusion.* Biophysical journal, 2016. **110**(5): p. 1110-1124.
90. Smirnova, Y.G., et al., *Solvent-exposed tails as prestalk transition states for membrane fusion at low hydration.* Journal of the American Chemical Society, 2010. **132**(19): p. 6710-6718.
91. Siegel, D.P., *Inverted micellar structures in bilayer membranes. Formation rates and half-lives.* Biophysical journal, 1984. **45**(2): p. 399-420.
92. Kolašinac, R., et al., *Deciphering the functional composition of fusogenic liposomes.* International Journal of Molecular Sciences, 2018. **19**(2): p. 346-361.
93. Kolašinac, R., et al., *Influence of environmental conditions on the fusion of cationic liposomes with living mammalian cells.* Nanomaterials, 2019. **9**(7): p. 1025-1041.
94. Bhattacharjee, S., *DLS and Zeta Potential - What they are and what they are not?* Journal of controlled release 2016. **235**: p. 337-351.
95. Brückel, T. and Förster, S., *Scattering - Introduction and Overview*, in *Scattering! Soft, Functional and Quantum Materials. Lecture Notes of the 50th IFF Spring School 2019*, Angst, M., et al., Editors. 2019, Forschungszentrum Jülich: Jülich.
96. Glatter, O. and Kratky, O., *Small angle x-ray scattering*. 1982, London; New York: Academic Press.
97. Guinier, A., and Fournet, G., *Small-angle scattering of X-rays*. 1955, New York: John Wiley & Sons, Inc.
98. Jackson, A.J., *Introduction to Small-Angle Neutron Scattering and Neutron Reflectometry.* NIST Center for Neutron Research, 2008.
99. Jaksch, S., *Small-angle scattering*, in *Scattering! Soft, Functional and Quantum Materials. Lecture Notes of the 50th IFF Spring School 2019*, Angst, M. et al., Editors. 2019, Forschungszentrum Jülich: Jülich.
100. Meurant, G., *An Introduction to Dynamic Light Scattering by Macromolecules* 2012: Elsevier. 472.
101. Ogendal, L., *Light Scattering: a brief introduction*, L. Ogendal., Editor. 2019, Copenhagen, Denmark: University of Copenhagen.
102. Pedersen, J.S., *Analysis of small-angle scattering data from colloids and polymer solutions: modeling and least-squares fitting.* Advances in colloid and interface science, 1997. **70**: p. 171-210.
103. Svergun, D., Koch, M., Timmins, P., and May, R., *Small Angle X-Ray and Neutron Scattering from Solutions of Biological Macromolecules*. 2013, Oxford: Oxford Scholarship Online.
104. Svergun, D.I., Feigin, L.A. and Taylor, G.W., *Structure analysis by small-angle X-ray and neutron scattering*. 1987, New York: Plenum Press.
105. Weyerich, B., Brunner-Popela, J. and Glatter, O., *Small-angle scattering of interacting particles. Generalized indirect Fourier transformation under consideration of the effective*

structure factor for polydisperse systems. Journal of applied crystallography, 1999. **32**(2): p. 197-209.
106. Disch, S., *The spin structure of magnetic nanoparticles and in magnetic nanostructures*. 2019. Vol. 21.
107. Radulescu A., Szekely, N. K. and Appavou, M-S., *KWS-2: Small angle scattering diffractometer.* Journal of large-scale research facilities,, 2015. **1**(A29).
108. Nallet, F., Laversanne, R. and Roux, D. *Modelling X-ray or neutron scattering spectra of lyotropic lamellar phases : interplay between form and structure factors.* Journal de Physique II, 1993. **3**(4): p. 487-502.
109. Hiemenz, P. and Rajagopalan, R., *Principles of colloid and surface chemistry*. 3rd ed. 2016.
110. Norde, W., *Colloids and interfaces in life sciences and bionanotechnology*. 2nd ed. 2011.
111. Sakho, E.H.M., et al., *Chapter 2 - Dynamic Light Scattering (DLS)*, in *Thermal and Rheological Measurement Techniques for Nanomaterials Characterization*, Thomas, S. et al., Editors. 2017, Elsevier. p. 37-49.
112. Mingard, K., et al., *Good Practice Guide for Improving the Consistency of Particle Size Measurement*. 2009, Hampton Road, Teddington, Middlesex, Scotland, UK: National Physical Laboratory.
113. Macey, M.G., *Flow cytometry: principles and applications*. 2007: Humana Press.
114. Shapiro, H.M., *Practical Flow Cytometry*. 2003: Wiley.
115. Heimburg, T., *Thermal biophysics of membranes*. 2007: Wiley-VCH.
116. Ali, S., et al., *A Differential Scanning Calorimetry Study of Phosphocholines Mixed with Paclitaxel and Its Bromoacylated Taxanes.* Biophysical Journal, 2000. **78**(1): p. 246- 256.
117. Demetzos, C., *Differential Scanning Calorimetry (DSC): a tool to study the thermal behavior of lipid bilayers and liposomal stability.* Journal of liposome research, 2008. **18**(3): p. 159-73.
118. Fidorra, M., Heimburg, T., and Seeger, H.M., *Melting of individual lipid components in binary lipid mixtures studied by FTIR spectroscopy, DSC and Monte Carlo simulations.* Biochimica et Biophysica Acta 2009. **1788**(3): p. 600-607.
119. Koshy, O., Subramanian, L. and Thomas, S., *Chapter 5 - Differential Scanning Calorimetry in Nanoscience and Nanotechnology*, in *Thermal and Rheological Measurement Techniques for Nanomaterials Characterization*, Thomas, S. et al., Editors. 2017, Elsevier. p. 109-122.
120. Almgren, M., Edwards, K. and Gustafsson, J., *Cryotransmission electron microscopy of thin vitrified samples.* Current opinion in colloid & interface science, 1996. **1**(2): p. 270-278.
121. Appavou, M.S., *Cryo-Transmission Electron Microscopy*, in *Scattering! Soft, Functional and Quantum Materials, Lecture Notes of the 50th IFF Spring School 2019*, Bruckel, T. et al. Editors. 2019, Förschungszentrum Jülich: Jülich, Germany.
122. Douglas, B.M. and Davidson, M.W., *Fundamentals of Light Microscopy*, in *Fundamentals of Light Microscopy and Electronic Imaging*. 2012.
123. Douglas, B.M. and Davidson, M.W., *Confocal laser scanning microscopy*, in *Fundamentals of Light Microscopy and Electronic Imaging*. 2012.
124. Egerton, R.F., *Physical principles of electron microscopy. An introduction to TEM, SEM, and AEM*, in *Handbook of biological confocal microscopy.*, Pawley, J.B. Editor. 2006, Springer: Berlin.
125. Elbaum, M., Wolf, S.G. and Houben, L., *Cryo-scanning transmission electron tomography of biological cells.* MRS Bulletin, 2016. **41**(7): p. 542-548.
126. Inkson, B.J., *2 - Scanning electron microscopy (SEM) and transmission electron microscopy (TEM) for materials characterization*, in *Materials characterization using nondestructive evaluation (NDE) methods*, G. Hübschen, et al., Editors. 2016, Woodhead Publishing. p. 17-43.
127. Inoué, S., *Foundations of Confocal Scanned Imaging in Light Microscopy*, in *Handbook Of Biological Confocal Microscopy*, J.B. Pawley, Editor. 2006, Springer US: Boston, MA. p. 1-19.
128. Kubitscheck, U., *Fluorescence Microscopy: From Principles to Biological Applications*. 2013, Weinheirn, Germany: Wiley-VCH Verlag GmbH & Co.

129. Lettinga, M.P. and Egelhaaf, S.U., *Light Microscopy*, in *Lecture Notes of the42nd IFF Spring School 2011: Macromolecular Systems in Soft and Living Matter*, Dhont, J. et al., Editors. 2011, Forschungszentrum Juelich.
130. Merkel, R., *Light microscopy*, in *Lecture Notes of the 46th IFF Spring School 2015: Functional Soft Matter*, Dhont, J. et al., Editors. 2015, Forschungszentrum Jülich.
131. Muller, S.A. and Engel, A., *Structure and mass analysis by Scanning Transmission Electron Microscopy*. Micron, 2001. **32**(1): p. 21-31.
132. Müller, S.A. and Engel, A., *Biological Scanning Transmission Electron Microscopy: imaging and single molecule mass determination.* International Journal for Chemistry, 2006. **60**(11): p. 749-753.
133. Murray, R.G.E. and Robinow, C.F., *Light Microscopy*, in *Methods for General and Molecular Microbiology*. 2007, American Society of Microbiology.
134. Pawley, J.B., *Handbook of biological confocal microscopy*. 3rd edition ed. 2006, Berlin: Springer.
135. Sagalowicz, L., et al., *Crystallography of dispersed liquid crystalline phases studied by cryo-Transmission Electron Microscopy*. Journal of microscopy, 2006. **221**(2): p. 110- 121.
136. Severs, N.J., *Freeze-fracture electron microscopy.* Nature protocols, 2007. **2**(3): p. 547- 576.
137. Sheppard, C.J.R. and Shotton, D.M., *Confocal Laser Scanning Microscopy*. The quarterly review of biology, 1999. **74**(1).
138. Hersch, N., et al., *The constant beat: cardiomyocytes adapt their forces by equal contraction upon environmental stiffening.* Biology open, 2013. **2**(3): p. 351-361.
139. Papahadjopoulos-Sternberg, B., *The power of freeze-fracture electron microscopy in membrane exploration.* Biophysical journal, 2016. **110**(3): p. 581.
140. Pinto da Silva, P. and Branton, D., *Membrane splitting in freeze-ethching. Covalently bound ferritin as a membrane marker.* Journal of cell biology, 1970. **45**(3): p. 598-605.
141. Sutterby, J.L., *Falling sphere viscometer.* Journal of Physics E: Scientific Instruments, 1973. **6**(10): p. 1001-1005.
142. Happel, J. and Brenner, H., *Low Reynolds number hydrodynamics: with special applications to particulate media*. 1965: Prentice-Hall.
143. Ammann, C., Meier, P. and Merbach, A., *A simple multinuclear NMR thermometer.* Journal of magnetic resonance 1982. **46**(2): p. 319-321.
144. Keeler, J., *Understanding NMR spectroscopy*. 4th ed. 2002, University of Cambridge: Willey.
145. Knight, J. and Knight, M., *Solid State NMR: basic principles and practice.* Organic Process Research & Development, 2012. **16**(9): p. 1572-1572.
146. Kooijman, E.E., et al., *Magic angle spinning 31P NMR spectroscopy reveals two essentially identical ionization states for the cardiolipin phosphates in phospholipid liposomes.* Biochimica et Biophysica Acta, 2017. **1859**(1): p. 61-68.
147. Laws, D.D., Bitter, H-M.L. and Jerschow, A., *Solid-State NMR Spectroscopic Methods in Chemistry.* Angewandte Chemie International Edition, 2002. **41**(17): p. 3096-3129.
148. Linseisen, F.M., Bayerl, S. and Bayerl, T.M., *^{2}H-NMR and DSC study of DPPC-DODAB mixtures.* Chemistry and Physics of Lipids, 1996. **83**(1): p. 9-23.
149. Schiller, J., et al., *^{31}P NMR Spectroscopy of Phospholipids: From Micelles to Membranes.* Current analytical chemistry, 2007. **3**(4): p. 283-301.
150. Markley, J.L., et al., *Recommendations for the presentation of NMR structures of proteins and nucleic acids.* Journal of biomolecular NMR, 1998. **12**(1): p. 1-23.
151. Rance, M. and Byrd, R.A., *Obtaining high-fidelity spin-12 powder spectra in anisotropic media: phase-cycled Hahn echo spectroscopy.* Journal of Magnetic Resonance, 1983. **52**(2): p. 221-240.
152. Fung, B.M., Khitrin, A.K. and Ermolaev, K., *An improved broadband decoupling sequence for liquid crystals and solids.* Journal of magnetic resonance 2000. **142**(1): p. 97-101.
153. Felgner, P.L., et al., *Lipofection: a highly efficient, lipid-mediated DNA-transfection procedure.* Proceedings of the National Academy of Sciences, 1987. **84**(21): p. 7413- 7417.
154. Radler, J.O., et al., *Structure of DNA-cationic liposome complexes: DNA intercalation in multilamellar membranes in distinct interhelical packing regimes.* Science, 1997. **275**(5301): p. 810-814.

155. Koynova, R., Wang, L. and MacDonald, R.C., *Cationic phospholipids forming cubic phases: lipoplex structure and transfection efficiency.* Molecular pharmaceutics, 2008. **5**(5): p. 739-44.
156. Pozharski, E.V. and MacDonald, R.C., *Single lipoplex study of cationic lipoid-DNA, self-assembled complexes.* Molecular pharmaceutics, 2007. **4**(6): p. 962-974.
157. Chernomordik, L.V. and Kozlov, M.M., *Mechanics of membrane fusion.* Nature Structural & Molecular Biology, 2008. **15**(7): p. 675-683.
158. Hart, S.L., *Lipid carriers for gene therapy.* Current drug delivery, 2005. **2**(4): p. 423- 428.
159. Khalil, I.A., et al., *Uptake pathways and subsequent intracellular trafficking in nonviral gene delivery.* Pharmacological reviews, 2006. **58**(1): p. 32-45.
160. Lacoeuille, F., et al., *Lipid nanocapsules for intracellular drug delivery of anticancer drugs.* Journal of nanoscience and nanotechnology, 2007. **7**(12): p. 4612-4617.
161. Simberg, D., et al., *DOTAP (and other cationic lipids): chemistry, biophysics, and transfection.* Critical reviews in therapeutic drug carrier systems, 2004. **21**(4): p. 257- 317.
162. Koltover, I., et al., *An inverted hexagonal phase of cationic liposome-DNA complexes related to DNA release and delivery.* Science, 1998. **281**(5373): p. 78-81.
163. Miller, C.R., et al., *Liposome-cell interactions in vitro: effect of liposome surface charge on the binding and endocytosis of conventional and sterically stabilized liposomes.* Biochemistry, 1998. **37**(37): p. 12875-12883.
164. O'Brien, P.J., et al., *Bio-Orthogonal Mediated Nucleic Acid Transfection of Cells via Cell Surface Engineering.* ACS central science, 2017. **3**(5): p. 489-500.
165. Braun, T., *Fusogene und Endozytotische Liposomen: Vergleichende Untersuchungen zum Wirkstofftransport am Beispiel von Doxorubicin und Aclacinomycin A.* 2017, Rheinischen Friedrich-Wilhelms-Universität Bonn: Bonn, Germany.
166. Moch, M., et al., *Effects of plectin depletion on keratin network dynamics and organization.* Public Library of Science, 2016. **11**(3).
167. Zuhorn, I.S., Kalicharan, R. and Hoekstra, D., *Lipoplex-mediated transfection of mammalian cells occurs through the cholesterol-dependent clathrin-mediated pathway of endocytosis.* Journal of biological chemistry, 2002. **277**(20): p. 18021-18028.
168. Heinze, M., et al., *Novel cationic lipids based on malonic acid amides backbone: transfection efficacy and cell toxicity properties.* Bioconjugate chemistry, 2010. **21**(4): p. 696-708.
169. Kim, B.K., et al., *Transfection property of a new cholesterol-based cationic lipid containing tri-2-hydroxyethylamine as gene delivery vehicle.* Journal of microbiology and biotechnology, 2012. **22**(6): p. 866-871.
170. Malamas, A.S., et al., *Design and evaluation of new pH-sensitive amphiphilic cationic lipids for siRNA delivery.* Journal of controlled release 2013. **171**(3): p. 296-307.
171. Kumar, V.V., *Lipid molecular shapes and membrane architecture.* Indian journal of biochemistry & biophysics, 1993. **30**(3): p. 135-138.
172. Frolov, V.A., Shnyrova, A.V. and Zimmerberg, J., *Lipid polymorphisms and membrane shape.* Cold spring harbor perspectives in biology, 2011. **3**(11): p. a004747-a004762.
173. Balazs, D.A. and Godbey, W., *Liposomes for use in gene delivery.* Journal of drug delivery, 2011. **2011**: p. 326497-3264109.
174. Farhood, H., Serbina, N. and Huang, L., *The role of dioleoyl phosphatidylethanolamine in cationic liposome mediated gene transfer.* Biochimica et Biophysica Acta 1995. **1235**(2): p. 289-295.
175. Ferrari, M.E., et al., *Synergy between cationic lipid and co-lipid determines the macroscopic structure and transfection activity of lipoplexes.* Nucleic acids research, 2002. **30**(8): p. 1808-16.
176. Gullapalli, R.R., Demirel, M.C. and Butler, P.J., *Molecular dynamics simulations of DiI-C18(3) in a DPPC lipid bilayer.* Physical chemistry chemical physics, 2008. **10**(24): p. 3548-60.
177. Boonstra, S., et al., *Hemagglutinin-mediated membrane fusion: a biophysical perspective.* Annual review of biophysics, 2018. **47**: p. 153-173.
178. Burger, K.N.J., *Chapter 11 - Morphology of Membrane Fusion*, in *Current Topics in Membranes*, R.M. Epand, Editor. 1997, Academic Press. p. 403-445.
179. Sharma, S. and Lindau, M., *The fusion pore, 60 years after the first cartoon.* FEBS Letters, 2018. **592**(21): p. 3542-3562.

180. Akimov, S.A., et al., *Phosphatidylcholine membrane fusion Is pH-Dependent.* International Journal of Molecular Sciences, 2018. **19**(5): p. 1358-1373
181. Faneca, H., et al., *Cationic liposome-based systems for nucleic acid delivery: from the formulation development to therapeutic applications*, in Drug Delivery Systems: Advanced Technologies Potentially Applicable in Personalised Treatment. Advances in Predictive, Preventive and Personalised Medicine, Coelho, J. Editor. 2013. Vol. 4. Springer, Dordrecht
182. Vaccaro, L., et al., *Plasticity of Influenza Haemagglutinin fusion peptides and their interaction with lipid bilayers.* Biophysical journal, 2005. **88**(1): p. 25-36.
183. Bulavin, L. and Lebovka, N., *Physics of Liquid Matter: Modern Problems: Proceedings*. Vol. 171. 2015, Kyiv, Ukraine.
184. Koynova, R., Wang, L. and MacDonald R.C., *An intracellular lamellar-nonlamellar phase transition rationalizes the superior performance of some cationic lipid transfection agents.* Proceedings of the National Academy of Sciences, 2006. **103**(39): p. 14373-14378.
185. Siegel, D.P., et al., *Intermediates in membrane fusion and bilayer/nonbilayer phase transitions imaged by time-resolved cryo-transmission electron microscopy.* Biophysical journal, 1989. **56**(1): p. 161-169.
186. Cevc, G., *Membrane electrostatics.* Biochimica et Biophysica Acta 1990. **1031**(3): p. 311-382.
187. Graber, Z.T., Shi, Z. and Baumgart, T., *Cations induce shape remodeling of negatively charged phospholipid membranes.* Physical Chemistry Chemical Physics 2017. **19**(23): p. 15285-15295.
188. Raja, M. and Vales, E., *Effects of sodium chloride on membrane fusion and on the formation of aggregates of potassium channel KcsA in Escherichia coli membrane.* Biophysical chemistry, 2009. **142**(1): p. 46-54.
189. Schultz, Z.D., et al., *Magnesium-induced lipid bilayer microdomain reorganizations: implications for membrane fusion.* The journal of physical chemistry, 2009. **113**(29): p. 9932-9941.
190. Lira, R.B., et al., *Highly efficient protein-free membrane fusion: a giant vesicle study.* Biophysical Journal, 2019. **116**(1): p. 79-91.
191. Wolf, H. and Gingell, D., *Conformational response of the glycocalyx to ionic strength and interaction with modified glass surfaces: study of live red cells by interferometry.* Journal of cell science, 1983. **63**: p. 101-12.
192. Mabrey, S. and Sturtevant, J.M., *Investigation of phase transitions of lipids and lipid mixtures by sensitivity differential scanning calorimetry.* Proceedings of the National Academy of Sciences, 1976. **73**(11): p. 3862-3866.
193. Wilkinson, D.A. and Nagle, J.F., *Dilatometric study of binary mixtures of phosphatidylcholines.* Biochemistry, 1979. **18**(19): p. 4244-9.
194. Middel, V., et al., *Dysferlin-mediated phosphatidylserine sorting engages macrophages in sarcolemma repair.* Nature communications, 2016. **7**: p. 12875-12886.
195. Mondal Roy, S. and Sarkar, M., *Membrane fusion induced by small molecules and ions.* Journal of lipids, 2011. **2011**: p. 528784-528798
196. Ortiz, A., et al., *Membrane fusion and the lamellar-to-inverted-hexagonal phase transition in cardiolipin vesicle systems induced by divalent cations.* Biophysical journal, 1999. **77**(4): p. 2003-2014.
197. Pinot, M., et al., *Polyunsaturated phospholipids facilitate membrane deformation and fission by endocytic proteins.* Science, 2014. **345**(6197): p. 693-697.
198. Singer, S.J. and Nicolson, G.L., *The fluid mosaic model of the structure of cell membranes.* Science, 1972. **175**(4023): p. 720-731.
199. Stamatatos, L., et al., *Interactions of cationic lipid vesicles with negatively charged phospholipid vesicles and biological membranes.* Biochemistry, 1988. **27**(11): p. 3917- 3925.
200. sraelachvili, J.N. and Wennerstrom, H., *Role of hydration and water structure in biological and colloidal interactions.* Nature, 1996. **379**(6562): p. 219-225.
201. Tanford, C., *Interfacial free energy and the hydrophobic effect.* Proceedings of the National Academy of Sciences, 1979. **76**(9): p. 4175-4176.
202. Lewis, R.N. and McElhaney, R.N., *Membrane lipid phase transitions and phase organization studied by Fourier transform infrared spectroscopy.* Biochimica et Biophysica Acta, 2013. **1828**(10): p. 2347-2358.

203. Cevc, G., *Isothermal lipid phase transitions.* Chemistry and Physics of Lipids, 1991. **57**(2): p. 293-307.
204. Wu, H.L., Sheng, Y.J. and Tsao, H.K., *Phase behaviors and membrane properties of model liposomes: temperature effect.* Journal of chemical physics, 2014. **141**(12): p. 124906-124917.
205. Alessandrini, A. and Facci, P., *Phase transitions in supported lipid bilayers studied by AFM.* Soft Matter, 2014. **10**(37): p. 7145-7164.
206. Koynova, R. and Tenchov, B., *Lipids: Phase Transitions*, in *Wiley Encyclopedia of Chemical Biology*, Begley, T.P., Editor. 2008, John Wiley & Sons, Inc.
207. Taylor, K.M.G. and Morris,, R.M., *Thermal analysis of phase transition behavior of liposomes.* Thermochimica Acta 1995. **248**: p. 289-301.
208. Siegel, D.P., *Inverted micellar intermediates and the transitions between lamellar, cubic, and inverted hexagonal lipid phases. I. Mechanism of the L-alpha-H-II phase transitions.* Biophysical journal, 1986. **49**(6): p. 1155-1170.
209. Siegel, D.P., *Energetics of intermediates in membrane fusion: comparison of stalk and inverted micellar intermediate mechanisms.* Biophysical journal, 1993. **65**(5): p. 2124- 2140.
210. Heinrich, M., et al., *Dynamic sorting of lipids and proteins in membrane tubes with a moving phase boundary.* Proceedings of the National Academy of Sciences, 2010. **107**(16): p. 7208-7213.
211. Hoopes, M.I., Faller, R. and Longo, M.L., *Lipid domain depletion at small localized bends imposed by a step geometry.* Langmuir, 2011. **27**(6): p. 2783-2788.
212. Tian, A. and Baumgart, T., *Sorting of lipids and proteins in membrane curvature gradients.* Biophysical journal, 2009. **96**(7): p. 2676-2688.
213. Lindblom, G. and Rilfors, L., *Cubic phases and isotropic structures formed by membrane lipid-possible biological relevance.* Biochimica et Biophysica Acta, 1989. **988**: p. 221-256.
214. Seddon, J.M., et al., *Inverse micellar phases of phospholipids and glycolipids. Invited Lecture.* Physical Chemistry Chemical Physics, 2000. **2**(20): p. 4485-4493.
215. Yang, Y., Yao, H. and Hong, M., *Distinguishing bicontinuous lipid cubic phases from isotropic membrane morphologies using ^{31}P Solid-State NMR spectroscopy.* The Journal of Physical Chemistry 2015. **119**(15): p. 4993-5001.
216. Winter, R., *Synchrotron X-ray and neutron small-angle scattering of lyotropic lipid mesophases, model biomembranes and proteins in solution at high pressure.* Biochimica et Biophysica Acta - Protein Structure and Molecular Enzymology, 2002. **1595**(1): p. 160-184.
217. Angelov, B., et al., *Long-Living Intermediates during a lamellar to a diamond-cubic lipid phase transition: s Small-Angle X-Ray Scattering investigation.* Langmuir, 2009. **25**(6): p. 3734-3742.
218. Nele, V., et al., *Effect of formulation method, lipid composition, and PEGylation on vesicle lamellarity: A Small-Angle Neutron Scattering Study.* Langmuir, 2019. **35**(18): p. 6064-6074.
219. Fong, C., et al., *Monodisperse nonionic phytanyl ethylene oxide surfactants: High throughput lyotropic liquid crystalline phase determination and the formation of liposomes, hexosomes and cubosomes*. Soft Matter, 2010. **6**: p. 4727-4741
220. Yaghmur, A., et al., *Emulsified microemulsions and oil-containing liquid crystalline phases.* Langmuir, 2005. **21**(2): p. 569-577.
221. Tran, N., et al., *Nanostructure and cytotoxicity of self-assembled monoolein–capric acid lyotropic liquid crystalline nanoparticles.* RSC Advances, 2015. **5**(34): p. 26785-26795.
222. Yang, L. and Huang, H.W., *Observation of a membrane fusion intermediate structure.* Science, 2002. **297**(5588): p. 1877-1879.
223. Koynova, R. and Tenchov, B., *Phase transitions and phase behavior of lipids*, in *Encyclopedia of Biophysics*, G.C.K. Roberts, Editor. 2013, Springer p. 1841-1854.
224. Demurtas, D., et al., *Direct visualization of dispersed lipid bicontinuous cubic phases by cryo-electron tomography.* Nature Communications, 2015. **6**: p. 8915-8923.
225. Glauert, A.M., *Electron microscopy of lipids and membranes.* Journal of the Royal Microscopical Society, 1968. **88**(1): p. 49-70.
226. Funari, S.S. and Rapp, G., *A continuous topological change during phase transitions in amphiphile/water systems.* Proceedings of the National Academy of Sciences, 1999. **96**(14): p. 7756-7759.

227. Meyer, H.W., et al., *Hydration of DMPC and DPPC at 4 degrees C produces a novel subgel phase with convex-concave bilayer curvatures.* Chemistry and physics of lipids, 2000. **105**(2): p. 149-66.
228. Tenchov, B., Koynova, R. and Rapp, G., *New ordered metastable phases between the gel and subgel phases in hydrated phospholipids.* Biophysical Journal, 2001. **80**(4): p. 1873-1890.
229. Jacoby, G., et al., *Metastability in lipid based particles exhibits temporally deterministic and controllable behavior.* Scientific Reports, 2015. **5**: p. 9481-9488.
230. Kirsch, S.A. and Böckmann, R.A., *Coupling of membrane nanodomain formation and enhanced electroporation near phase transition.* Biophysical Journal, 2019. **116**(11): p. 2131-2148.
231. Ting, C.L., et al., *Metastable prepores in tension-free lipid bilayers.* Physical Review Letters, 2018. **120**(12): p. 128103.
232. Nieh, M.P., et al., *Highly aligned lamellar lipid domains induced by macroscopic confinement.* Langmuir, 2003. **19**(17): p. 6936-6941.
233. Matsuki, H., et al., *Thermotropic and barotropic phase behavior of phosphatidylcholine bilayers.* International Journal of Molecular Sciences, 2013. **14**(2): p. 2282-2302.
234. Ogunyankin, M.O. and Longo, M.L., *Metastability in pixelation patterns of coexisting fluid lipid bilayer phases imposed by e-beam patterned substrates.* Soft Matter, 2013. **9**(6): p. 2037-2046.
235. Rappolt, M. and Rapp, G., *Structure of the stable and metastable ripple phase of dipalmitoylphosphatidylcholine.* European biophysics journal, 1996. **24**(6): p. 381–386.
236. Arnold, K., *Chapter 19 - Cation-Induced Vesicle Fusion Modulated by Polymers and Proteins*, in *Handbook of Biological Physics*, R. Lipowsky and E. Sackmann, Editors. 1995, North-Holland. p. 903-957.
237. Kozlovsky, Y., et al., *Stalk phase formation: effects of dehydration and saddle splay modulus.* Biophysical Journal, 2004. **87**(4): p. 2508-2521.
238. Kozlovsky, Y. and Kozlov, M.M., *Stalk model of membrane fusion: solution of energy crisis.* Biophysical Journal, 2002. **82**(2): p. 882-895.
239. Kuzmin, P.I., et al., *A quantitative model for membrane fusion based on low-energy intermediates.* Proceedings of the National Academy of Sciences, 2001. **98**(13): p. 7235-7240.
240. May, S., *Structure and energy of fusion stalks: the role of membrane edges.* Biophysical journal, 2002. **83**(6): p. 2969-2980.
241. Ellens, H., et al., *Membrane fusion and inverted phases.* Biochemistry, 1989. **28**(9): p. 3692-3703.
242. Asano, K., *Fusion between HVJ and cell membrane.* Annual reports of the College of Medical Technology, Kyoto University 1988. **8**(1): p. 18-36.
243. Teissier, E., et al., *Mechanism of inhibition of enveloped virus membrane fusion by the antiviral drug Arbidol.* Public Library of Science, 2011. **6**: p. e1587-15100.
244. de Campo, L., et al., *Reversible phase transitions in emulsified nanostructured lipid systems.* Langmuir, 2004. **20**(13): p. 5254-5261.
245. Bulbake, U., et al., *Liposomal formulations in clinical use: an updated review.* Pharmaceutics, 2017. **9**(2) 33 pages.
246. Gurunathan, S., et al., *Nanoparticle-Mediated Combination Therapy: Two-in-One Approach for Cancer.* International Journal of Molecular Science, 2018. **19**(10): p. 3264-32101.
247. Nisini, R., et al., *The multirole of liposomes in therapy and prevention of infectious diseases.* Frontiers in Immunology, 2018. **9**(155).
248. Deshpande, P.P., Biswas, S. and Torchilin, V.P., *Current trends in the use of liposomes for tumor targeting.* Nanomedicine 2013. **8**(9): p. 1509-1528.
249. Olusanya, T.O.B., et al., *Liposomal drug delivery systems and anticancer drugs.* Molecules, 2018. **23**(4): p. 907-924.
250. Lamichhane, N., et al., *Liposomes: clinical applications and potential for image-guided drug delivery.* Molecules, 2018. **23**(2): p. 288-305.
251. Xing, H., Hwang, K. and Lu, Y., *Recent developments of liposomes as nanocarriers for theranostic applications.* Theranostics, 2016. **6**(9) p. 1336–1352.
252. De Silva, L., et al., *Characterization, optimization, and in vitro evaluation of Technetium-99m-labeled niosomes.* International journal of nanomedicine, 2019. **14**: p. 1101-1117.
253. Phillips, W., Goins, B. and Bao, A., *Radioactive liposomes.* Wiley interdisciplinary reviews. Nanomedicine and nanobiotechnology, 2009. **1**: p. 69-83.

254. Berg, G.E., et al., *Iodine-131 treatment of hyperthyroidism: significance of effective half-life measurements.* Journal of nuclear medicine 1996. **37**(2): p. 228-232.
255. Park, S.Y., et al., *Peptidoglycan recognition protein Pglyrp2 protects mice from psoriasis-like skin inflammation by promoting regulatory T cells and limiting Th17 responses.* The journal of immunology, 2011. **187**(11): p. 5813-5823.
256. Murray, I.P., Spiro, M.J. and Stanbury, J.B., *The metabolism of iodine in the thyroid gland.* Journal of chronic diseases, 1961. **14**: p. 473-83.
257. Gregoriadis, G., *Liposome technology*. 3rd ed. Vol. 1. 2006, London UK: CRC Press.
258. Monzel, C., et al., *Measuring fast stochastic displacements of bio-membranes with dynamic optical displacement spectroscopy.* Nature Communications, 2015. **6**: p. 8162- 8170.
259. Tavano, L., Mazzotta, E. and Muzzalupo, R., *Nanovesicular formulations for cancer gene therapy.* Current pharmaceutical design, 2017. **23**(35): p. 5327-5335.
260. Zylberberg, C., et al., *Engineering liposomal nanoparticles for targeted gene therapy.* Gene therapy, 2017. **24**(8): p. 441-452.
261. Heurtault, B., et al., *Physico-chemical stability of colloidal lipid particles.* Biomaterials, 2003. **24**(23): p. 4283-300.
262. Oh, J.-R. and Ahn, B-C., *False-positive uptake on radioiodine whole-body scintigraphy: physiologic and pathologic variants unrelated to thyroid cancer.* American journal of nuclear medicine and molecular imaging, 2012. **2**(3): p. 362-385.
263. Srivatsan, A. and Chen, X., *Recent advances in nanoparticle-based nuclear imaging of cancers.* Advances in cancer research, 2014. **124**: p. 83-129.
264. Kumar, V., *Radiolabeled white blood cells and direct targeting of micro-organisms for infection imaging.* The quarterly journal of nuclear medicine and molecular imaging, 2005. **49**(4): p. 325-338.
265. van der Geest, T., et al., *Radionuclide imaging of liposomal drug delivery.* Expert Opinion on Drug Delivery, 2016. **13**(9): p. 1231-1242.
266. Li, S., et al., *Characterization of cationic lipid-protamine-DNA (LPD) complexes for intravenous gene delivery.* Gene therapy, 1998. **5**(7): p. 930-937.

A. List of abbreviations

1D	One-dimensional
2D	Two-dimensional
3D	Three-dimensional
AIDS	Acquired Immune Deficiency Syndrome
DAPI	4′,6-diamidino-2-phenylindole
DMEM-F12	Dulbecco's Modified Eagle Medium
DNA	Deoxyribonucleic acid
EDTA	Ethylenediaminetetraacetic acid
FDA	The Food and Drug Administration
GFP	The green fluorescent protein
mRNA	Messenger Ribonucleic acid
siRNA	small interfering Ribonucleic Acid
USA	The United States of America

List of publications:

Kolašinac et al. *Deciphering the Functional Composition of Fusogenic Liposomes*, Int. J. Mol. Sci, 2018, 19(2), 346; https://doi.org/10.3390/ijms19020346

Kolašinac et al. *Influence of environmental conditions on the fusion of cationic liposomes with living mammalian cells*, Nanomaterials, 2019, 9(7), 1025, https://doi.org/10.3390/nano9071025

Kolašinac et al. *Delivery of the Radionuclide ^{131}I to Cancer Cells using Fusogenic Liposomes as Nanocarriers*, International Journal of Nanomedicine, 2019 (submitted)

- Biennial Meeting of the German Biophysical Society, Düsseldorf, Germany
  2nd poster prize of the poster presentation: *Deciphering the functional principles of fusogenic liposomes*, September 16-19, *2018*

- IHRS BioSoft Symposium "Biomolecular Machines: Simulations Meet Experiments" – Talk: *Deciphering the functional principles of fusogenic liposomes*, April 23-24, 2018

- SoftComp Topical Workshop: Filaments, Membranes, Cells, and their Interactions

  Curie Institute and Forschungszentrum Jülich, Jülich (Germany) - Poster presentation: *Deciphering the functional principles of fusogenic liposomes*, January 28-31, *2018*

- Presentation and Communication Skills Course, Helmholtz Association, Stuttgart (Germany) – Five minutes presentation of Ph.D. work, August 5-6, 2017

- FEBS-EMBO lecture course: Molecular Architecture, Dynamics and Function of Biomembranes

  Federation of European Biochemical Societies (FEBS) / European Molecular Biology Organization (EMBO) / The University of Utrecht, Cargèse (France) - Poster presentation of the Ph.D. thesis, June 12 – 21, *2017*